UNIVERSIDADE ESTADUAL PAULISTA
"JÚLIO DE MESQUITA FILHO"

INSTITUTO DE QUÍMICA

MUHAMMAD SUFAID KHAN

Estudos da atividade para redução de oxigênio e da estabilidade de nanopartículas de PdNi e PdCu de diferentes composições suportadas em carbono

Studies of oxygen reduction activity and stability of carbon-supported PdNi and PdCu nanoparticles of different compositions

Araraquara

2018

MUHAMMAD SUFAID KHAN

Estudos da atividade para redução de oxigênio e da estabilidade de nanopartículas de PdNi e PdCu de diferentes composições suportadas em carbono

Studies of oxygen reduction activity and stability of carbon-supported PdNi and PdCu nanoparticles of different compositions

Tese apresentada ao Instituto de Química, Universidade Estadual Paulista, como parte dos requisitos para obtenção do título de Doutor em Química.

Orientadora: Profª. Drª. Hebe de las Mercedes Villullas

Araraquara

2018

FICHA CATALOGRÁFICA

Khan, Muhammad Sufaid
K45e Studies of oxygen reduction activity and stability of carbon-supported PdNi and PdCu nanoparticles of different compositions / Muhammad Sufaid Khan. – Araraquara: [s.n.], 2018
103 p.: il.

Thesis (doctor) – Universidade Estadual Paulista, Instituto de Química
Advisor: Hebe de las Mercedes Villullas

1. Oxygen – Industrial applications. 2. Palladium catalysts. 3. Nanoparticles. 4. Electrocatalysis. 5. Fuel cells. I. Title.

Elaboração: Seção Técnica de Aquisição e Tratamento da Informação
Biblioteca do Instituto de Química, Unesp, câmpus de Araraquara

UNIVERSIDADE ESTADUAL PAULISTA

Câmpus de Araraquara

CERTIFICADO DE APROVAÇÃO

TÍTULO DA TESE: "Studies of oxygen reduction activity and stability of carbon-supported PdNi and PdCu nanoparticles of different compositions"

AUTOR: MUHAMMAD SUFAID KHAN
ORIENTADORA: HEBE DE LAS MERCEDES VILLULLAS

Aprovado como parte das exigências para obtenção do Título de Doutor em QUÍMICA, pela Comissão Examinadora:

Profª. Drª. HEBE DE LAS MERCEDES VILLULLAS
Departamento de Físico-Química / Instituto de Química - UNESP - Araraquara

Profª. Drª. MARGARIDA JURI SAEKI
Departamento de Química / Instituto de Biociências - UNESP - Botucatu

Prof. Dr. ASSIS VICENTE BENEDETTI
Departamento de Físico- Química / Instituto de Química - UNESP - Araraquara

Profa. Dra. JANAINA FERNANDES GOMES
Departamento de Engenharia Química / Universidade Federal de São Carlos - UFSCar - São Carlos

Profa. Dra. ELISABETE INACIO SANTIAGO
CNEN / INSTITUTO DE PESQUISAS ENERGETICAS E NUCLEARES

Araraquara, 23 de fevereiro de 2018

Personal information

Name: Muhammad Sufaid Khan

Date of Birth: 01 March, 1984

Nationality: Pakistani

Present address: Av: Itápolis, 2161, Kit: 02, Bairro Quitandinha, Araraquara (SP).

Email: sufaidkhan1984@gmail.com

Academic record

PhD studies (Chemistry). Instituto de Química –UNESP, Campus de Araraquara, Araraquara (SP), Brasil (2014 - 2018).

M.S./M.Phil. in Physical Chemistry. National Centre of Excellence in Physical Chemistry, University of Peshawar, Peshawar Khyber Pukhtunkhwa (KPK), Pakistan, 2014.

Master in Physical Chemistry. Institute of Chemical Sciences University of Peshawar, Khyber Pukhtunkhwa (KPK), Pakistan, 2009.

Graduation. Govt. Post Graduate Jahanzeeb College Swat, University of Malakand, Khyber Pukhtunkhwa (KPK), Pakistan, 2006.

List of Publications

1. **Muhammad Sufaid Khan.,** et al. Removal of basic dye from aqueous solution by nanoscale zerovalent iron (NZVI) as adsorbent. Journal of Chemical Society of Pakistan, v. 35, n. 3, p. 745-748, 2013.

2. Jan Nisar; **Muhammad Sufaid Khan**; Mudassir Iqbal and Muhammad Anas Khan. Catalytic Thermal Decomposition of Polyethylene Determined by Thermogravimetric Treatment. Journal of Chemical Society of Pakistan, v. 36, n. 5, p. 829-836, 2014.

3. Jan Nisar; **Muhammad Sufaid Khan;** Munawar Iqbal; Afzal Shah; Ghulam Ali; Murtaza Sayed; Rafaqat Ali Khan; Faheem Shah; Tariq Mahmood. Thermal decomposition study of polyvinyl chloride in the presence of commercially available oxides catalysts. Advances in Polymer Technology, v. -, p. 1-8, 2017**.**

4. Abdur Rashid; Abida Farooqi; Sardar Khan; Salman Zahir; shah Jehan: Seema Khattak: **Muhammad Sufaid Khan**: Raees Khan. Fluoride prevalence in groundwater around fluorite mining area in the flood plain of river Swat, Pakistan. Science of the Total Environment, 2018. Ms. Ref. No.: STOTEN-D-17-08735 (Submitted after minor corrections).

Participation in events / conferences

1. **KHAN, M. S**.; MILIAN, R. P.; GALLO, I. B. C.; VILLULLAS, H. M. Studies of oxygen reduction activity and stability of carbon-supported PdNi nanoparticles of different compositions. 46th World Chemistry Congress, 40a Reunião Anual da Sociedade Brasileira de Química, São Paulo – Brazil, 9th to 14th of July 2017.

2. **KHAN, M. S**.; MILIAN, R. P.; GALLO, I. B. C.; VILLULLAS, H. M. Carbon-supported PdCu nanoparticles: activity for oxygen reduction in alkaline solutions and stability studies. XVI Brazilian MRS Meeting, Gramado (RS), 10th to 14th of September 2017.

3. **KHAN, M. S**.; MILIAN, R. P.; GALLO, I. B. C.; VILLULLAS, H. M. Synthesis and characterization of carbon-supported PdNi nanocatalysts for electroreduction of oxygen. XV Brazilian MRS Meeting, Campinas (SP), 25th to 29th of September 2016.

4. **KHAN, M. S**.; MILIAN, R. P. ; GALLO, I. B. C.; VILLULLAS, H. M. Carbon-supported PdCu and PdNi nanoparticles for oxygen reduction electrocatalysis. 26th National and 14th International Chemistry Conference Chemical Society of Pakistan (CSP) 5th to 8th of October 2015.

DEDICATION

I dedicate this thesis
to my late parents.

ACKNOWLEDEGEMENTS

First and foremost, I praise and thank Allah, the Almighty, for giving me the strength and courage, to accomplish this work and for blessing me with many great people, whose guidance and assistance make this task possible for me. I would therefore like to express my thanks to all of them.

Prof. Dr. Hebe de las Mercedes Villullas, my supervisor, for accepting me as Ph. D student and for her tremendous support, guidance and patience during the fulfillment of this work.

Irã Gallo, my lab fellow, whose sincere help and professional suggestions contribute a lot to the completion of this work.

All my laboratory friends and colleagues, Felipe Ometto, Rosendo Parra Milian, Gabriel Martins de Alvarenga and Douglas Saraiva, for their wonderful company, suggestions and useful scientific discussion.

I thank my family members especially my respected brother Pardool Khan, Assistant Professor in Physics, for his support and encouragement in this higher studies abroad and other family for their constant prayers, who all gave me courage and support all the time.

My Pakistani friends, especially Dr. Sabir Khan, Dr. Sajjad Hussain, Dr. Sajjad Ullah, Dr. Sardar Muhammad Hussain, Mian Abdul Ali, Dr. Ayaz Hassan, Sajjad Ali, Dr. Akbar Ali, Dr. Zia Ud din, Majid Ali and Wasid Ullah for always being around me throughout all the ups and downs I have been through.

Especial thanks to the Instituto de Química da Universidade Estadual Paulista "Júlio de Mesquita Filho", Câmpus de Araraquara, and to Deparmento de Físico-Química for providing a suitable environment and well-equipped laboratories for carrying out the research work and to the Laboratório Nacional de Luz Síncrotron (LNLS) for giving the opportunity to conduct X-ray absorption experiments.

Finally, I am thankful for the TWAS-CNPq fellowship that provided the opportunity for post-graduate studies.

ABSTRACT

The slow kinetics of the oxygen reduction reaction is the main cause of the severe performance losses of fuel cell cathode. Pt is the most active pure metal to catalyze this reaction. However, because of their limited availability and high price, the use of cheaper metals to act as catalysts in fuel cell electrodes is highly desirable. In this context, Pd-based catalysts are getting increasing attention. Thus, the main objective of this work was to study the oxygen reduction reaction on carbon-supported PdM (M = Ni, Cu) catalysts with different atomic ratios (Ni and Cu 10-50% in atoms), in acidic and alkaline solutions. The modified polyol method was used for the preparation of PdM nanoparticles that were then supported on carbon powder. The catalysts were characterized by X-ray diffraction (XRD) to investigate the crystalline structure and by X-ray absorption spectroscopy (XAS) to examine the electronic properties. The electrochemical behavior was studied by cyclic voltammetry. The PdNi/C and PdCu/C catalyst and a Pd/C reference sample were evaluated as electrocatalysts for the oxygen reduction reaction in acidic and alkaline solutions using the rotating ring disk electrode technique. Results showed formation of PdM alloys and an increase in the electronic occupation of the Pd 4d band. In both media, all PdM/C samples were more active for oxygen reduction than Pd/C, with activity increasing as the percentage of Ni or Cu increased. The production of hydrogen peroxide was small indicating that the reduction of oxygen proceeds mainly via the four-electron path. PdCu/C catalysts were more active than PdNi/C materials in acidic medium, but PdNi/C samples had better performance in alkaline solution. In addition, stability tests revealed that the presence of Ni and Cu considerably decreases the dissolution of Pd in acidic medium, although the stability of the materials was lower in alkaline than in acidic medium.

Keywords: Oxygen reduction reaction, Pd-based catalysts, PdM nanoparticles, electrocatalysis, Fuel cell cathode.

RESUMO

A cinética lenta da reação de redução de oxigênio é a principal causa das severas perdas de desempenho dos catodos de células a combustível. A Pt é metal puro mais ativo para catalisar esta reação. Entretanto, devido sua baixa abundância e alto custo, o uso de metais mais baratos para atuar como catalisadores nos eletrodos de células a combustível é muito desejável. Neste contexto, catalisadores baseados em Pd têm atraído cada vez mais atenção. Assim, o principal objetivo deste trabalho é estudar a reação de redução de oxigênio em catalisadores PdM (M = Ni, Cu) com diferentes composições (Ni e Cu 10-50% em átomos), em soluções ácidas e alcalinas. O método do poliol modificado foi utilizado para preparar as nanopartículas PdM, que foram posteriormente suportadas em pó de carbono. Os catalisadores foram caracterizados por difração de raios X para investigar a estrutura cristalina e por espectroscopia de absorção de raios X para determinar as propriedades eletrônicas. O comportamento eletroquímico foi examinado por voltametria cíclica. Os materiais PdNi/C e PdCu/C, assim como uma amostra de Pd/C usada como material de referência, foram testados como eletrocatalisadores para a reação de redução de oxigênio em meio ácido e alcalino utilizando a técnica do eletrodo de disco-anel rotatório. Os resultados mostraram formação de ligas PdM e um aumento na ocupação eletrônica da banda 4d do Pd. Em ambos os meios, os materiais PdM/C se mostraram mais ativos para a redução de oxigênio que o Pd/C, com atividades que aumentam à medida que cresce a percentagem de Ni or Cu. A produção de peróxido de hidrogênio foi baixa, indicando que a redução de oxigênio ocorre principalmente via 4 elétrons. Os catalisadores PdCu/C se mostraram mais ativos que os de PdNi/C em meio ácido, mas as amostras de PdNi/C foram mais ativas em meio alcalino. Além disso, testes de estabilidade revelaram que a presença de Ni ou Cu diminui consideravelmente a dissolução de Pd em meio ácido, mas a estabilidade destes materiais em meio básico é menor que em ácido.

Palavras-chave: Redução de oxigênio, catalisadores baseados em Pd, nanopartículas PdM, eletrocatálise. cátodo

LIST OF FIGURES

LIST OF TABLES

LIST OF ABBREVIATIONS

AFC	Alkaline Fuel Cell
AST	Accelerated Stability Test
CV	Cyclic Voltammetry
DAFC	Direct Alcohol Fuel Cell
DMFC	Direct Methanol Fuel Cell
ECSA	Electrochemical Active Surface Area
EXAFS	Extended X-Ray Absorption Fine Structure
MA	Mass activity
ORR	Oxygen Reduction Reaction
PEMFC	Proton Exchange Membrane Fuel Cell
RHE	Reversible Hydrogen Electrode
RRDE	Rotating Ring Disk Electrode
SA	Specific activity
XAS	X-Ray Absorption Spectroscopy
XANES	X-Ray Absorption Near Edge Structure
XRD	X-Ray Diffraction

SUMMARY

1. INTRODUCTION

Alternative ways for energy production as well as renewable energy sources have become increasingly relevant over the last years. The production of energy from fossil fuels causes environmental pollution, which has a considerable impact on climate and public health. To avoid and/or reduce the impact of fossil fuels burning on human health and environment, it becomes of paramount importance to develop greener and cost-effective sustainable energy systems. Among other possibilities, the use of electrochemical devices to convert chemical energy into electricity is presently considered a viable approach to clean energy generation. In particular, the development of fuel cell technology [1,2] is considered as one of the most promising ways of obtaining clean energy [3].

1.1. Fuel cells

Fuel cells are electrochemical devices where the oxidation of the fuel at the anode and the reduction of oxygen at the cathode side occur in such a way that allows the production of electricity. Electricity is produced from the charge-transfer processes occurring at the electrodes (anode and cathode), where a catalyst is often used to accelerate the electrochemical reactions [1,2].

Sir William Robert Grove was the first to demonstrate, in 1839, a fuel cell [4]. The concept of fuel cell started from a succession of experiments on water electrolysis in a setup for which the proposed named was gas voltaic battery. That gas voltaic battery was composed of two platinum electrodes immersed in a dilute sulfuric acidic electrolyte. He observed that during electrolysis the passage of current through the cell lead to the breaking up of water molecules into hydrogen and oxygen. Furthermore, Groove realized that when the power supply was taken out, a small current circulated through the cell due to the opposite reaction.

Although the concept of the alkaline fuel cell was known from the beginning of the 20th century, the viability of alkaline fuel cells was demonstrated in 1959 by Frances Thomas Bacon, at Cambridge University, by developing an alkaline fuel cell known as Bacon cell. That Bacon cell had power capacity of 5 to 6 kW. However, a high gas pressure (20 to 40 bar) was required during operation, which made the Bacon cell heavy [2].

Moreover, in 1960, Pratt and Whitney used the licensed patent of Bacon and constructed an engine. The main focus of this modification to engine was to minimize the gas pressure by using a strong basic solution. The Pratt and Whitney manufactured engine was used in the Apollo spacecraft. Research on fuel cells continued and in 1960s Thomas Grubb and Leonard Niedrach also developed a fuel cell which was used for power generation in the Gemini spacecraft [2]. History of fuel cell development is found in literature [5].

Generally, a fuel cell is composed of two electrodes immersed in an electrolyte, in which the electrochemical oxidation of the fuel at the anode and a reduction reaction at the cathode allow converting chemical energy in to electricity. An electric current is produced as the electrons released in the oxidation reaction circulate through the external circuit towards the cathode and an electrolyte present between the anode and cathode conducts the ionic charges between the two electrodes. At the current stage, there are several different types of fuel cells [1,2]. The main types in different stages of development to be marketable are classified on the bases of the type of electrolyte and are summarized in Table 1.

Table 1 – Classification of fuel cells based on types of electrolytes. Adapted from reference [6].

Type	Electrolyte	Operating temperature	Fuel
Alkaline fuel cell (AFC)	35-45 % KOH	60-90 °C	Pure hydrogen
Polymer electrolyte membrane fuel cell (PEMFC)	Proton exchange membrane and anion exchange membrane	60-90 °C	Pure hydrogen, methanol, ethanol
Phosphoric acidic fuel cell (PAFC)	100% H_3PO_4	180-220 °C	Hydrogen
Molten carbonate fuel cell (MCFC)	Molten carbonates (62 % LiO_2CO_3, 38 % K_2CO_3)	550-650 °C	Hydrogen, hydrocarbons, carbon monoxide
Solid oxide fuel cell (SOFC)	Stabilized zirconia and yttria	800-1000 °C	Hydrogen, hydrocarbons, carbon monoxide

1.1.1. Proton Exchange Membrane Fuel Cell (PEM)

Proton Exchange Membrane (PEM) fuel cells are also known as Polymer Electrolyte Fuel Cells (PEFCs). A PEM fuel cell possesses higher power capacity and smaller volume and are lighter compared to the other types of fuel cells. When the PEMFC is fed with hydrogen fuel, the oxidation of hydrogen and the reduction of oxygen produce electricity, water and heat [7]. Hence, the operational process of this type of fuel cell is environmentally friendly. The reactions that occur in the H_2/O_2 PEMFC are:

Anode reaction	$H_2 \rightarrow 2H^+ + 2e^-$	(1)
Cathode reaction	$½\ O_2 + 2H^+ + 2e^- \rightarrow H_2O$	(2)
Overall reaction	$H_2 + ½\ O_2 \rightarrow H_2O$	(3)

On the anode catalyst, the hydrogen molecules are oxidized to H^+ liberating electrons that are transported through the external circuit. On the cathode catalyst, oxygen molecules are reduced. The transport of H^+ from anode to cathode occurs through the electrolyte. Both electrochemical reactions occur on the surface of a catalyst. In cells that operate at low temperature the catalyst is usually Pt and the electrolyte is a proton-exchange membrane. During power production, losses related to the reaction kinetics (activation loss), resistance (ohmic loss) and concentration depletion (mass-transport loss) reduce the power efficiency.

Inside the PEM fuel cell, the porous carbon electrodes have catalysts that usually consist of Pt or Pt-based alloys materials in the form of nanoparticles. The solid polymer membrane that acts as electrolyte is usually Nafion®. A scheme of a PEMFC is shown in Figure 1.

The PEMFCs is a low temperature fuel cell and its temperature rises up to 80 -100 °C in operation. Low temperature operation and low warm-up time of components are advantages of the PEMFC. The general applications of the PEMFCs are vehicles, portable electronic devices and back-up, among others.

Figure 1 - Schematic diagram of a H_2/O_2 PEM fuel cell. Reproduced from reference [7].

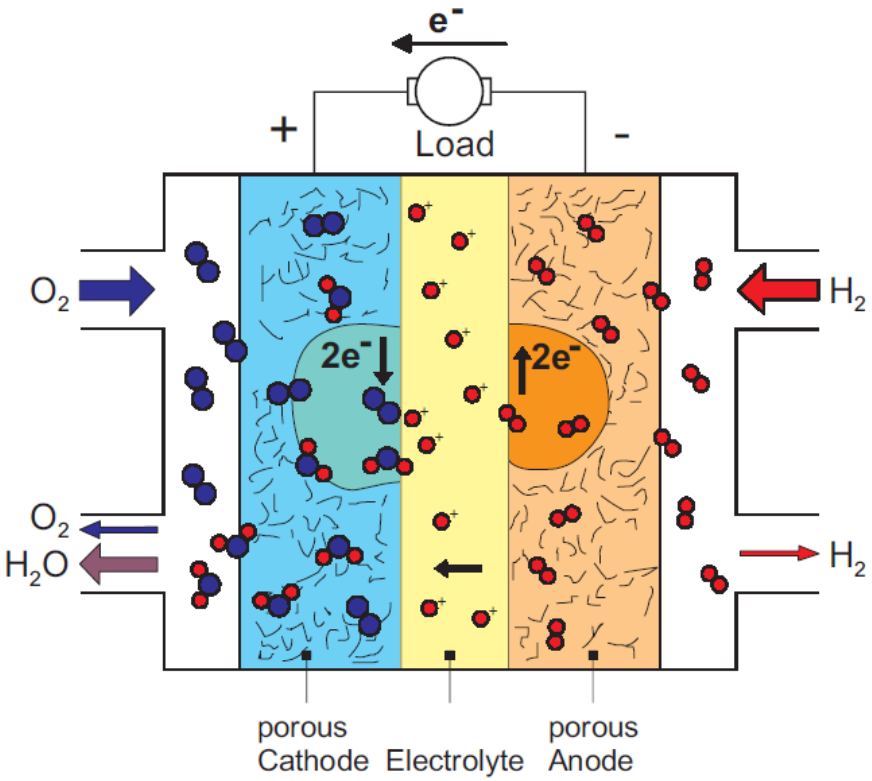

Generally, this type of fuel cell gives a potential of 0.7 V at full load. To obtain higher voltages several fuel cells can be connected in series (stacks). Stacks of different fuel cell types are made on the bases of production capacity from several kilowatts to tens of megawatts.

Although the use of hydrogen as fuel in PEMFC produces higher current densities, production of pure hydrogen, storage and delivery from one station to another involve technical challenges. Hence, utilization of alternative fuels without those requirements is desirable for the future energy need. The use of liquid fuels (such as methanol, ethanol, etc.) in Direct Alcohol Fuel Cells (DAFCs), which are PEMFCs fed with alcohol, seems to have several advantages regarding storage and distribution. From a thermodynamic point of view, the alcohol oxidation efficiency is about 97 %, which is higher than that of hydrogen oxidation (83 %). The hydrogen volume energy capacity is 2.6 kWh/L, which is lower than that of ethanol (6.3 kWh/L) and methanol (4.8 kWh/L), respectively. Therefore, alcohols are considered viable fuels to replace hydrogen to satisfy future energy demand [8,9].

1.1.2. Alkaline fuel cells

The Alkaline Fuel Cell (AFC) is considered a very important type of cell and it was used in space technology. The AFC is operated at low temperature, about 100 °C. The electrolyte used in AFCs is an aqueous solution of KOH. The electrolyte concentration is 85 wt.% and 35 to 50 wt.% KOH for AFCs operated at high and low temperature, respectively. The KOH electrolyte is embedded in a solid matrix (usually asbestos). Different types of non-precious elements are used as electrocatalysts for cathode and anode. Despite the many advantages of AFCs, there are also some drawbacks, like poisoning by carbon dioxide. Even a small amount of CO_2 can badly affect the stability and efficiency of AFCs due to formation of carbonate [5]. Therefore, in the last few years great attention was given to develop alkaline exchange membrane fuel cell (AEMFC), because they have some advantages over PEMFCs [10].

The use of anion exchange membranes in alkaline fuel cells has many advantages, such as enhanced ORR kinetics in the alkaline environment and the possibility of using cheaper metals as electrocatalysts or Pt-free materials that are more stable in alkaline than in acidic media [11]. In addition, there are more options for fuels to be used in alkaline medium as substitute of hydrogen [12]. Over the last years, a large amount of reports began to focus on AEMFCs as the availability of appropriate AEMs was growing [13]. However, the amount of data on activity and stability of catalysts in alkaline media available in the literature is much lesser than for acidic environments.

Generally, the PEM and AEM fuel cells are similar. The principal difference is that the solid membrane is acidic (proton exchange) in the PEMFCs and alkaline (anion exchange) in AEMFCs. The differences between a PEMFC and an AEMFC are illustrated in Figure 2. In the AEMFC, the hydroxide ions move from the cathode to the anode, while in the PEMFC the hydrogen ion move from the anode to the cathode of the fuel cell.

Figure 2 - Schematic diagrams of the PEMFC and AEMFC. Reproduced from reference [10]. Permission to reproduce this figure is not required.

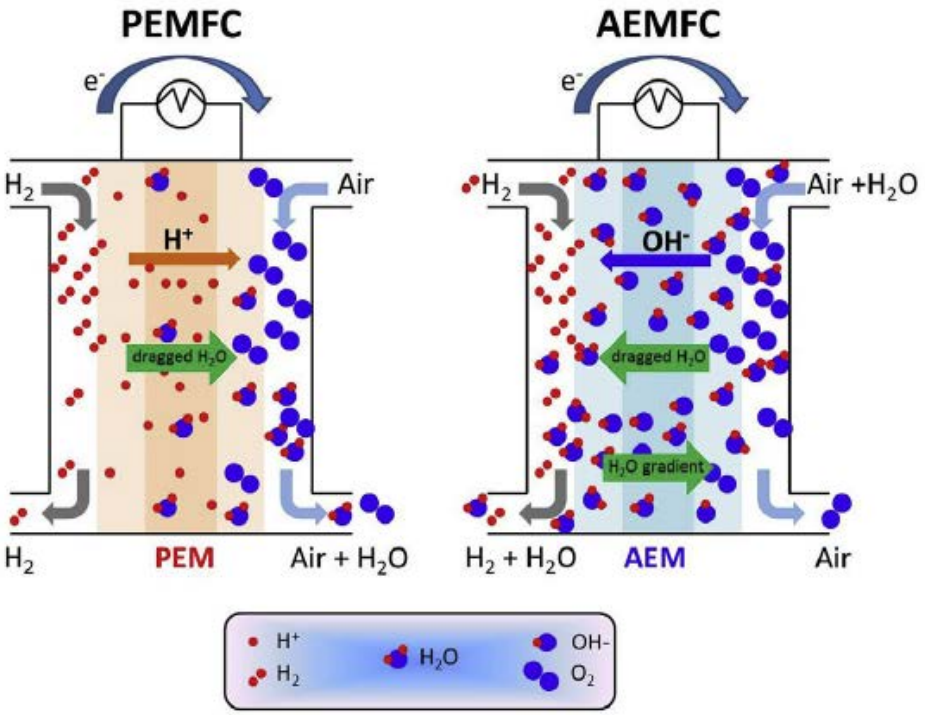

It should be kept in mind that during the electrochemical process in the AEMFC, the hydroxide ions and water are not moving as in the same direction as protons are transported in the PEM fuel cells. The reduction of oxygen at the cathode and the oxidation of hydrogen occurring at the anode of the AEMFC are given by the following reactions:

$$\tfrac{1}{2}\, O_2 + H_2O + 2e^- \rightarrow 2OH^- \qquad (4)$$

$$2\, OH^- + H_2 \rightarrow 2H_2O + 2e^- \qquad (5)$$

As shown in reaction (5), water is formed as a product like in a PEMFC, but in the AEMFCs water is produced at the anode and at the same time water reacts at the cathode. This unique water movement situation together with the high pH medium show the distinctive nature of the AEM fuel cells [10].

Over the last two decades, several different aspects of fuel cell technology have been widely investigated [14]. Overall, PEMFCs and AEMFCs are presently

regarded as adequate systems for energy generation [15,16]. While research on this area has led to significant progress, the cell performance is still affected by the sluggish kinetics of oxygen reduction, which produces considerable losses of cell potential [1,2].

1.2. The oxygen reduction reaction

The oxygen reduction reaction (ORR) plays a crucial role in biological process needed to sustain life, such as respiration, in corrosion, in many industrial reactions and in electrochemical energy conversion systems.

The ORR plays a significant role in electrochemistry. In particular, ORR electrocatalysis [17,18,19,20,21] is one of the most important research areas related to the development of fuel cell catalysts.

The ORR is a multi-step process. It is known that in an acidic medium it occurs by two distinct routes: the direct reduction to water, which involves the transfer of 4 electrons, and the reduction via hydrogen peroxide, which involves the transfer of 2 electrons [18,22,23]:

$$O_2 + 4H^+ + 4e^- \rightarrow 2H_2O \quad (6)$$

$$O_2 + 2H^+ + 2e^- \rightarrow H_2O_2 \quad (7)$$

The hydrogen peroxide formed in the two-electron route can diffuse to solution or be reduced to water [23]:

$$H_2O_2 + 2H^+ + 2e^- \rightarrow 2H_2O \quad (8)$$

These routes are shown in the simplified reaction scheme of Figure 3.

Figure 3 - Simplified ORR mechanism in acidic medium, adapted from reference [23].

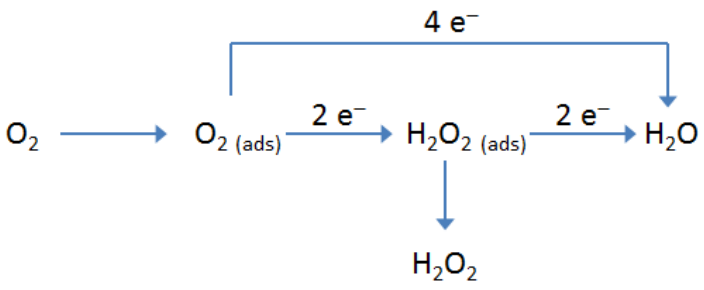

Similarly, the electrochemical reactions in alkaline medium, in which ORR proceeds either by a two-electron or through four-electron pathways, are [18,22,23]:

$$O_2 + 2H_2O + 4e^- \rightarrow 4OH^- \quad (9)$$

$$O_2 + H_2O + 2e^- \rightarrow HO_2^- + OH^- \quad (10)$$

$$HO_2^- + H_2O + 2e^- \rightarrow 3OH^- \quad (11)$$

Besides reactions (6) to (11) that take place in aqueous media, in non-aqueous aprotic solvents the ORR can also involve one-electron path, in which O_2 is converted into superoxide (O_2^{2-}) [18].

The thermodynamic electrode potentials at standard conditions for O_2 reduction reactions are presented in Table 2. The actual mechanism through which the ORR occurs might be much more difficult and include different intermediates, which initially depended on the electrode nature, electrocatalyst and medium.

Table 2 – Thermodynamic electrode potentials of electrochemical O_2 reduction, adapted from reference [21].

Electrolyte	ORR reactions	Thermodynamic electrode potential at standard conditions, V
Acidic aqueous solution	$O_2 + 4H^+ + 4e^- \rightarrow 2H_2O$ $O_2 + 2H^+ + 2e^- \rightarrow H_2O_2$ $H_2O_2 + 2H^+ + 2e^- \rightarrow 2H_2O$	1.229 0.70 1.76
Alkaline aqueous solution	$O_2 + H_2O + 4e^- \rightarrow 4OH^-$ $O_2 + H_2O + 2e^- \rightarrow OH_2^- + OH^-$ $OH_2^- + H_2O + 2e^- \rightarrow 3OH^-$	0.401 -0.065 0.865
Non-aqueous aprotic solvents	$O_2 + e^- \rightarrow O_2^-$ $O_2^- + e^- \rightarrow O_2^{2-}$	Value strongly dependent on solvent used

The oxygen molecule adsorbs in different ways on the surface of a catalyst and that influences the reduction mechanism [18,23], as shown in Figure 4. For instance, the adsorption of oxygen following the model of Griffith occurs only in metals that have at least two unpaired electrons in valence orbitals. On the other hand, the adsorption of oxygen as in the bridge model occurs in metals with at least one unpaired electron. Adsorption according to the model proposed by Pauling takes place when the distance between the catalytic sites is much larger than the oxygen-oxygen bond length or when there are steric impediments that hinder the adsorption of the two atoms of the oxygen molecule. On Pauling's model, the oxygen molecule adsorbs on a single catalytic site, as can be observed in the scheme of Figure 4.

Figure 4 - Models for O_2 adsorption and reduction mechanism. Adapted from reference [23].

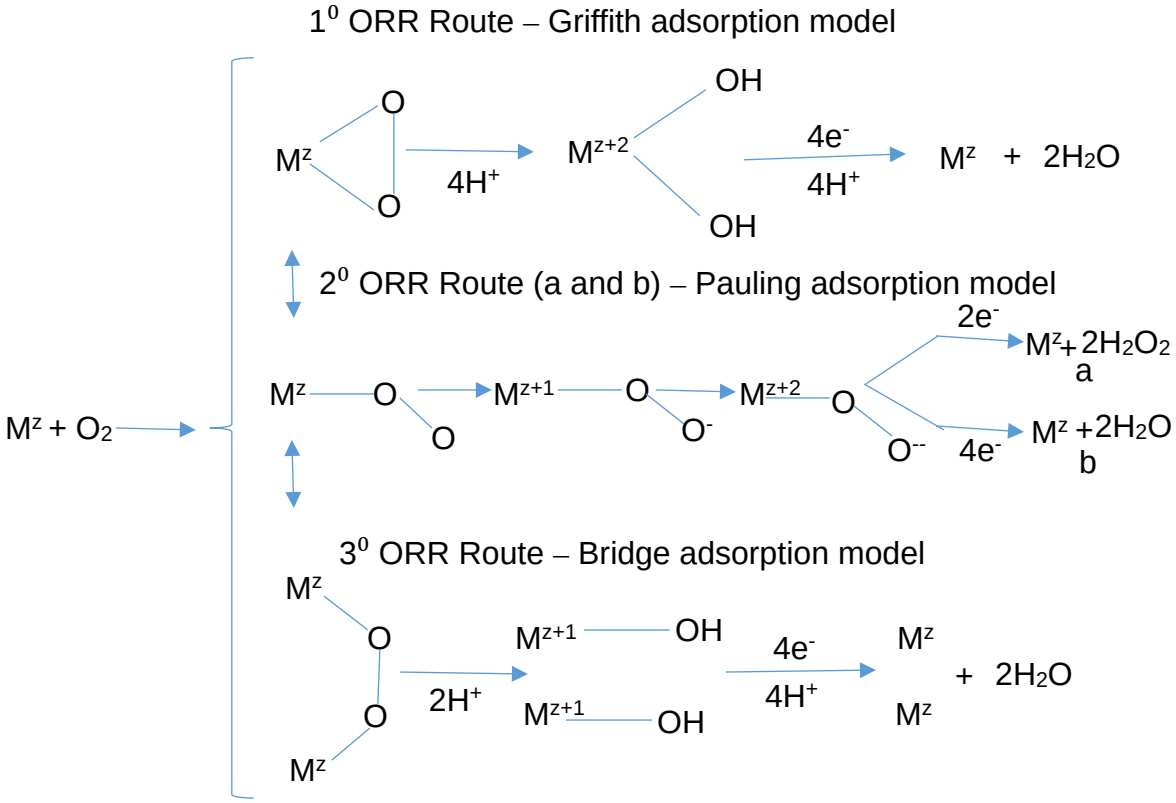

1.3. Catalysts for oxygen reduction

Generally, the 4-electron O_2 reduction is extremely non-reversible. In this regard, one of the challenges is to get experimental potentials closer to the thermodynamic reversible potential of this process at room temperature. For example, if Pt electrodes are utilized in acidic or basic media under ambient conditions, the deviation from thermodynamic electrode potential (1.23 V vs RHE) is quite large and the experimental potential value is hardly around 1 V. At room temperature, the exchange current density of ORR on Pt, which is the most active metal in acidic solutions, lays between 10^{-7} and 10^{-10} A cm^{-2} [21].

Therefore, to overcome the limitation imposed by the ORR slow kinetics it is necessary to increase the activity of the catalysts. So far, the approach to this problem consisting in alloying Pt with first-row transition metals has been relatively successful. Pt-based binary systems such as PtFe [24-30], PtCo [27, 30-32], PtNi [27,30,32], PtCu [27,33], etc., have shown enhanced catalytic activities. The additional advantage of this approach is the partial substitution of Pt by other less expensive metals. Most significant results were discussed in review articles [34-36].

Pt is still the most commonly used metal in carbon-supported catalyst materials for fuel cells reactions in acidic or alkaline media [37], but it is an expensive and rare metal. To overcome the drawbacks of high costs, the development of new and cheaper electrocatalysts is needed. Viable catalysts to substitute expensive Pt-based materials must have the ability of selectively catalyzing the four-electron reduction of oxygen to produce water at low overpotentials, with low H_2O_2 production. Another issue is the catalyst stability because good durability is needed for fuel cell technology commercialization.

1.3.1. Palladium and palladium-alloy catalysts

In the search for catalysts less expensive than Pt and Pt-based materials, new materials for ORR electrocatalysis have been suggested as an alternative to Pt, such as Pd and Pd-based alloys [38-40]. This is a promising approach because the cost of Pd is much lower than the cost of Pt [41] and it is more abundant in the earth crust. Besides that, Pd and Pt belong to same group of the periodic table and have several similar properties. Consequently, the catalytic

behavior of Pd should be expected to be close to that of Pt for some processes. However, several research works showed that in acidic solution the ORR catalytic activity of Pd is considerably lower than that of Pt [39,42]. Moreover, Pd catalysts have lower durability in acidic medium [43-45]. Despite the lower activity, in acidic environments Pd-based catalysis are alcohol tolerant and that is advantageous for PEMFCs fed with methanol and ethanol [40].

Several studies of the ORR were done for Pd-based catalyst in acidic solutions, such as PdNi [44-47], PdCo [47,48], PdAg [47] and PdCu [47,49], reporting activities for the ORR better than for Pd.

Generally, it is considered that Pd alloys with metals with smaller atomic size than Pd enhance the ORR catalytic performance [39]. Ni is one of the best options for alloying with Pd to improve the catalytic performance for the ORR. Literature results show improved catalytic activity for a PdNi thin film prepared by sputtering [50] compared with Pd, but lower than the activity of Pt. Another group synthesized a PdNi alloy through metallic reductive precipitation, but its catalytic performance was poorer than for the PdNi thin film alloy prepared by sputtering [51]. Data for carbon-supported PdNi, PdFe and PdCo [44] evidenced that the second metal increases the stability, but dissolution still occurs.

In acidic medium, Pd and Pd-based catalysts have low stability against Pd dissolution [43-45]. Pd is much more stable in OH^- solutions and, hence, great attention was given to catalysts for ORR in alkaline medium. Jiang et al. found that Pd/C showed higher activity than Pt/C for the ORR at room temperature and up to 60^{o}C [52]. In other studies, the ORR activity and stability of Pd nanocubes in alkaline medium was found to be similar or better than Pt [53]. Generally, Pd-based materials show better catalytic performance in alkaline solutions than in acidic [54].

Ni is one of the non-noble metals showing attractive performance as electrode material in combination with Pd. PdNi/C electrocatalysts are considered to be economically feasible, while they are also more efficient catalysts compared to Pd/C and Pt/C in alkaline solution [55]. Pd-based alloys with nonprecious metals also show enhanced activity and stability in alkaline medium [40,55-57]

Considering that Cu helps to improve the ORR catalytic performance of Pt and Pd have similar electronic shells, it is reasonable to expect that PdCu alloys might have enhanced catalytic performance. Theoretical calculations predicted

that PdCu in 50:50 atomic composition should show high catalytic activity for ORR [58] and literature results showed improved performances for PdCu materials [59-64].

Generally, comparison of published results for PdNi and PdCu materials is very difficult because materials properties and the experimental conditions of ORR measurements differ. Some results about the catalytic activities for ORR of PdCu and PdNi materials in acidic and alkaline solutions are summarized in Table 3 to illustrate the divergences among them. Results for ORR on Pd and Pd-based catalysts were discussed in review articles [20,39,54,65].

Table 3 – Summary of some results for PdCu and PdNi electrocatalysts reported in the literature.

Preparation method	Nominal composition	XRD size	EDX composition	Mass activity	Specific activity	Particle size (nm)	Medium	Ref.
Simple Galvanic Replacement	Mesoporous PdCu	–	Pd:Cu 85:15 EDS	–	0.6 mA/cm^2 Half wave 0.84 V	3	0.1 M $HClO_4$	[64]
Copper metal organic framework	PdCu 1 (2 wt.% Cu and 13.6 wt % Pd) PdCu 2 (0.25 wt.% Cu and 16.2 wt.% Pd)	0.3869 nm 0.3907 nm	–	Pt>PdCu in $HClO_4$ at half wave 0.85 V PdCu 1>Pd>PdCu 2 in NaOH	Pt>PdCu in $HClO_4$ Half wave PdCu1> Pd > PdCu2 in NaOH	4 ± 1.1 4 ± 1.5 4 ± 1.5	0.1 M $HClO_4$ 0.1 M NaOH	[66]
Dealloying	PdCu 50:50	–	–	0.15 A/mg $_{Pd}$	0.22 mA/cm^2 at 0.9 V	Around 7	0.1 M $HClO_4$	[61]
Co-impregnated, HT	PdCu 1:1 PdCu 1:3	∽0.388 nm ∽0.384 nm	49.1:50.9 24.8:75.2 ICP-AES 47.5:10.7	At 0.85 V, at 600 ºC 95 and 135 mA/mg $_{Pd}$	–	21 ± 5.1 23.3 ± 8.3	0.6 M $HClO_4$	[67]
Colloidal synthesis and HT	PdCu 1:1	–	–	23 mA/mg $_{Pd}$ at 0.9V and 500 ºC	33 µA/cm$^2_{Pd}$ at 0.9V and 500 ºC	10 ± 2.5 at 500 ºC	0.1 M $HClO_4$	[62]
Modified polyol method and HT	PdNi 80:20		83.7:16.3 83.4:16.6 at 500ºC	At 0.7 V and 500 ºC 100 mA/mg $_{Pd}$ at	At 500 ºC 4 mA/µc at 0.7 V	5.6-6.7	0.5 M H_2SO_4	[51]
Modified Galvanic Replacement	PdNi 1:1	0.3798 nm	–	∽600mA/g $_{Pd}$	∽1440 µA/m^2	30 and shell thickness 5	0.1 M KOH	[55]
Electrochemical dealloying in acidic solution	PdNi 20:80	0.3820 nm	91:9 dealloying EDS	1.1 mA/µg at 0.80 V 0.4 mA/µg at 0.85 V	–	~ 10 pore size	0.1 M $HClO_4$	[68]
One-step mild dealloying of PdNiAl precursor alloy	Nanoporous PdNi Alloy	–	75:25 EDS	0.18 A/mg at 0.9 V	0.21 mA/cm^2 $_{Pd}$ at 0.9V	~ 5	0.1 M $HClO_4$	[69]

Mass activity: current/mass; Specific Activity: current/area; HT: Heat Treatment

1.3.2. Stability challenges

Besides the required higher catalytic activities, the catalyst stability is also an important challenge for commercialization of the fuel cell system. For practical applications of fuel cells, lifetime is a very important factor. There are different lifetime required, which depend upon the application of the fuel cells. For example, The American Department of Energy proposed lifetime of 20,000 hours for buses, 3,000 to 5,000 hours for cars and 40,000 for stationary uses. It is noticed that the lifetime of fuel cell for stationary applications is higher than automotive use. The difference is basically due to the energetic working conditions and differences in the voltage due to on/off. The pre-commercial PEM fuel cell stack still does not fulfill these requirements. There are many factors that affect the lifetime of the PEMFC [70,71], which include degradation of the catalyst layer, the gas diffusion layer and the membrane.

So far, carbon-supported Pt or Pt-based catalysts have higher durability than other materials in the acidic environment of PEMFCs [37,72]. Nevertheless, their durability is still insufficient [72,73]. The factors that affect the durability of the catalyst layer are agglomeration, sintering, leaching and contamination by impurities [72,74,75,76]. Generally, literature reports show that nanoparticles supported on carbon have stability to some extent [34,77] The corrosion of carbon causes degradation of the catalyst layer and different carbon forms [78,79,80] and other alternatives as mixed carbon-oxide supports are investigated [26,81,82].

In last decade, many studies reported addition of non-precious elements to Pd electrocatalysts that lead to ORR performance analogous to that of Pt. However, in acidic media those materials do not have the stability needed for practical application. That is another reason for the interest in AEMFCs, because non-precious metals and alloys shows much higher stability in alkaline solution than in acidic medium [11,40,83,84].

2. OBJECTIVE

To study systematically the activity of carbon-supported PdNi and PdCu catalysts of different compositions for the oxygen reduction reaction of nanostructured catalysts in acidic and alkaline solutions, and to correlate their performances with chemical and electronic properties, aiming to contribute to the development of efficient Pt-free catalysts.

In this regard, some specific objectives are:

✓ To optimize a synthesis methodology to prepare carbon-supported PdCu and PdNi nanoparticles with different compositions,

✓ To characterize the structural and electronic properties,

✓ To evaluate activity for oxygen reduction reaction and the percentage of hydrogen peroxide formed in acidic and alkaline solutions,

✓ To check the stability of the prepared materials in acidic and basic media.

✓ To correlate the catalytic activities with the catalysts properties.

3. MATERIALS AND METHODS

3.1. Synthesis of electrocatalysts

For the preparation of the electrocatalysts, PdNi and PdCu nanoparticles were obtained in colloidal state using the modified polyol method [85] and subsequently supported on carbon powder (Vulcan XC-72). The polyol method is a colloidal method, which was developed by Fievet et al. [86] for preparing Ni nanoparticles from the reduction of a Ni-precursor by a polyalcohol (ethylene glycol or diethylene glycol). In this method, the alcohol works as reducing agent as well as solvent. The modified polyol process was first proposed for the synthesis of FePt magnetic particles in dioctylether using a long-chain alcohol as reducer (1, 2 hexadecanediol) [85]. This method produces nanoparticles smaller than those obtained in a glycol and it was used in several works in our group [28,31,44,87,88] introducing minor modifications.

In this work, PdNi and PdCu nanoparticles with different atomic compositions (Pd:M with M = Ni or Cu, 90:10, 80:20, 70:30, 60:40 and 50:50) were prepared in dioctylether. The metal precursors (Pd (II) acetylacetonate, Ni (II) acetylacetonate and Cu (II) acetylacetonate, Aldrich) and the reducer 1, 2 hexadecanediol were dissolved in dioctylether and the solution was heated up to 110 ^{o}C under argon atmosphere. Then, to prevent excessive growth and agglomeration, oleic acidic and oleylamine were added to the mixture, which was further heated until reflux (298 ^{o}C) and kept at this temperature until the formation of the nanoparticles (i.e. black dispersion). At that point, the heat source was turned off and the reaction mixture was let to cool to room temperature. The nanoparticles were separated and cleaned (flocculation by addition of ethanol, centrifugation, and re-dispersion in hexane, repeated until clean solution as described in ref. [31]). Finally, the nanoparticles were supported on carbon powder by constant stirring in medium of hexane for 12 hours. The resulting material was filtered using a PVDF membrane of 0.22 μm (Millipore) pore size and thoroughly washed with ethanol, acetone, and ultra-pure water. After the washing steps, the catalysts were dried in furnace at 80 ^{o}C for 2 hours. All catalysts were prepared with 20 wt.% metal loading on carbon. The same procedure was employed for the preparation of a Pd/C sample that was used as reference material.

3.2. X-ray diffraction (XRD) measurements

The X-ray diffractograms were obtained on a Rigaku equipment, model D Max 2500PC, in the range of 20 to 100 degrees in 2θ, with scan rate of 1^{o} min^{-1} and Cu Kα incident radiation (wavelength of 1.5406 Å). XRD data were used to estimate the crystallite average size and the lattice constant.

3.3. X-ray absorption spectroscopy (XAS)

When X-rays strike a sample, radiation can either be scattered or absorbed by the electrons. When the absorption process occurs, electrons are then raised to higher levels of energy. At certain energy of the incident X-ray, there is a sharp rise in absorption, which is named absorption edge. The edge energies correspond to the binding energies of the electrons in the K, L, M, etc., shells of the absorbing element. The absorption edges are labeled in the order of increasing energy, K, LI, LII, LIII, MI, and so on. Both K and L levels can be used in the hard X-ray range (5 to 35 keV) and in the tender-soft X-ray range (0.9 to 5.5 keV), thus allowing most elements to be investigated by XAS. The excited state of the atom with one of the core levels left empty and a photoelectron will ultimately decay soon after absorption. A higher energy core level electron occupies the deeper hole created by the emission of electron after absorption of X-rays. In this process, X-ray of well-defined energy is emitted and is characteristic of the atom and can be used to identify and quantify the atoms in a system. An X-ray absorption spectrum is generally divided into two distinct portions: X-ray absorption near edge structure (XANES) usually within 30 eV of the absorption edge and the extended X-ray absorption fine structure (EXAFS), in the region between 50 and 1,000 eV above the absorption edge [89]. In the XANES region transitions of core electrons to bound levels take place, due to which a sudden increase of absorption is observed, whereas in the EXAFS region the ejected photoelectrons experience multiple scattering from the electrons of neighboring atoms.

In this work, the electronic properties of PdNi/C, PdCu/C and Pd/C catalysts were analyzed by X-ray absorption spectroscopy (XAS) in the Tender X-ray energy region. All measurements were carried out at the SXS beam line of the

Brazilian Synchrotron Light Laboratory (LNLS) around the Pd L3 absorption edge (3,173 keV; $2p_{3/2} \rightarrow 4d$ transitions). The catalyst was placed on a carbon tape (double-sided) adhered on a sample holder and spectra were collected with samples inside a high-vacuum chamber. Energy calibration was made with a Mo foil. Spectra were obtained in TEY (total electron yield) mode. Energy resolution was 2.2 eV. For each sample, spectra were collected in three distinct regions of the sample, in order to ensure data reproducibility.

3.4. Electrochemical measurements

3.4.1. Electrode preparation

An ultra-thin layer of catalyst deposited on a glassy carbon disk (0.247 cm^2 geometric area) was employed as working electrode in the electrochemical measurements [90]. For that, the proper amount of catalyst powder was suspended in 1 mL of isopropanol containing 15 µL of Nafion solution (Aldrich) under continuous ultrasonic stirring for 15 minutes. The complete suspension of the catalyst powder resulted in a black ink, which was then applied on the glassy carbon electrode. An adequate volume of suspension was applied with the aid of a micro-syringe so to have a layer with a total load of 30 µg cm^{-2} of metals. After the formation of the catalyst ultra-thin layer over the electrode surface, it was hydrated by ultra-pure water. All electrochemical experiments were conducted at room temperature (24-25 ^oC).

3.4.2. Cyclic voltammetry and ORR activity measurements

The electrochemical measurements were made in a conventional three-electrode electrochemical cell. The working electrode was the ultra-thin layer of catalyst deposited on the disk of a ring-disk electrode purchased from Pine Instrument Company (glassy carbon disk and Pt ring). Only the disk was connected for cyclic voltammetry (CV) and accelerated stability tests. The ORR was studied using the rotating ring-disk electrode (RRDE) technique. A platinum wire was used as auxiliary electrode and a reversible hydrogen electrode (RHE) as reference electrode, in acidic and alkaline media.

The general electrochemical behavior of PdNi/C, PdCu/C and Pd/C catalysts was examined by CV. For all materials, CV curves were recorded in Ar-saturated acidic (0.5 M H_2SO_4) and basic (0.1 M NaOH) solutions. The CV studies were carried out in the potential range of 0.05 V to 1.0 V (vs. RHE), with scan rate of 0.05 V s^{-1} for both media.

The evaluation of catalytic activity for the ORR was performed by measuring polarization curves at a sweep rate of 0.005 V s^{-1} in O_2-saturated acidic and alkaline solutions. The polarization curves were taken in potential range of 0.1 V to 1.0 V. The RRDE used for these measurements has a glassy carbon disk (0.247 cm^2 geometric area) surrounded by a Pt ring (0.186 cm^2 geometric area) vs. RHE. The ORR was evaluated from the current generated by the reaction on the disk while the amount of H_2O_2 formed was monitored by means of the oxidation current on the ring. In alkaline solutions, the RRDE was operated at different rotation speeds (1225, 1600, 2025, 2500 rpm) while in acidic solution the polarization curves were recorded only at rotation rate of 2500 rpm.

3.4.3. Determination of the Pd electrochemical surface area

The electrochemical active surface area (ECSA) of Pd was evaluated from the charge of PdO reduction. For that, cyclic voltammetry curves taken in 0.5 M H_2SO_4 solution saturated with Ar were measured between 0.050V and different upper potential limits (up to 1.65 V). The upper limit was increased in intervals of 0.050 V and 0.025 V. These experiments were done with scan rate of 0.05 V s^{-1}. A fresh catalyst layer was used for each different potential limit.

The charges were calculated from integration of the reduction peaks of PdO for each experiment done with different potential limit. After integration of the reduction peaks from the CV curves, the charges were plotted against the upper potential limit to estimate the potential where a PdO layer is completed [32]. For the ECSA calculation a reduction charge density of 424 $\mu C\ cm^{-2}$ for the reduction of a PdO monolayer was used [32].

3.4.4. Stability tests

Long-term accelerated stability tests were carried out by continuously cycling the potential (150 cycles) between 0.05 V and 1.0 V (vs. RHE) at a scan rate of 0.05 V s^{-1} in Ar-saturated 0.5 M H_2SO_4 solution. In alkaline solution (0.1 M NaOH), the catalysts were submitted to 1,000 cycles done in same potential range and with the same sweep rate than for acidic solution.

4. RESULTS AND DISCUSSION

4.1. PdNi/C catalyst

4.1.1. X-ray diffraction analysis

The structural properties of the PdNi/C and Pd/C catalysts were evaluated from X-ray diffraction (XRD) measurements. The diffraction patterns obtained are shown in Figure 5. At 2θ around 25 degrees there is a diffraction peak that corresponds to the (002) planes of the carbon support. The other peaks correspond to the signals typical of the face centered cubic (fcc) Pd structure (PDF 87-643).

Figure 5 - (a) X-ray diffraction data for PdNi/C and Pd/C catalysts. (b) Enlarged region of diffraction of (220) planes (~ 66.5º) showing the shift in peak position for PdNi/C catalysts. Catalysts are indicated in the figure.

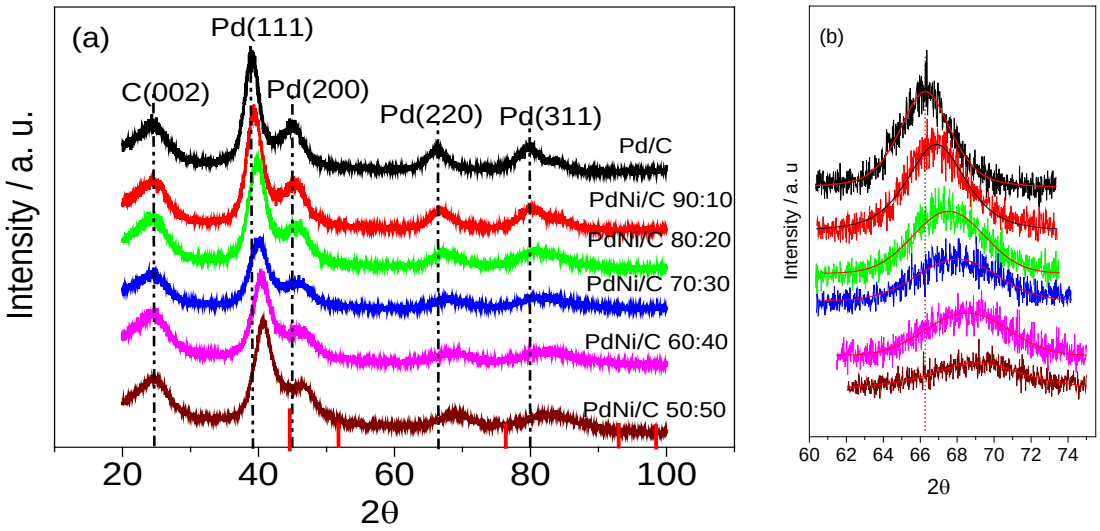

In general, the main peaks for PdNi/C samples lie between the signals of Pd/C and those of pure Ni (PDF #04-0850). The 2θ values for the diffraction signals of pure Ni are indicated with red lines at the bottom of Figure 5(a). This shift in peak position is usually taken as proof of alloy formation that causes a lattice constant contraction. The shift in 2θ towards higher values is more significant in the case of the PdNi/C 50:50 material, most likely because of a

higher incorporation of the second metal, which leads to a smaller lattice spacing, as compared to the other PdNi/C materials and to the Pd/C reference sample. The addition of Ni produced also a decrease in crystallite size, evidenced by the increase in the width of the peaks.

The average crystallite sizes were calculated using Scherrer´s equation [91]:

$$D = \frac{0.9\lambda}{\omega \cos\theta} \qquad (12)$$

where λ is the wavelength of the incident radiation, ω is the peak width at half intensity and θ is the position of the maximum intensity. The factor 0.9 appears as result of considering that the particles are spherical [91]. For all calculations, the (220) peak of the Pd fcc structure was used due to the fact that the broad carbon peak does not affect this region.

The apparent lattice parameter (a_{exp}) at (220) diffraction and the corresponding Pd-Pd distance (d_{fcc}) were calculated as:

$$a_{exp} = \frac{\sqrt{2}\lambda}{sen\theta} \qquad (13)$$

$$d_{fcc} = \frac{\sqrt{2}}{2} a_{exp} \qquad (14)$$

The results obtained for PdNi/C and Pd/C catalysts from the XRD study are summarized in Table 4. The decrease in lattice constant with increasing atomic percentage of Ni indicates that solid solutions are formed between Pd and Ni.

Overall, the lattice parameter values estimated from XRD results for Pd/C and PdNi/C show that Ni was incorporated to some degree into the Pd lattice. The change in the lattice parameter also justifies the decrease in Pd-Pd interatomic distances for all PdNi/C catalysts.

Table 4 – Structural characteristics of Pd/C and PdNi/C nanocatalysts derived from XRD data.

Catalyst	Crystallite size (nm)	Lattice constant (Å)	Pd-Pd distance (Å)
Pd/C	2.9	3.988	2.820
PdNi/C 90:10	2.5	3.956	2.797
PdNi/C 80:20	2.1	3.921	2.773
PdNi//C 70:30	1.9	3.898	2.756
PdNi/C 60:40	1.8	3.871	2.737
PdNi/C 50:50	1.6	3.845	2.719

The lattice parameter changes with composition as illustrated in Figure 6.

Figure 6 - Variation of the lattice parameters with atomic percentage of Ni.

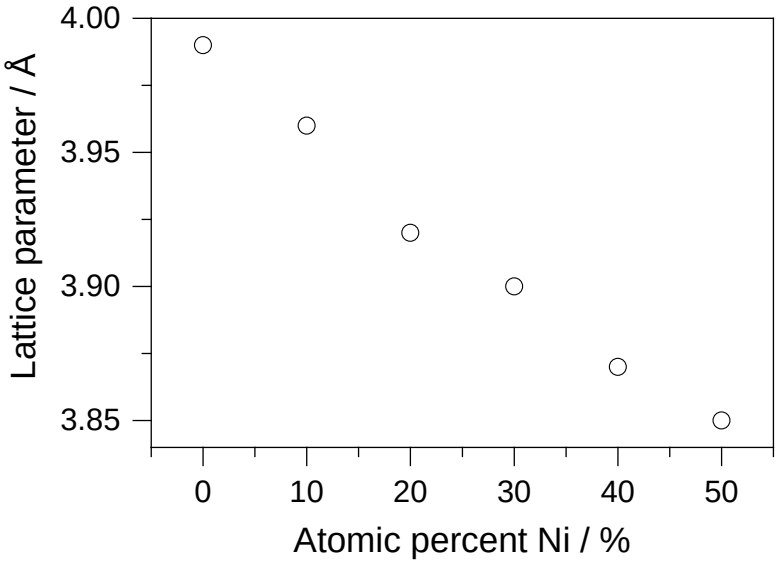

The calculated lattice parameter for Pd/C (3.988 Å) is larger than the literature value for Pd metal (3.890 Å) and the calculated values for PdNi/C samples are larger than for solid solutions [92], as shown in Figure 7.

Figure 7 - Lattice parameters against Ni molar fraction obtained for PdNi/C samples and reported for solid solutions in ref. [92].

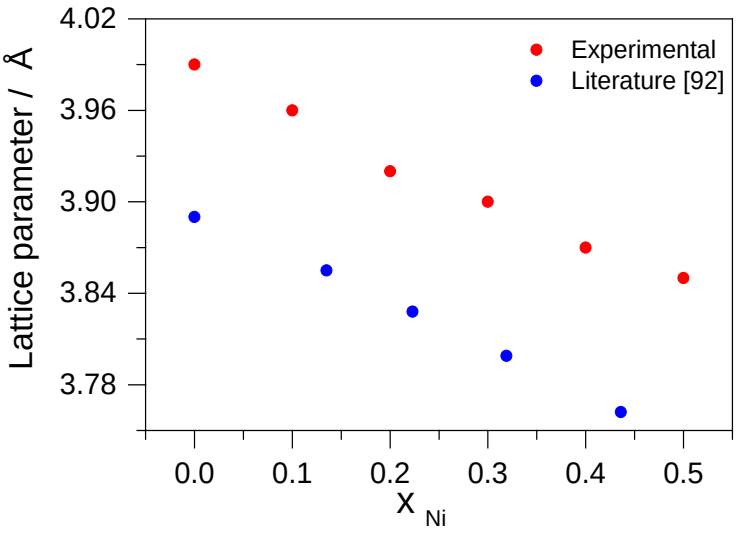

The larger values obtained indicate uniform strain for Pd/C and for PdNi/C samples [91]. Moreover, the points in Figure 7 lay on almost parallel lines meaning that uniform strain of Pd/C and PdNi/C samples is similar.

The alloy compositions were calculated using Vegard's law, neglecting the uniform strain:

$$x_M = \frac{a - a_0}{a_M - a_0} \qquad (15)$$

where a represents the experimental value of lattice parameter for the PdNi/C electrocatalysts, a_M is the lattice parameter for a PdNi solid phase and a_0 the lattice parameter of Pd/C. The calculated values are shown in Table 5.

Table 5 – Calculated Pd:Ni ratios for PdNi alloys derived from XRD data.

Catalyst	Calculated Pd:Ni ratio	Nominal
PdNi/C 90:10	91:09	90:10
PdNi/C 80:20	79:21	80:20
PdNi//C 70:30	73:27	70:30
PdNi/C 60:40	63:37	60:40
PdNi/C 50:50	57:43	50:50

4.1.2. X-ray absorption spectroscopy (XAS) results

The XAS technique allows a quantitative analysis of the electron occupancy of the Pd 4d band. This is important in the current research work because the adsorption of oxygen happens through the interaction with the outermost electrons of Pd, which are those in 4d band. Therefore, the occupancy of these orbitals could affect the strength of adsorption on the surface.

Generally, such studies can be carried out for Pt, Au and other metals using in situ conditions that simulate the real environment at which the catalytic reaction happens. However, the energy of absorption at the Pd L3 edge (3.173 keV) is lower than the minimum energy value that can be used in the beamlines where in situ experiments can be performed. Therefore, the XAS experiments were carried out under conditions of high vacuum. It is also important to emphasize that measurements were done in triplicate for a better statistical representation.

Each sample of prepared catalysts was introduced into the analysis chamber fixed to a conducting carbon tape. In this way, the mass of material could not be controlled and the raw XAS spectra involve different energy differences between the pre and post-edge regions. Then, data normalization was done with the XAS data processing Athena software [93]. The normalized XAS spectra for PdNi/C materials and Pd/C are presented in Figure 8.

It is seen that the intensity of the absorption peak is lower for PdNi/C than for Pd/C and the decrease follows the Ni percentage, which indicates that Ni addition leads to an increase in electronic occupation of Pd 4d band.

Figure 8 - Normalized X-ray absorption spectra measured around the Pd L3 edge for Pd/C and PdNi/C catalysts. Inset: absorption peak region enlarged.

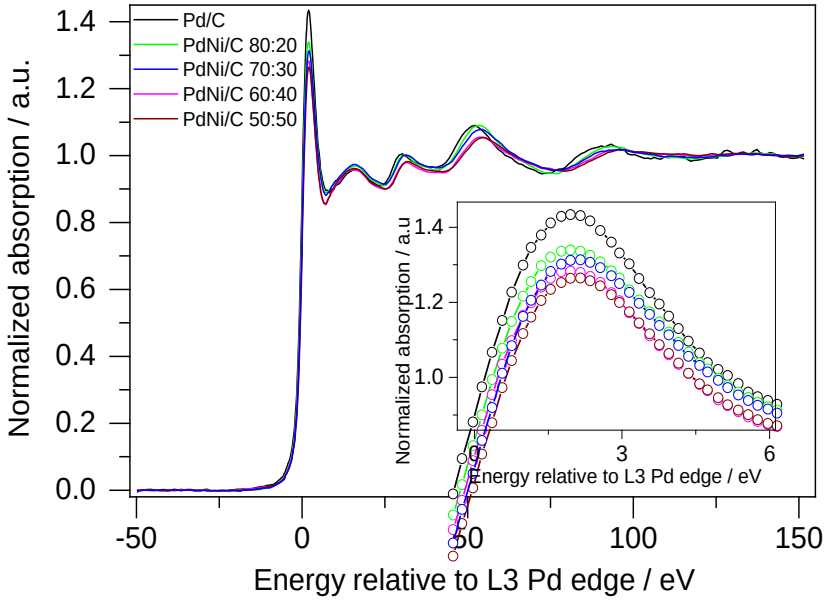

A better comparison requires separation of the transitions to unbound states from those to bound states. This was done using the method proposed by Shukla et al. [25] that consists in adjusting to the spectrum a theoretical arc tangent curve combined with a Lorentzian curve, which integral is proportional to the band vacancy. The results are presented in Figure 9. Clearly, the vacancy of the 4d band of Pd decreases with increasing percentage of Ni.

Figure 9 - Integral values of the Lorentzian curves adjusted to spectra against percentage of Ni.

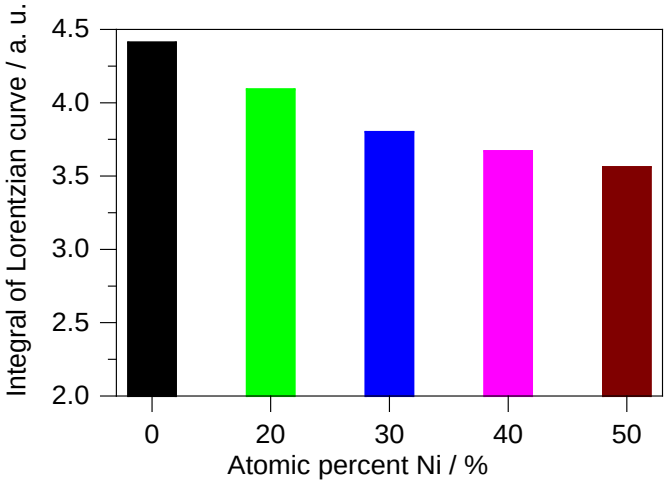

4.1.3. Electrochemical characterization in acidic medium

CV curves registered in Ar-saturated 0.5 M H_2SO_4 for Pd/C and PdNi/C catalysts with different compositions are shown in Figure 10.

Figure 10 – Cyclic voltammetry curves (5th cycles) of the Pd/C and PdNi/C catalysts in 0.5 M H_2SO_4 saturated with Ar. Sweep rate: 0.05 V s^{-1}.

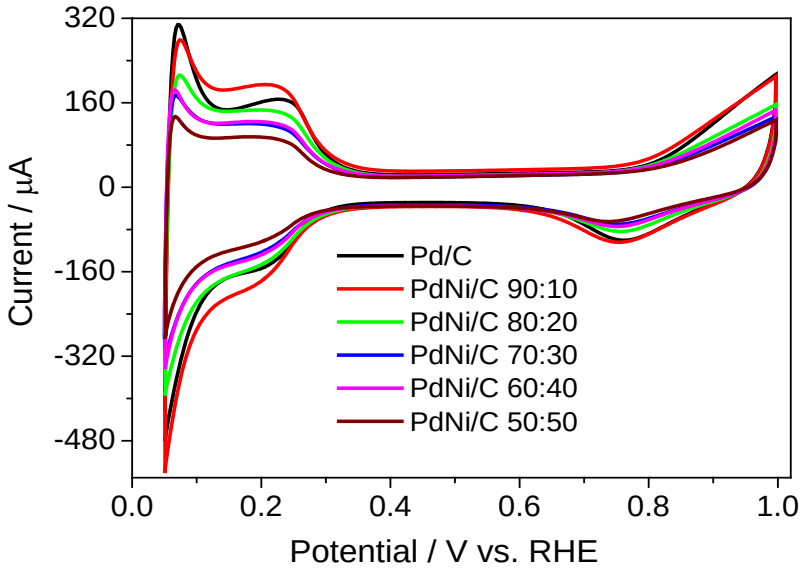

All voltammograms for PdNi/C have shapes similar to that of Pd/C and similar shapes to those reported in the literature for Pd/C and Pd-M/C catalysts [44]. Prior to 0.4 V, the current peaks are related to hydrogen adsorption/desorption phenomena, which occur in the potential range of 0.05 V to 0.3 V. The reduction of Pd oxides formed in the positive scan appears as a cathodic current peak observed around 0.80 V. As seen in Figure 10, the curves clearly have different charges related to these processes, which means that the Pd surface area varies. Pd/C seems to have the highest area, while PdNi/C 50:50 has the lowest one. The fact that carbon-supported PdNi catalysts have a lower Pd area is quite apparent in the hydrogen adsorption/desorption charge. In general, this can be taken as confirmation of the presence of Ni on the surface of the nanoparticles.

4.1.4. Determination of Pd electrochemically active surface area

The electrochemical surface area (ECSA) is an important factor for calculation of kinetic parameters for an electrocatalyst. Therefore, different methods were proposed in the literature for its determination. For instance, a well-known method applicable to ECSA determination of Pt and Pt/C is the H_2 adsorption/desorption charge method. However, the same method is not valid to evaluate the ECSA for Pd because hydrogen adsorption and absorption occur on Pd electrocatalyst, although some authors use it [60]. Therefore, calculation of the ECSA from hydrogen adsorption/desorption charges was considered not accurate way to determine the ECSA for Pd/C and PdNi/C electrocatalysts. Therefore, in the present work the surface oxide reduction method was chosen for estimation of the ECSA that was calculated as:

$$\mathrm{ECSA}_{(\mathrm{Pd})} = \frac{\mathrm{Q}_{\mathrm{PdO}} / \mu\mathrm{C}}{420\ \mu\mathrm{C\ cm}^{-2}} \qquad (16)$$

where Q_{PdO} is the charge measured from a CV recorded up to the potential limit corresponding to the formation of a monolayer of oxide. That potential was estimated from the change in slope of plots of PdO reduction charge vs. potential limit [27,32]. The literature value of charge for a PdO monolayer on 1 cm^2 area is 424 μC [32].

Sets of CVs for Pd/C and PdNi/C materials recorded in 0.5 M H_2SO_4 with different upper potential limit between 1.0 V and 1.65 V (vs. RHE) are shown in Figure 11. The potential window for these experiments was selected according to the literature [27,94].

Figure 11 - CV curves measured for different upper potential limits and the corresponding plots of charges vs. potential limit. Catalyst indicated in the figure. Ar-purged 0.5 M H_2SO_4 solution. Sweep rate 0.05 V s^{-1}.

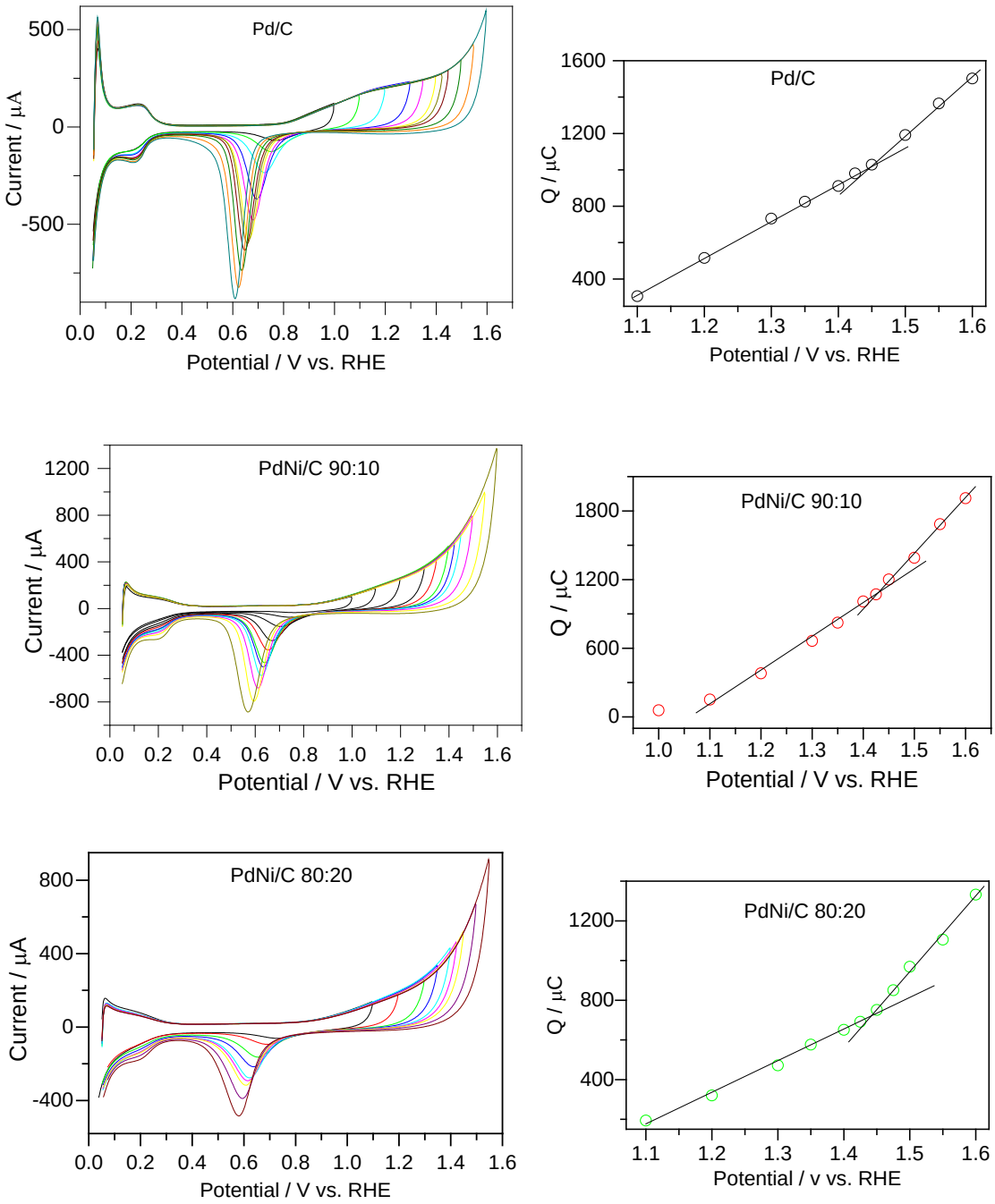

Figure 11 - (Continuation).

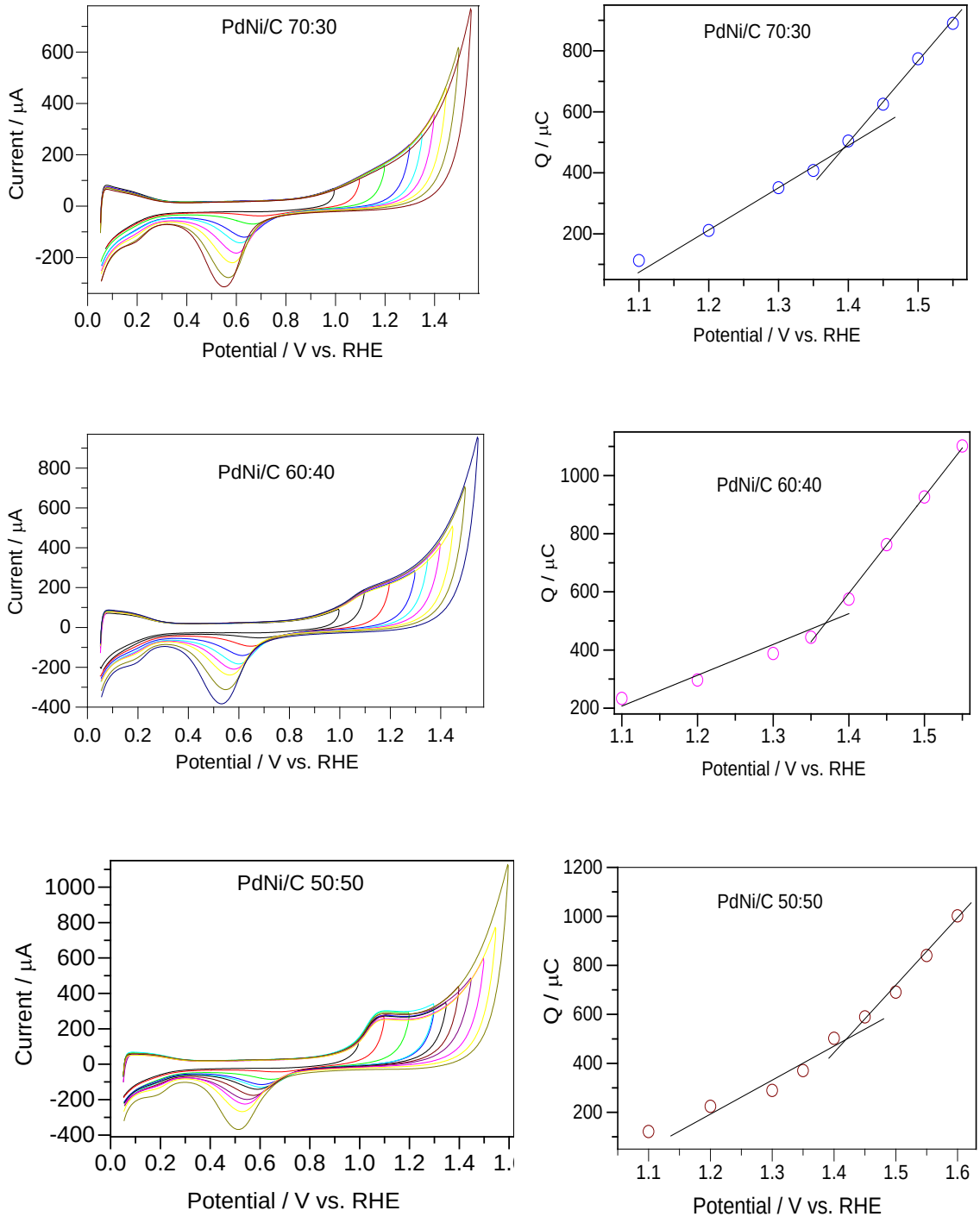

For most materials, the potential of PdO monolayer formation was about 1.45 V in good agreement with literature [27]. Lower values were obtained for PdNi/C 70:30, PdNi/C 60:40 and PdNi/C 50:50 compared to the Pd/C and other PdNi/C samples. This may be due to some degree of interference of the second

metal, *i.e.,* Ni. The calculated Pd ECSA values Pd/C and PdNi/C are displayed in Table 6 and show that the ECSA decreases as the percentage of Ni increases.

Table 6 – ECSA of Pd calculated from PdO reduction charges.

Catalyst	ECSA of Pd (cm^2)
Pd/C	3.4
PdNi/C 90:10	2.4
PdNi/C 80:20	1.9
PdNi/C 70:30	1.4
PdNi/C 60:40	1.4
PdNi/C 50:50	1.0

4.1.4. Oxygen reduction in acidic medium

In general practice, the kinetic parameters of ORR can be calculated by using a rotating ring disk electrode (RRDE) [95]. This technique allows a controlled transport of the oxygen molecules from the interior of the electrolyte medium to the surface of the electrode while monitoring the current due to the reduction of oxygen as a function of potential. The H_2O_2 formation can be monitored by its oxidation at the ring electrode.

Figure 12 shows a set of results for ORR studies carried out for Pd/C and PdNi/C catalysts obtained in O_2-saturated 0.5 M H_2SO_4 aqueous electrolyte. The current at the disk (ORR) and the ring (H_2O_2 oxidation) are those for polarization curves measured at 2500 rpm.

By analyzing Figure 12 (b), it is concluded that in acidic medium the current is controlled by mass transport from 0.1 V to 0.2 V. This current is called limiting current (iL), and results from the high reaction rate at high overpotentials, which makes the O_2 concentration at the electrode surface equal to zero.

Figure 12 - (a) ORR Polarization curves for PdNi/C and Pd/C catalysts measured in 0.5 M H_2SO_4 solution saturated with O_2 (b) H_2O_2 oxidation currents at the ring. Inset: Percentage of H_2O_2 formed at disk potential of 0.6 V vs. atomic percent of Ni. Rotation rate: 2500 rpm. Sweep rate: 0.005 V s^{-1}.

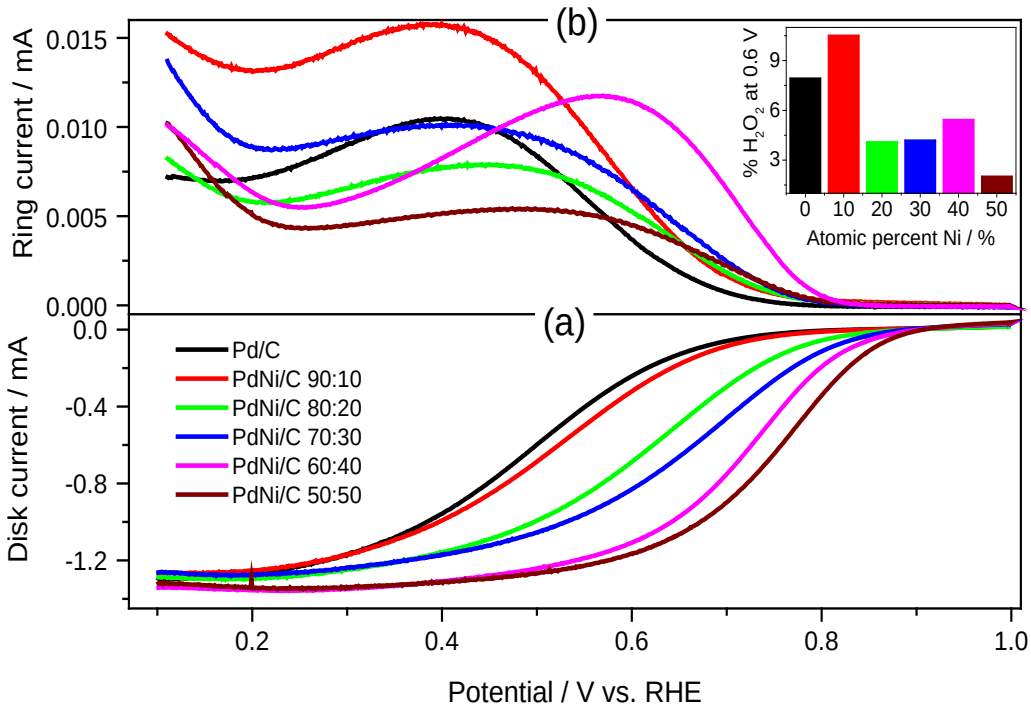

The limiting current is given by the Levich equation [95]:

$$iL = 0.62nFAD^{2/3}\nu^{-1/6}\omega^{1/2}C^{0}_{O2} \qquad (17)$$

where n is the number of electrons, F is the Faraday constant (96485 C mol^{-1}), D is the diffusion coefficient of O_2, A is the electrode area, ν is kinematic viscosity of the solution (0.01 cm^2 s^{-1}), ω is the rotation rate and C^0_{O2} is the bulk concentration of O_2. Values for D and C^0_{O2} were taken from literature [50].

At very low overpotentials, the current is controlled by the reaction kinetics (ik), which depends on the activity of the catalyst and reflects the kinetics of the ORR. In the intermediate potential region both, kinetics and mass transport, determine the measured current (i).

The ORR polarization curves for Pd/C and PdNi/C catalysts suggest that the electrochemical reaction is under kinetic and mixed activation-diffusion control in almost the entire potential range of measurements.

As said above, the rotating ring disk electrode technique allowed assessment of the amount of H_2O_2 formed during the ORR. The amount of H_2O_2 compared to the amount of O_2 reduced allows determining if the ORR proceeds by two-electron or by four-electron routes. A high rotation rate (2500 rpm) causes an increase in current due to enhanced oxygen transport. Considering the small amounts of H_2O_2 detected (Figure 12 (a) and inset), the ORR pathway seems to be mostly a four-electron transfer reaction to water [23].

The percentage of H_2O_2 can be calculated as:

$$\%H_2O_2 = 100\left(2\frac{ir/N}{id + ir/N}\right) \quad (18)$$

where i_r is the current measured on the ring, i_d is the current measured on the disk and N is the collection efficiency of the disk-ring electrode, which depends on the dimensions of the gap between the disk and the ring. As shown in the inset of Figure 12 (a), the production of H_2O_2 is in most cases lower for PdNi/C catalysts, indicating that the addition of Ni favors the ORR via 4 electrons.

The measured current (i) depends on the limiting (iL) and kinetic (ik) currents, which are related by the Koutecky- Levich equation:

$$\frac{1}{i} = \frac{1}{i_K} + \frac{1}{i_L} \quad (19)$$

For all materials, the kinetic currents were calculated at 0.80 V by using Koutecky- Levich equation.

The catalytic activities for Pd/C and PdNi/C for ORR can be analyzed as specific activity and mass activity. The specific activity is given by the kinetic current divided by the surface area of Pd (ECSA), *i.e.,* it is a current density, and the mass activity by normalization with respect to Pd mass:

$$As = \frac{ik}{ESCA_{Pd}} \quad (20)$$

$$Am = \frac{ik}{W} \quad (21)$$

where W is the loading of Pd (in this work the total Pd + Ni was kept at 30 $\mu g/cm^2$). This kind of normalization emphasizes how economically interesting the catalysts

are. In fuel cells, the performance of the catalyst is also analyzed on the costs, in terms of kW/$.

The ik value at 0.9 V is usually chosen for Pt catalysts to avoid inclusion of any concentration polarization, but the overpotential of the ORR on Pd is larger than for Pt. Thus, we made calculation for 0.80 V. Figure 13 shows the mass activity and specific activity against the percentage of Ni.

Figure 13 - Mass activity (a) and specific activity (b) for ORR in 0.5 M H_2SO_4 solution against atomic percentage of Ni.

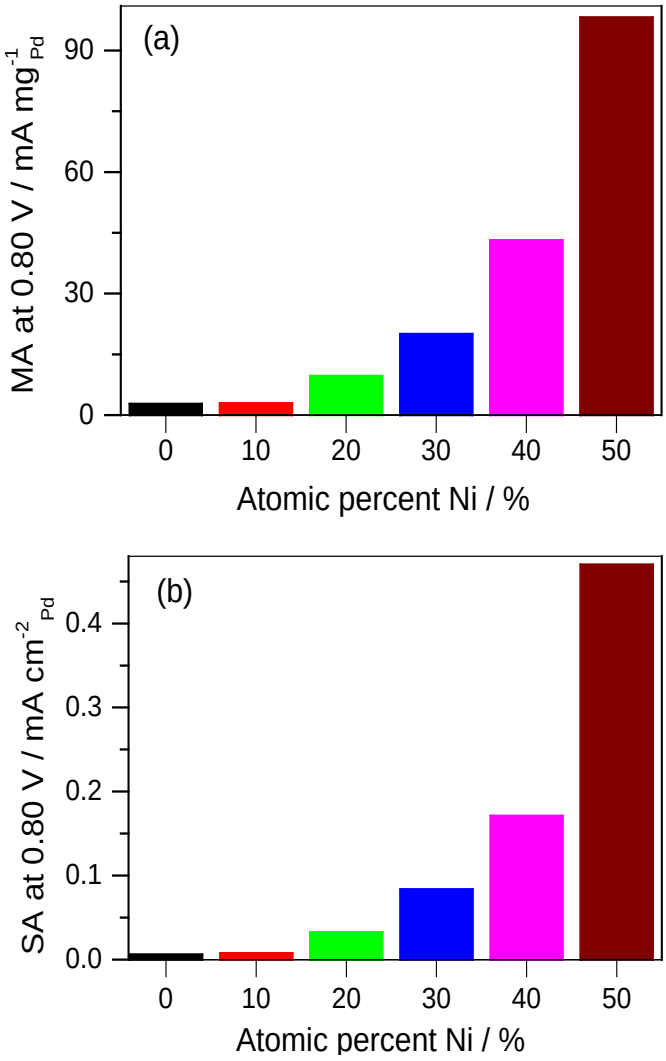

This analysis showed that the mass activity of pure Pd/C is lower than for all PdNi/C catalysts, and that specific and mass activity increases as the percentage of Ni increases.

The higher activities of PdNi/C samples might be due to some electronic effect due to the presence of Ni or to changes in the Pd-Pd distance. Figure 14 (a) shows that current density of ORR at 0.8 V increases as the addition of Ni leads to increasing occupancy of Pd 4d band. Figure 14 (b) shows that there is also a correlation with the Pd-Pd distance.

Figure 14 - Specific activity for ORR at 0.8 V in acidic solution of Pd/C and PdNi/C of different compositions. (a) Against the integral of Lorentzian curve adjusted to XAS spectra. (b) Against the XRD-derived Pd-Pd distance.

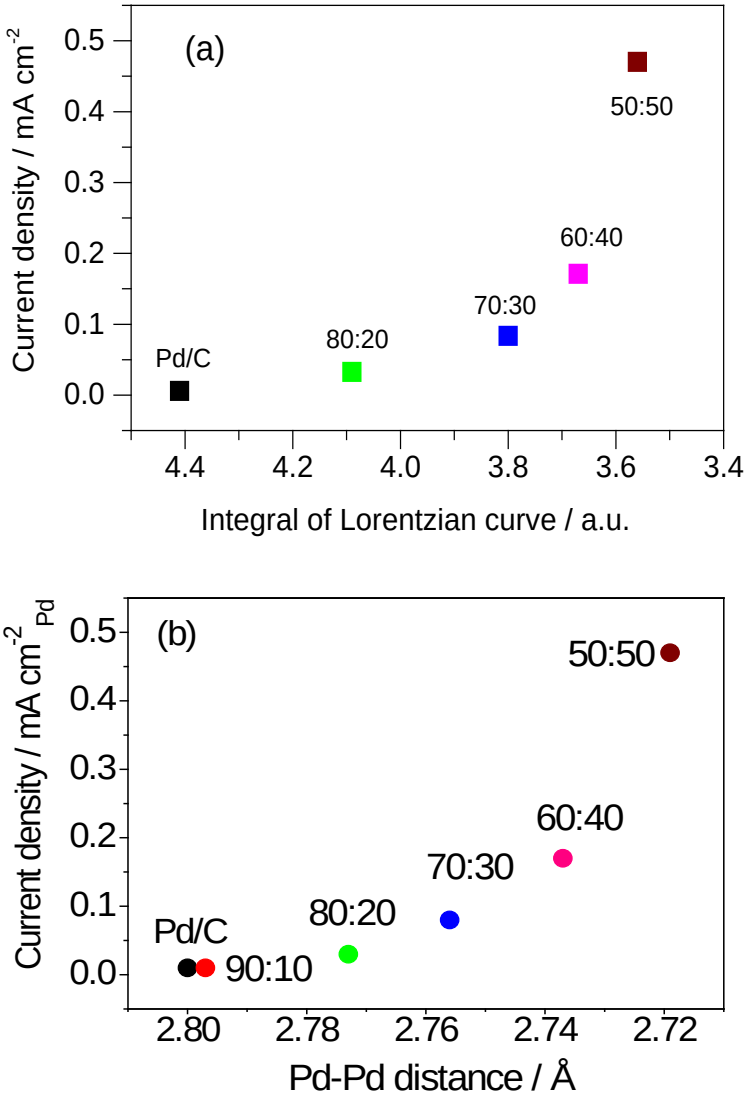

In general, the trends observed lead to conclude that in acidic solution it is not possible to attribute the enhancement of ORR activity by Ni only to electronic

effects or to the distance between Pd atoms. It is likely that both effects play a role.

The plots of potential against log ik (mass-transport corrected Tafel plots) for the ORR on Pd/C and PdNi/C electrocatalysts are given in Figure 15. Two regions having different slopes are clearly identified (60 mV/dec and 120 mV/dec). These calculated Tafel slopes are in agreement with literature values [23].

Figure 15 - Mass-transport corrected Tafel plots of ORR on the Pd/C and PdNi/C samples. Lines with slopes of -60 mV/dec and -120 mV/dec are shown.

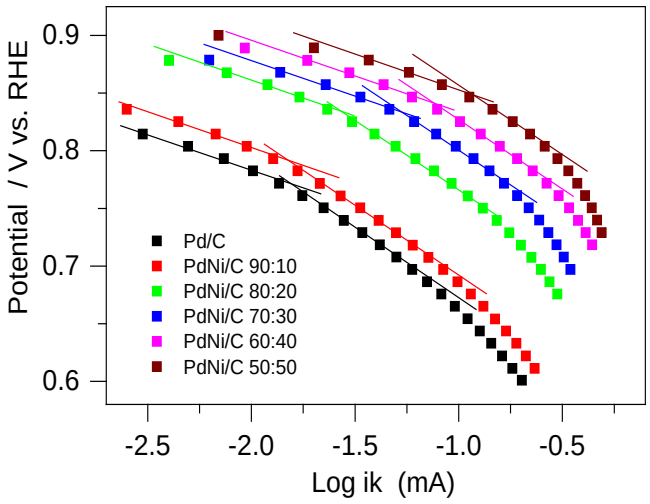

The Tafel slope is a parameter that shows how rapidly the overpotential rises for a ten-fold increase of the reaction current. The change from -60 mV/dec at low current densities to the -120 mV/dec value observed at higher overpotentials is well known for Pt and Pd electrodes and for nanoparticles [96]. The change is due to the variation of oxygen coverage of the surface. In the low overpotential region the adsorption of oxygen follows a Temkin isotherm and at higher overpotentials the coverage decreases and adsorption follows a Langmuir isotherm [23].

4.1.5. Accelerated stability tests in acidic medium

For accelerated stability tests, Pd/C and PdNi/C catalysts were continuously cycled (5-150) from 0.050 V to 1.0 V and the changes in charge were evaluated.

The voltammetry curves obtained for Pd/C and PdNi/C samples of all compositions are depicted in Figure 16.

Figure 16 - Cyclic voltammetry curves taken for stability tests for Pd/C and PdNi/C catalyst in 0.5 M H_2SO_4 solution from 0.050 to 1.0 V vs RHE. Sweep rate 0.050 V s^{-1}.

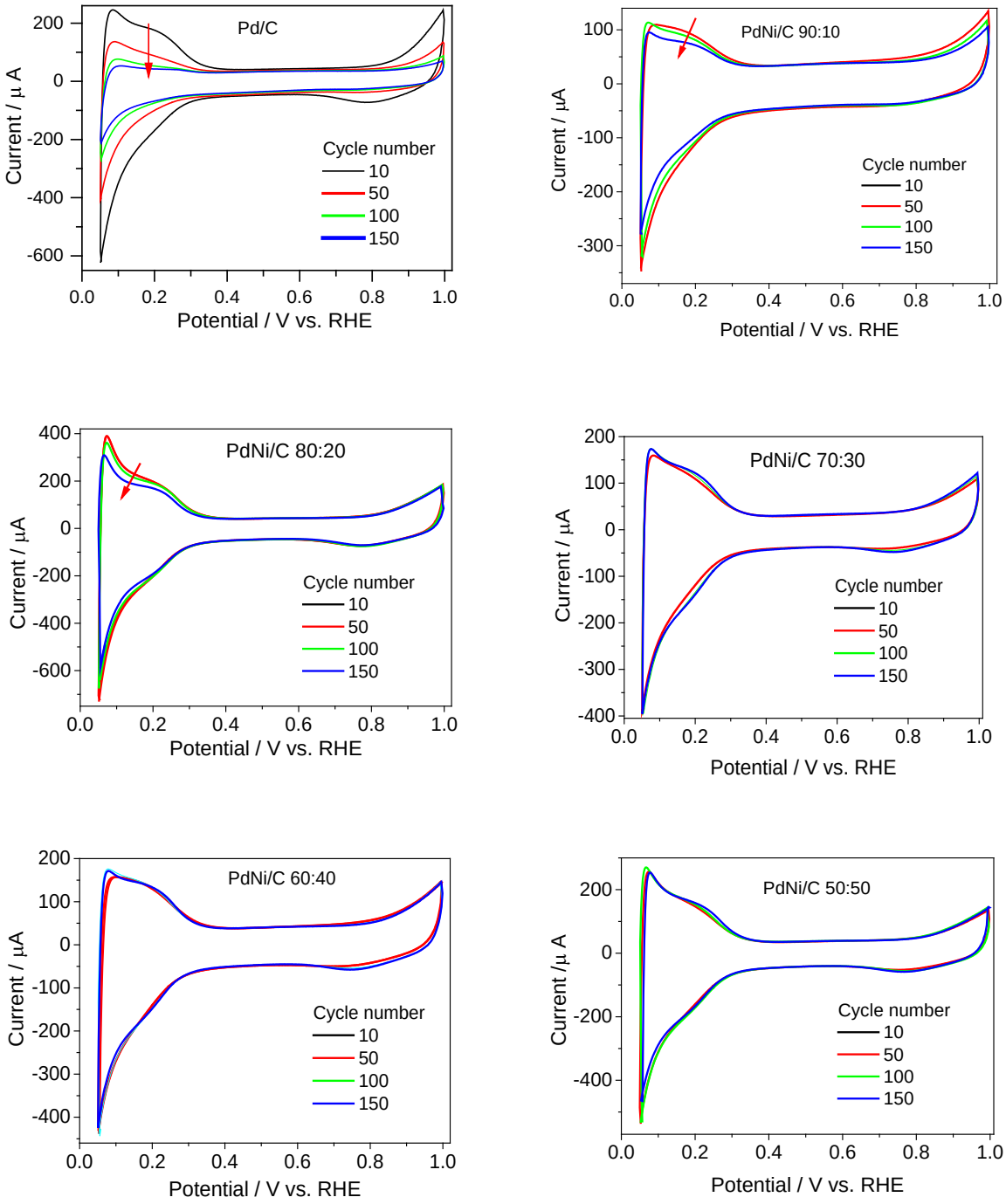

It can be seen that repeated cycling has a noticeable effect on the Pd/C reference catalyst. Changes are seen for PdNi/C 90:10, PdNi/C 80:20, which displayed a loss of charge less pronounced than Pd/C. The current-potential curves for PdNi/C 70:30, 60:40 and 50:50 did not suffer any significant change. Thus, accelerated stability tests show a higher stability for PdNi/C catalysts compared to the Pd/C sample.

Generally, all PdNi/C catalysts presented better stability than pure Pd/C, as indicated by the relative variation of the total charge presented in Figure 17. It is interesting to note that after 150 cycles, the largest charge variation occurred in Pd/C that drops to about 90 % of its initial value while for PdNi/C materials the variation of charge observed is smaller. In summary, PdNi/C catalysts are more stable than Pd/C, in agreement with previous results obtained by the group for other Pd-based catalysts [44]. Cui et al. investigated PtNi/C and observed Ni dissolution in acidic medium. They correlated better catalytic performance for methanol oxidation to changes of the Pt-Ni surface sites [81].

Figure 17 - Relative charge variations during accelerated stability tests for Pd/C and PdNi/C in 0.5 M H_2SO_4.

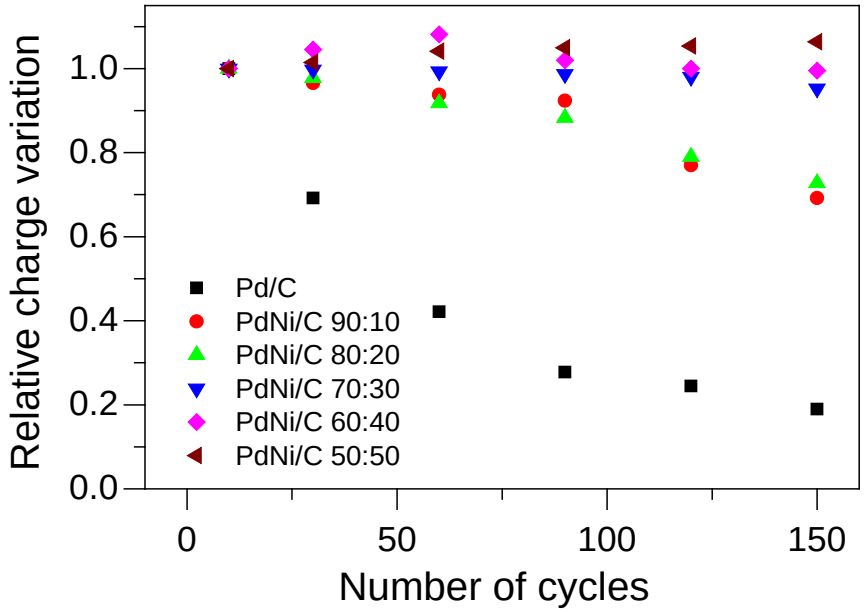

Interestingly, the charge involved in the CVs for PdNi/C 60:40 and 50:50 increases a little bit during cycling. This indicates that during continuous potential cycling some surface Ni is dissolved and more Pd is exposed to the solution.

4.1.6. Electrochemical studies in alkaline solution

In the same way as for acidic medium, electrochemical properties of Pd/C and PdNi/C electrocatalysts with different compositions were studied by cyclic voltammetry in Ar-saturated 0.1 M NaOH solution. The CVs were measured at scan rate of 0.05 V s^{-1} in potential range of 0.05 V to 1.0 V (vs. RHE). A comparison of typical current-potential curves is shown in Figure 18.

Figure 18 – Cyclic voltammetry curves (5th cycles) of the Pd/C and PdNi/C catalysts in Ar-saturated 0.1 M NaOH. Sweep rate: 0.05 V s^{-1}.

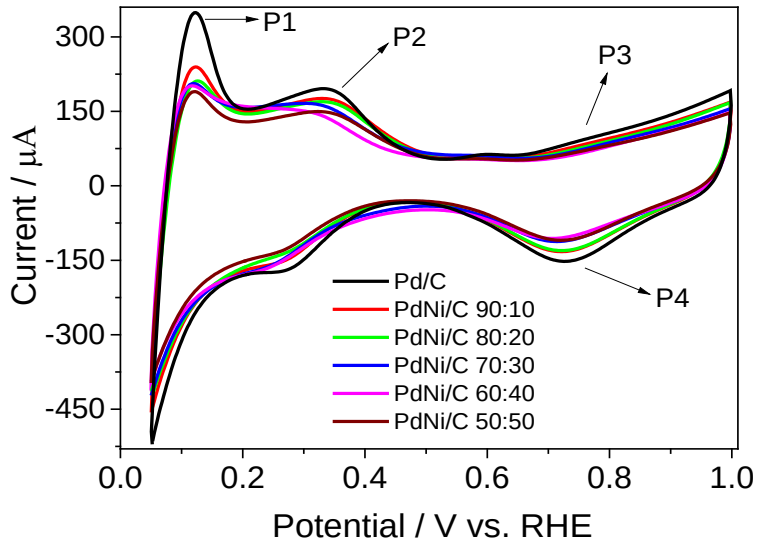

Different processes are observed in the CVs in alkaline solution. In the positive-going potential scan, the curve for Pd/C shows three current peaks that are related to different electrochemical processes happening on the surface of catalyst. Peaks P1 and P2, in the potential range of between 0.050 V and around 0.50 V (vs. RHE), are attributed to the oxidation of absorbed/adsorbed hydrogen:

$$Pd\text{–}H_{abs/ads} + OH^- \rightarrow Pd + H_2O + e^- \quad (22)$$

Process P3 in Figure 18 appears to begin around 0.6 V and can be ascribed to the production of the Pd (II) oxide layer. The electrochemical mechanism of this oxidation process is not clear. It is believed that OH^- ions are initially chemisorbed in the early stage of oxide formation, and later on higher valence oxides are formed at higher potentials according to:

$$Pd + OH^- \leftrightarrow Pd\text{-}OH_{ads} + e^- \quad (23)$$

$$Pd\text{-}OH_{ads} + OH^- \leftrightarrow Pd\text{-}O + H_2O + e^- \quad (24)$$

$$Pd\text{-}OH_{ads} + Pd\text{-}OH_{ads} \leftrightarrow Pd\text{-}O + H_2O \quad (25)$$

The adsorption of OH^- (equation 23) partially overlaps with the hydrogen desorption peak P2. The reduction process at peak potential of 0.720 V (peak P4) corresponds to the reduction of Pd (II) oxide:

$$Pd\text{-}O + H_2O + 2e^- \leftrightarrow Pd + 2\ OH^- \quad (26)$$

Generally, Figure 18 shows that the CV curves of PdNi/C electrocatalysts are similar to CV shape of Pd/C. However, the hydrogen adsorption/desorption region involves smaller intensity for P1 and P2 current peaks. This indicates that for the catalysts that contain Ni peaks P1 and P2 the amount of Pd on the surface is smaller. Also, peaks P1 and P2 might be shifted positively or negatively, and this shift could be related to the interference of nickel oxide formation. PdNi/C 90:10 involves higher hydrogen adsorption/desorption currents among the PdNi/C samples of different compositions while PdNi/C 50:50 shows the lowest one. The decrease in hydrogen adsorption/desorption charge may be due to the alloy formation effect, *i.e.,* small lattice size in PdNi/C compared to the Pd/C.

In the potential range from 0.5 V to 1.0 V there is a slight shift to lower positive values of the onset potential of the Pd oxides formation as the Ni content increases. Generally, the oxide region is initiated at 0.530 V and the reduction region lies between 0.95 V and 0.50 V. Similar cyclic voltammetry behavior is reported in literature for PdNi materials [44,97].

4.1.7. Oxygen reduction in alkaline solution

In alkaline medium, ORR polarization was registered at several rotation speeds (1225, 1600, 2025 and 2500 rpm). Sets of polarization curves are shown in Figure 19.

Figure 19 - ORR polarization curves at various rotation rates for Pd/C and PdNi/C catalysts in 0.1 M NaOH solution. Sweep rate: 5 mV s^{-1}

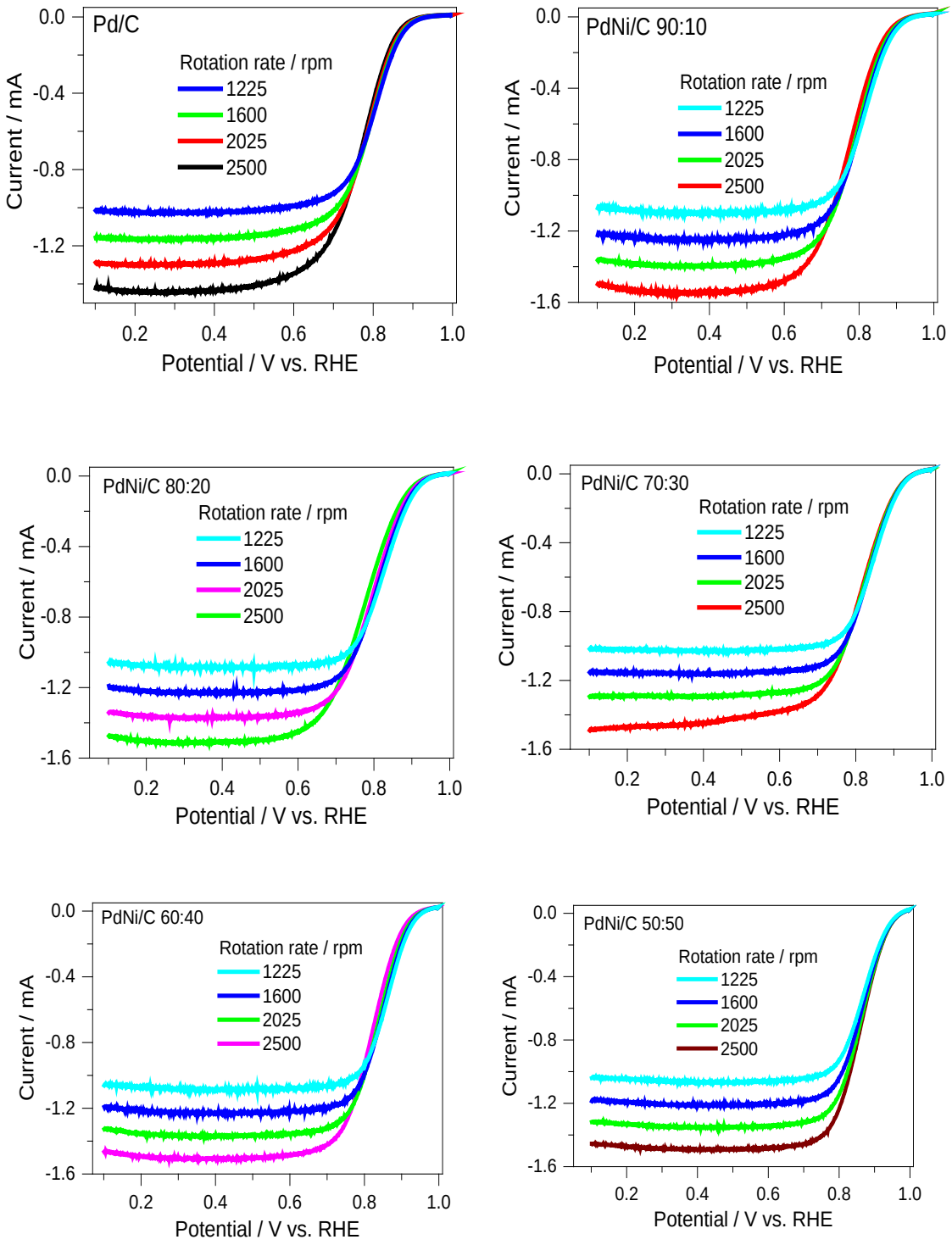

These ORR experiments were carried out keeping a continuous flow of O_2 gas at 0.1 M NaOH medium, on similar conditions that those set for ORR measurements in acidic medium.

The Levich plots derived from the ORR curves for Pd/C and PdNi/C of different compositions (Figure 20) are linear and show a small positive intercept associated to O_2 diffusion inside the catalyst ultra-thin layer, as expected [90]. Small differences in the slope could due to variations of ECSA and/or number of electrons transferred.

Figure 20 - Levich plots for Pd/C and PdNi/C catalysts. The linear fit shown only for Pd/C and PdNi/C 50:50, for clarity.

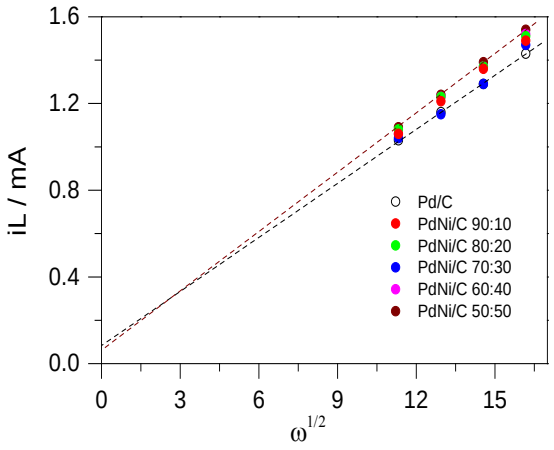

A comparison of the ORR polarization curves and the hydrogen peroxide oxidation currents registered at 2500 rpm for Pd/C and PdNi/C materials is presented in Figure 21.

All ORR curves exhibit a well-defined diffusion-limiting current region between 0.1 V to about 0.60 V and a mixed kinetic-diffusion control region up to 0.93 V. In the polarization curves (Figure 21 (b)), two characteristics are noticeable. First, the potential region of mixed kinetic-diffusion control on PdNi/C is shifted towards higher potentials compared to Pd/C following the increase in the percentage of Ni. The kinetic-diffusion controlled currents are gradually increasing as the percentage of Ni increases. The largest value is observed for PdNi/C 50:50. This shows that PdNi/C electrocatalysts have enhanced ORR activities in alkaline medium compared with Pd/C.

Figure 21 - (a) ORR Polarization curves for PdNi/C and Pd/C catalysts measured in 0.1 NaOH solution saturated with O_2 (b) H_2O_2 oxidation currents at the ring. Inset: Percentage of H_2O_2 formed at disk potential of 0.8 V vs. atomic percent of Ni. Rotation rate: 2500 rpm. Sweep rate: 0.005 V s^{-1}.

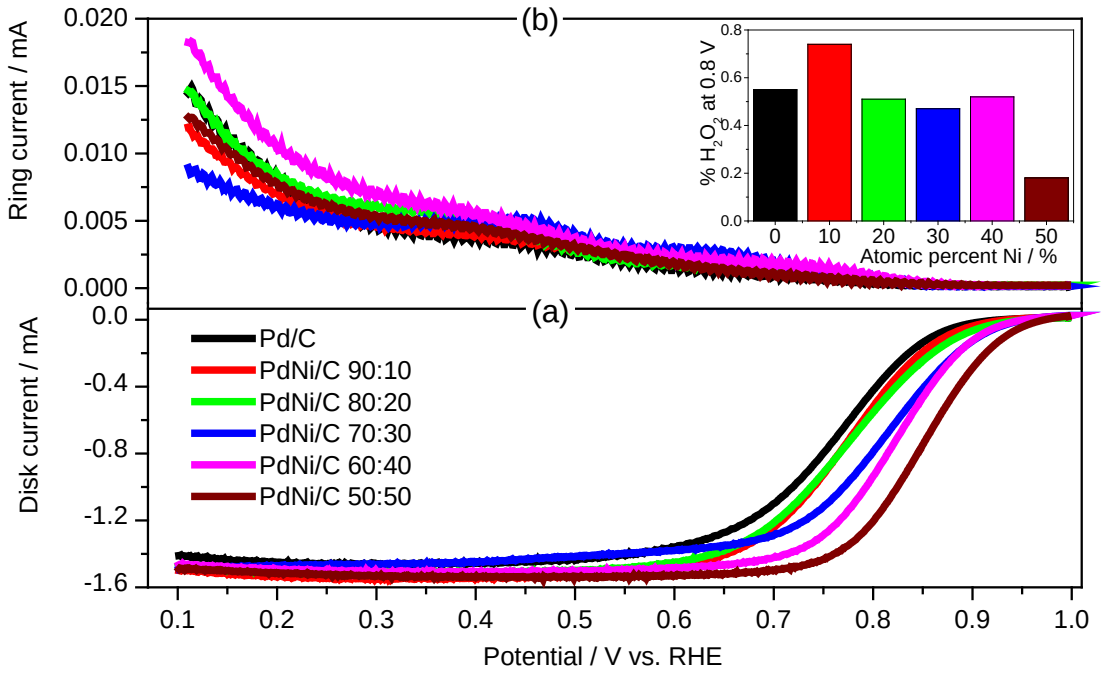

Additionally, small currents of hydrogen peroxide oxidation are detected on the ring electrode (Figure 21 (b)). Hydrogen peroxide is detected in the potential region that initiates at about 0.850 V and the current continuously grows up to 0.1 V. Our results agree with results that have been reported for thin Pd films supported on a Pt (111) [98] and Pd-Ni alloys [46].

To investigate the catalytic performance of the PdNi/C and Pd/C in detail, the kinetic current was estimated from the ORR polarization curves by considering the mass-transport correction given by the Koutecky Levich equation (equation 19). For all materials, the kinetic currents in alkaline solution were calculated at 0.850 V.

The mass and specific activities are plotted against the Ni atomic percentage in Figure 22. As in acidic solutions, this analysis shows that the mass activity and specific activity of pure Pd/C are lower than for all PdNi/C catalysts, and that performance improvement increases as the percentage of Ni increases.

Figure 22 - Mass activity (a) and specific activity (b) for ORR at 0.850 V in 0.1 M NaOH solution against atomic percentage of Ni.

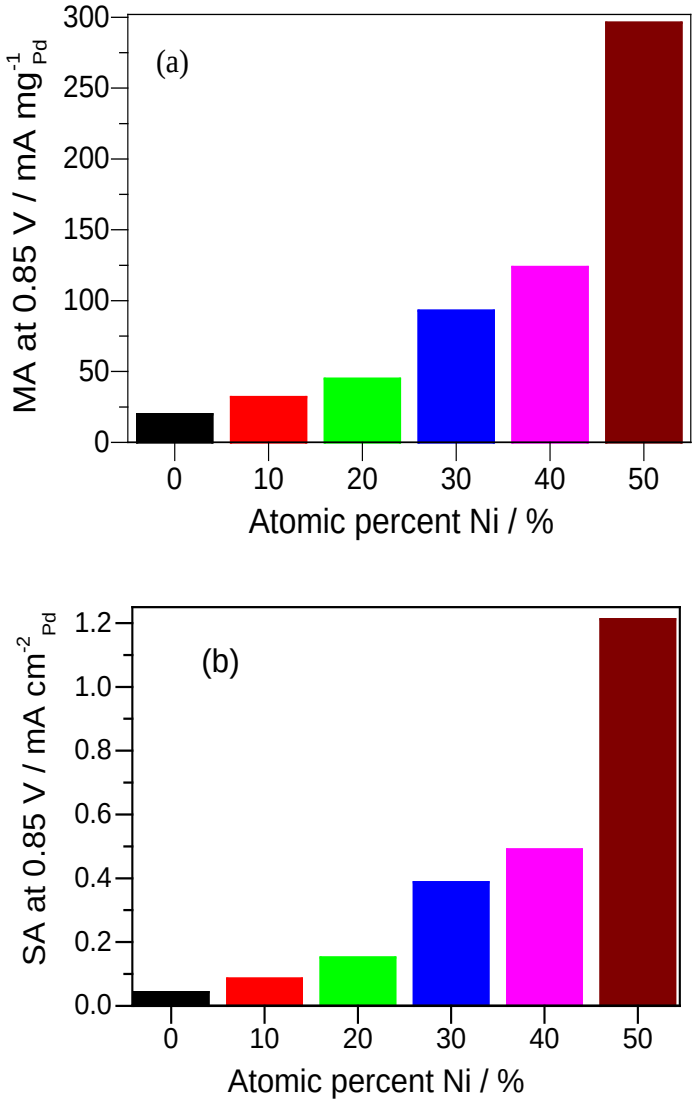

To analyze if the higher activities of PdNi/C samples might be due to some electronic effect due to the presence of Ni or to changes in the Pd-Pd distance, plots of current density of ORR at 0.850 V against those properties are presented in Figure 23. Similar to acidic solution, it is concluded that ORR activity is related to both electronic effects and Pd-Pd distance.

Figure 23 - Specific activity for ORR at 0.850 V in alkaline solution of Pd/C and PdNi/C of different compositions. (a) Against the integral of Lorentzian curve adjusted to XAS spectra. (b) Against the XRD-derived Pd-Pd distance.

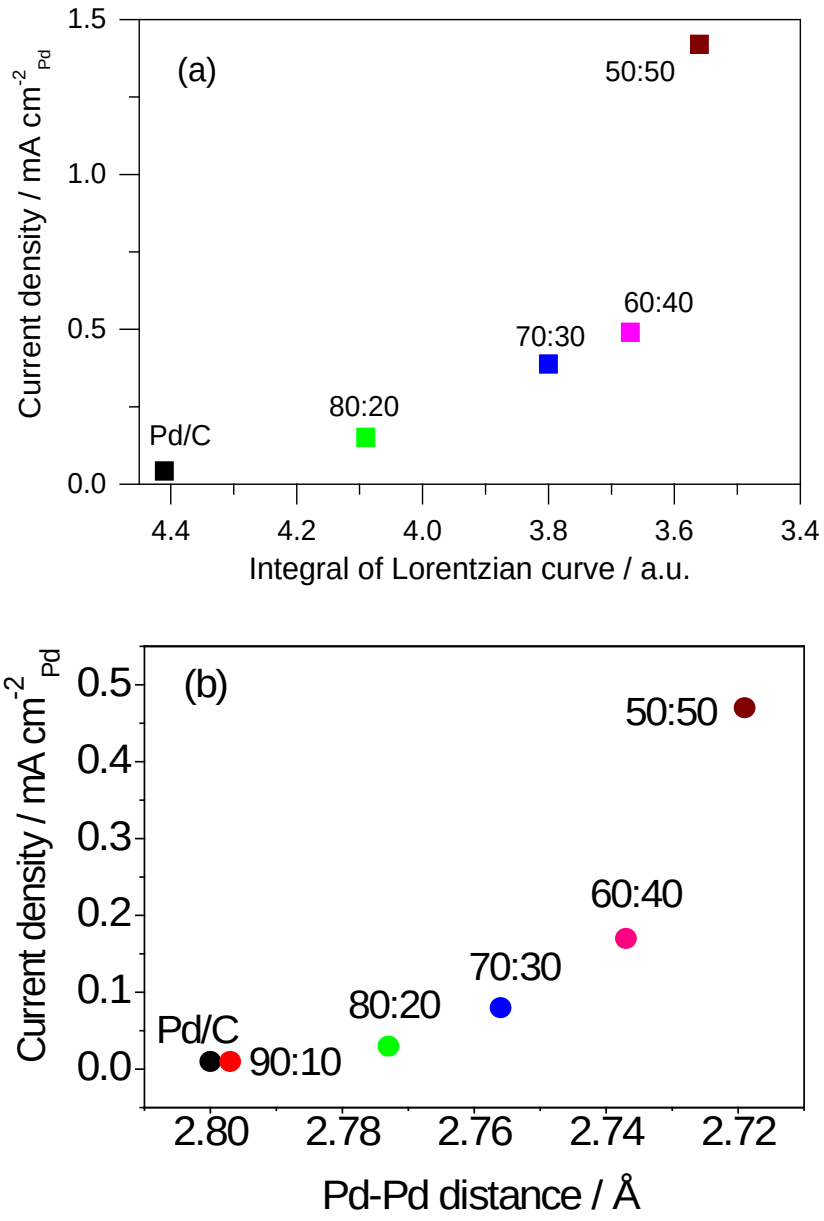

The Tafel plots for the ORR in alkaline solution are presented in Figure 24. Two well-defined regions of slopes of 60 and 120 mV/dec are seen, as expected.

Figure 24 - Mass-transport corrected Tafel plots of ORR on the Pd/C and PdNi/C samples in 0.1 M NaOH. Lines with slopes of 60 mv/dec and 120 mV/dec are shown.

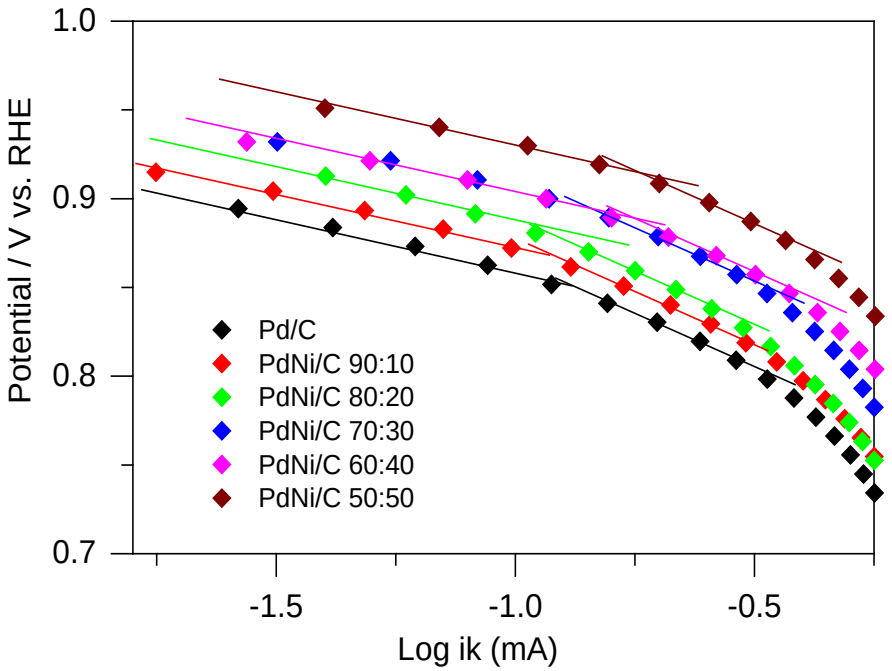

Based on the calculated values of specific activities, it is concluded that the all PdNi/C samples perform better than Pd/C for the ORR in alkaline medium and that enhancement follows the Ni percentage. A similar enhancing catalytic activity is reported in the literature for hollow Pd_1Ni_1/C in alkaline environment [55]. The formation of hydrogen peroxide occurs in small percentage indicating that the ORR proceeds mainly via 4 electrons. Generally, formation of hydrogen peroxide seems smaller on PdNi/C materials than on Pd/C.

In brief conclusion, the results clearly demonstrate that addition of Ni to Pd not only greatly enhances the mass for ORR but also leads to superior specific activity, in good agreement with results reported for PdNi in the literature [46,55,68,69]. It is believed that higher catalytic performance may be due to electronic effects as well as to surface effects.

4.1.8. Stability studied in alkaline solution

Accelerated stability test were done by continuously cycling the potential between 0.05 V and 1.0 V at 0.05 V s^{-1} in 0.1 M NaOH under Ar flow. The current-

potential profiles up to 1000 cycles for Pd/C and for all PdNi/C samples of different compositions are presented in Figure 24. For Pd/C, the charge increases as seen comparing the curves up to 500 cycles. Further cycling produces a decrease of charge.

Figure 25 - Cyclic voltammetry curves taken for stability tests for Pd/C and PdNi/C catalyst in 0.1 M NaOH solution from 0.050 to 1.0 V vs RHE. Sweep rate 0.050 V s^{-1}.

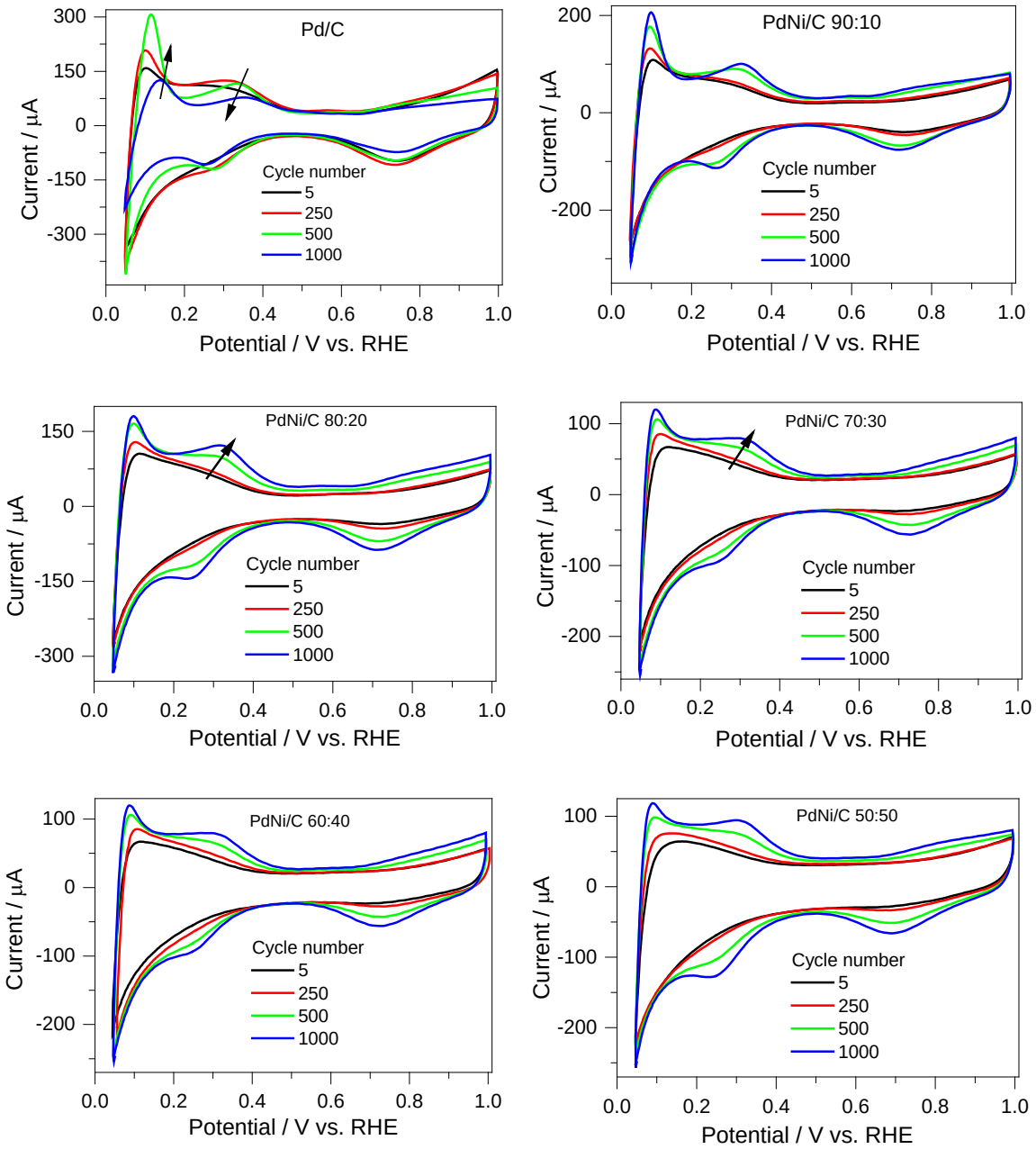

For all PdNi/C materials studied, small variations are observed up to 250 cycles and changes in charge become more pronounced for larger number of potential cycles. There is a steady increase in charge, which reflects an increase in Pd area, likely due to Ni leaching.

Figure 26 - Relative charge variations during accelerated stability tests for Pd/C and PdNi/C in 0.1 M NaOH solution.

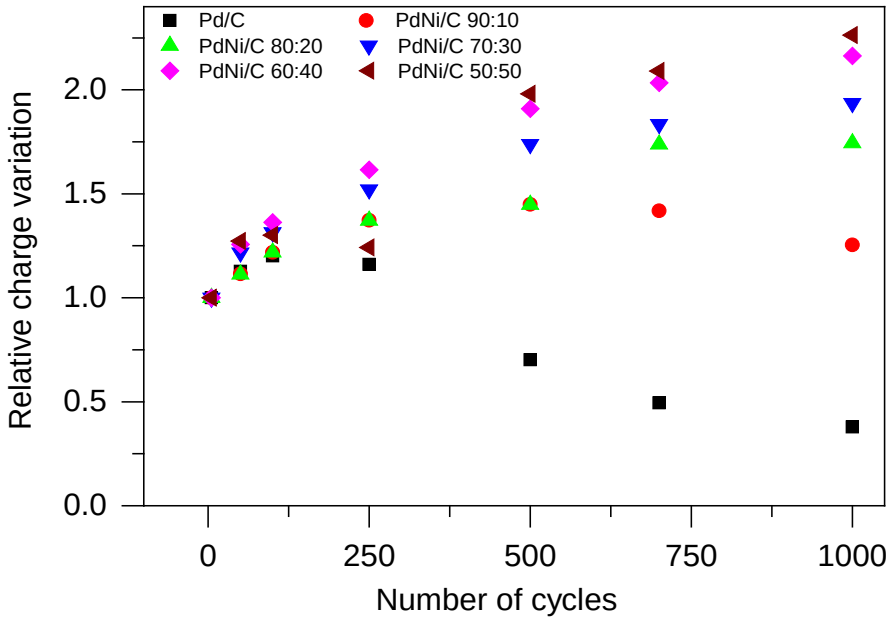

Overall, the activity for the ORR is higher in alkaline solution than in acidic medium. In contrast, the catalysts appears to be less stable.

4.2. PdCu/C catalyst

4.2.1. X-ray diffraction analysis

The physical properties of the Pd/C and PdCu/C catalysts were analyzed by X-ray diffraction and the patterns obtained is shown in Figure 27. The XRD patterns show the common signals of the face centered cubic (fcc) structure of Pd. Like for PdNi/C samples, XRD results for PdCu/C catalysts show that diffraction peaks are laying between those of Pd and Cu metal. For verification, the pure Pd and pure Cu peak angles are given in the bottom line of Figure 27.

Figure 27 - X-ray diffraction data for PdCu/C and Pd/C catalysts. Catalysts are indicated in the figure.

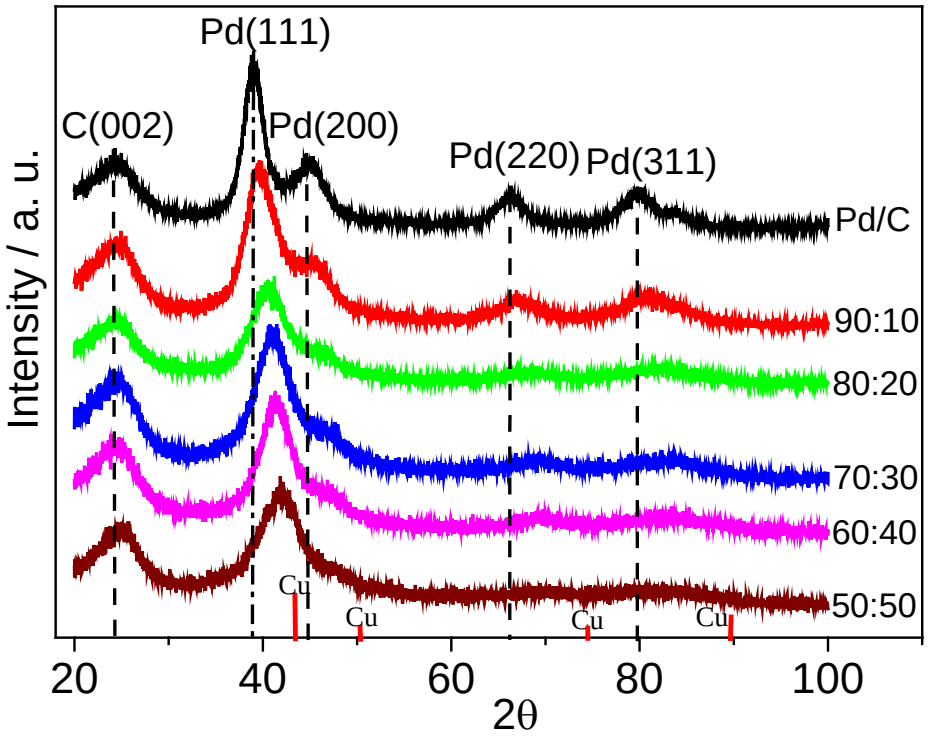

The shift in 2θ position is a confirmation of alloying between Pd and Cu. Such a shift reflects the contraction of the Pd fcc crystalline lattice caused by the partial replacement of Pd atoms (1.69 Å) with smaller sized Cu atoms (1.45 Å). Compared to the pure Pd/C, the signals for PdCu/C 90:10 and PdCu/C 80:20 are slightly shifted toward higher 2θ values. This suggests that a PdCu alloy with low Cu concentration was formed. For PdCu/C 70:30, PdCu/C 60:40 and PdCu/C 50:50, shift to higher 2θ angles is more pronounced as Cu percentage increases.

Moreover, as the percentage of Cu increases the width of XRD peaks increases and intensity decreases, allowing to conclude that the particles are becoming less crystalline and/or have smaller sizes [31].

Average crystallite size, lattice constant and Pd-Pd interatomic distance were calculating by using equations 12, 13 and 14. The results obtained from the XRD study for Pd/C and PdCu/C catalysts are summarized in Table 7. It is seen that the lattice constant and the Pd-Pd distance decrease with increasing atomic percentage of Cu indicating that solid solutions were formed between Pd and Cu.

Table 7 – Structural characteristics of Pd/C and PdCu/C nanocatalysts derived from XRD data.

Catalyst	Crystallite size (nm)	Lattice parameter (Å)	Pd-Pd distance (Å)
Pd/C	2.9	3.988	2.820
PdCu/C 90:10	2.1	3.939	2.783
PdCu/C 80:20	1.9	3.896	2.743
PdCu/C 70:30	2.1	3.846	2.720
PdCu/C 60:40	1.8	3.826	2.702
PdCu/C 50:50	2.1	3.779	2.691

A plot of lattice parameter against the atomic percentage of copper is presented in Figure 28.

Figure 28 - Variation of the lattice parameters with atomic percentage of Cu.

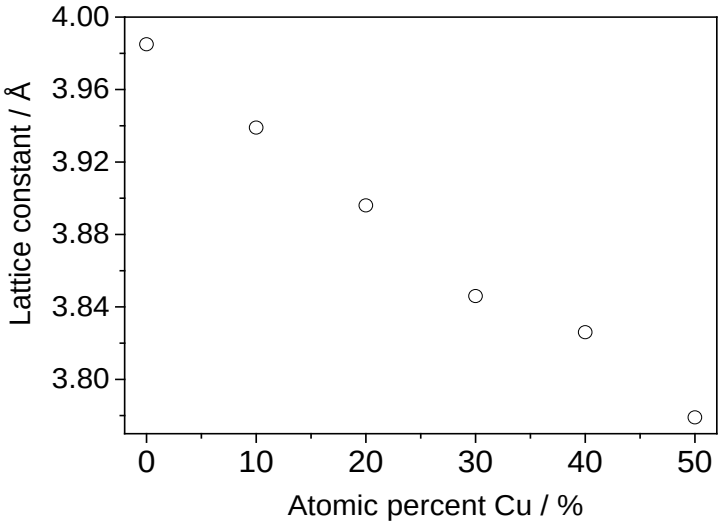

The composition of the PdCu solid solutions was estimated for our PdCu nanoparticles by applying Vegard´s law (equation 15). Because the single elements have not the same crystal structure, the literature value of lattice

parameter for the PdCu alloy having 48.1 % of Cu (a_M = 3.763 Å) [99] was used instead of using the lattice parameter of pure Cu. Results are presented in Table 8.

Table 8 – Calculated Pd:Cu ratios for PdCu alloys derived from XRD data.

Catalyst	Calculated Pd:Cu ratio	Nominal
PdCu/C 90:10	89:11	90:10
PdCu/C 80:20	80:20	80:20
PdCu//C 70:30	68:32	70:30
PdCu/C 60:40	63:37	60:40
PdCu/C 50:50	53:47	50:50

A comparison of our lattice parameter values for PdCu/C with the values for alloys [99] is presented in Figure 29. It is seen that distance between one set and other decreases as the molar fraction of Cu increases. This means that the lattice strain of Pd/C is not maintained and diminishes with Cu addition.

Figure 29 - Lattice parameters against Cu molar fraction obtained for PdCu/C samples and reported for solid solutions in ref. [99].

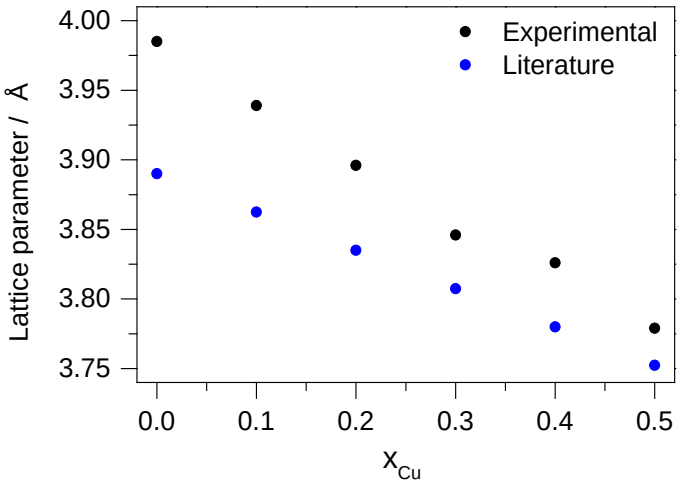

4.2.2. X-ray absorption spectroscopy (XAS) results

The normalized XAS spectra for all PdCu/C materials are displayed in Figure 30. Generally, it is seen that Cu leads to decrease of electronic vacancy of the Pd 4 d band compared to the pure Pd/C. However, the PdCu/C 50:50 catalyst presented the most intense absorption indicating an increase in the band vacancy. This phenomenon might be attributed to highest concentration of Cu oxides. The estimated integral of the Lorentzian curve adjusted to spectra is shown in Figure 31.

Figure 30 - Normalized X-ray absorption spectra measured around the Pd L3 edge for Pd/C and PdCu/C catalysts. Inset: absorption peak region enlarged.

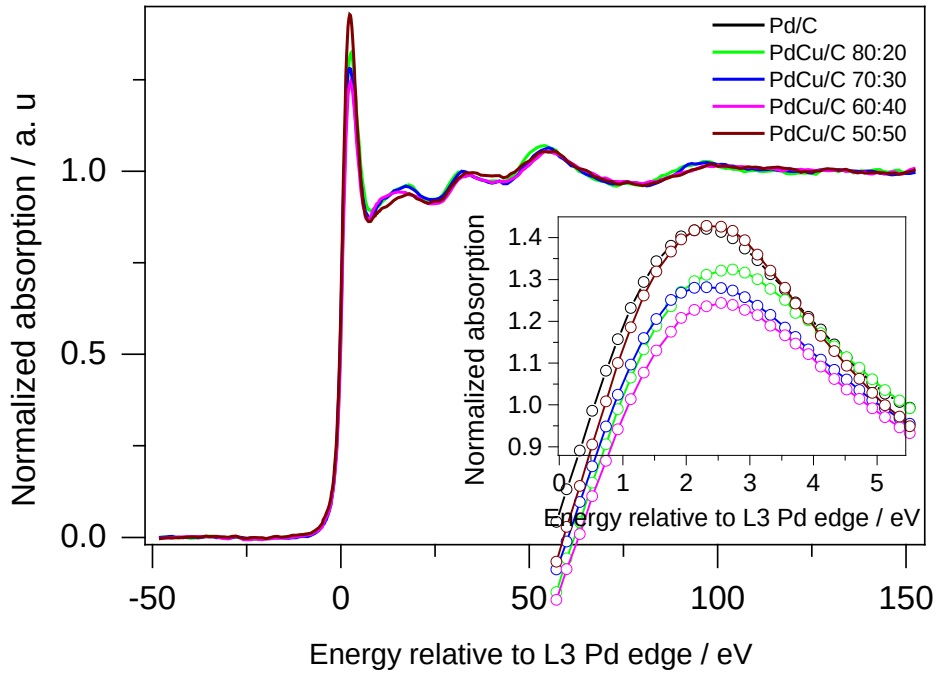

Figure 31 - Integral values of the Lorentzian curves adjusted to spectra against percentage of Cu.

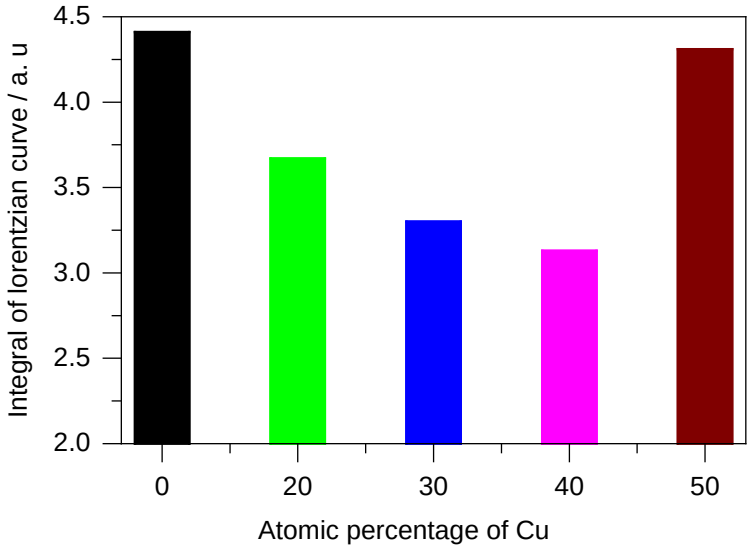

4.2.3. Cyclic voltammetry measurements

A comparison of typical current-potential curves is shown in Figure 32. The general shapes of CV curves for the PdCu/C materials are similar to that of Pd/C, in agreement with results found in the literature [63,66]. Additionally, in Figure 32, the curves clearly have different charges, which means that the Pd surface area varies. This variation is quite apparent in the hydrogen adsorption/desorption charge and reflects the fact that PdCu/C catalysts have lower Pd area than Pd/C. For instance, Pd/C obviously has the highest area, while PdCu/C 50:50 has the lowest one. In general, this can be taken as evidence of the presence of Cu on the surface of the materials.

Figure 32 – Cyclic voltammetry curves (5th cycles) of the Pd/C and PdCu/C catalysts in 0.5 M H_2SO_4 saturated with Ar. Sweep rate: 0.05 V s^{-1}.

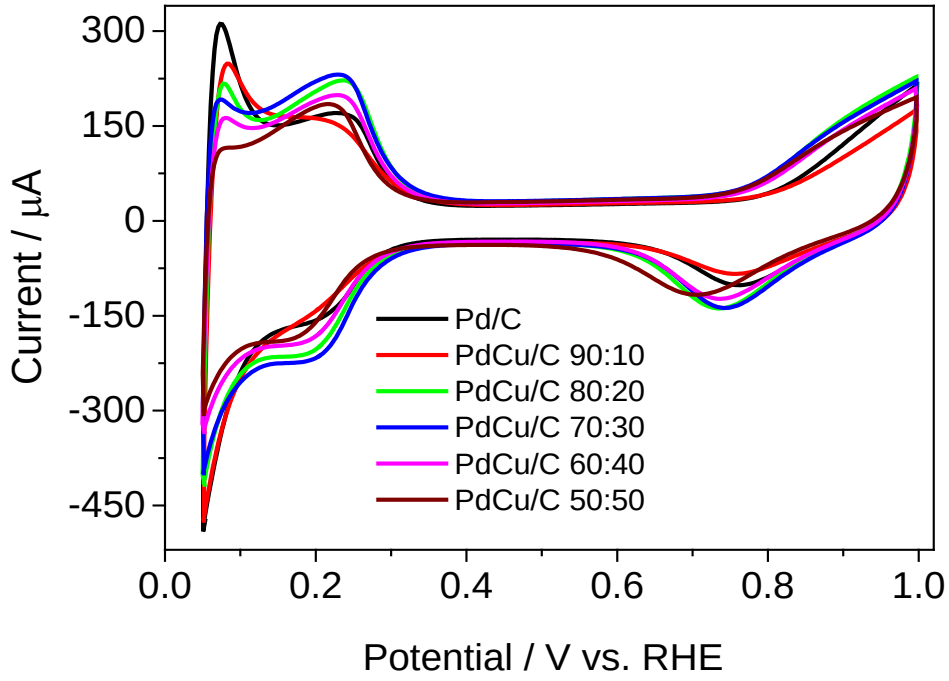

Also, it is seen in Figure 32 that as the Cu content increases there is a slight shift in the oxide reduction peak potential toward lower potential values that seems to follow the shift of the onset potential of the oxide formation. This behavior is different than that of PdNi/C catalysts (Figure 10). A plot of peak potential of the reduction of Pd oxide against Cu percentage is presented in Figure 33.

Figure 33 - Peak potential of PdO reduction from curves of Figure 32 vs. Cu percentage.

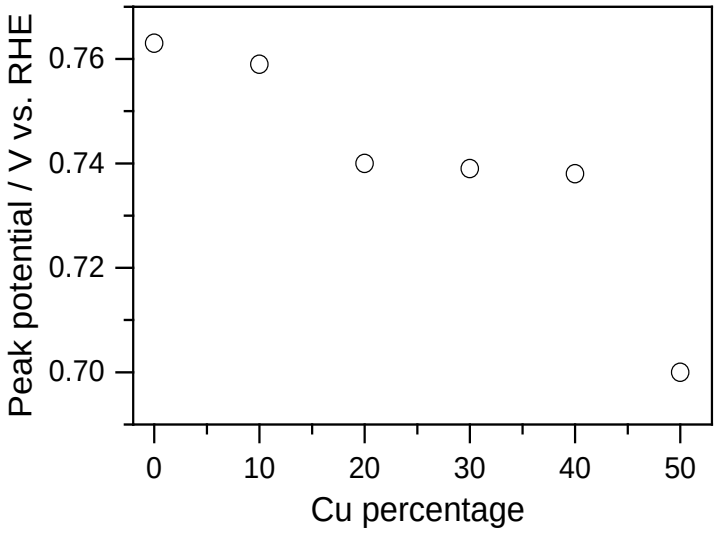

4.2.4. Determination of Pd electrochemical surface area for PdCu/C samples

The ECSA of Pd for PdCu/C samples was determined as described for PdNi/C. Figure 34 shows the CV curves registered for various upper potential limits from 1.0 V to 1.650 V in 0.5 M H_2SO_4 and the plots of reduction charge of PdO against the upper potential limit. Again, a fresh layer of catalysts was used for each curve. It is seen that for the PdCu/C 90:10 and 80:20, one reduction peak at about 0.5 V appears after reaching upper limit potential of 1.60 V that could be ascribed to Cu reduction. That process is not apparent for the PdCu/C samples with higher percentage of Cu.

Figure 34 - Cyclic voltammetry curves taken for stability tests for PdCu/C catalyst in 0.5 M H_2SO_4 solution from 0.050 to 1.0 V vs RHE. Sweep rate 0.050 V s^{-1}.

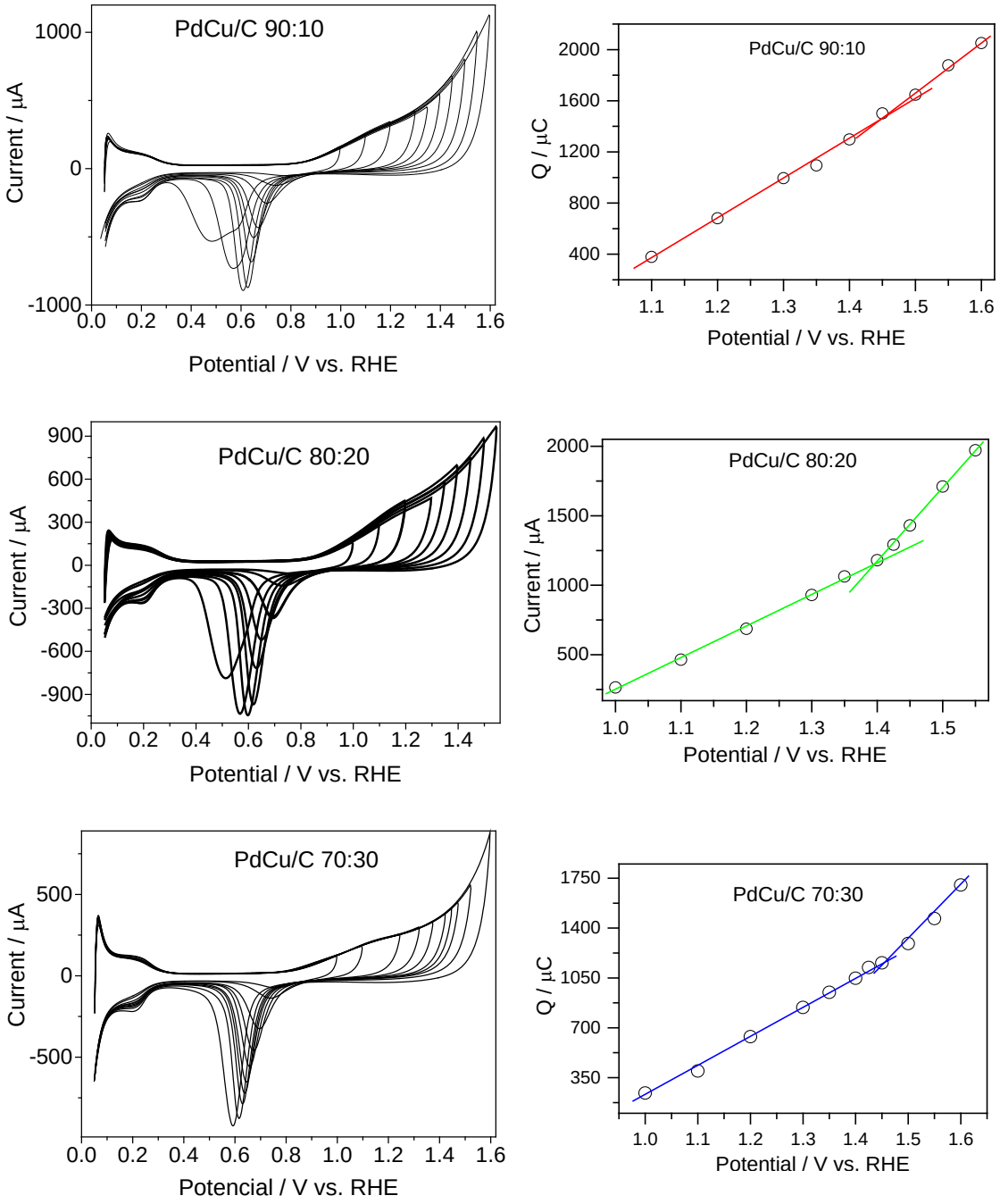

Figure 34 – (Continuation).

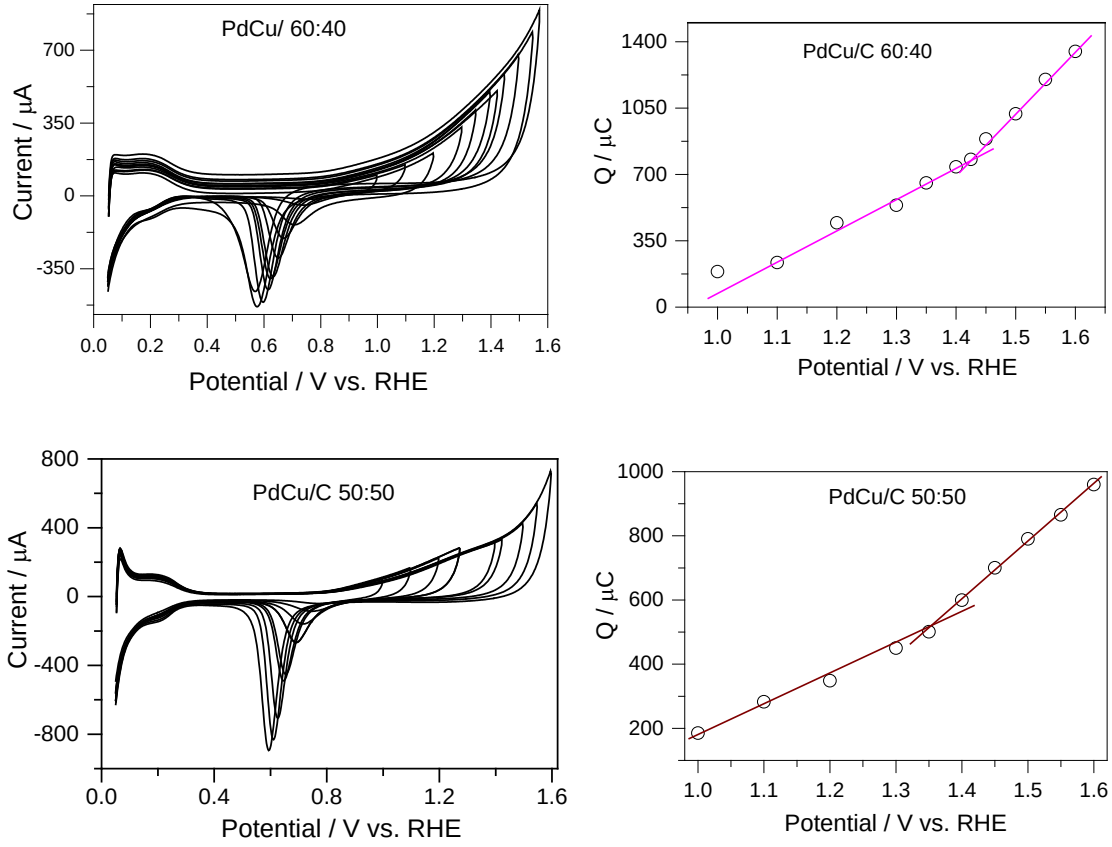

The values of ECSA of Pd estimated from the charge of reduction of a monolayer of Pd oxide are given in Table 9. It is seen that the ECSA of Pd decreases as the percentage of Cu in the PdCu/C samples increases.

Table 9 – ECSA of Pd calculated from PdO reduction charges.

Catalyst	ECSA of Pd (cm^2)
Pd/C	3.4
PdCu/C 90:10	3.1
PdCu/C 80:20	2.8
PdCu/C 70:30	2.7
PdCu/C 60:40	1.9
PdCu/C 50:50	1.8

4.2.5. Oxygen reduction reaction in acidic electrolyte

The catalytic activities for ORR were determined by using the rotating ring disk electrode (RRDE) technique under the same conditions used for the study of ORR on PdNi/C in acidic and alkaline media. Figure 35 presents a set of polarization curves of ORR (current at the disk) and the corresponding currents of H_2O_2 oxidation (current at the ring) measured in O_2-saturated 0.5 M H_2SO_4 solution at 2500 rpm. The ORR polarization curves show some differences in the limiting currents and a significant shift towards more positive potentials as the percentage of Cu increases. This evidences that Cu enhances the ORR activity.

Along the ORR reaction, the small current of H_2O_2 formation (Figure 35 b, inset) shows that the ORR proceeds mostly via four-electron transfer towards the water formation. Also, the percentage of hydrogen peroxide formed decreases as the Cu content increases. These results agree with literature data [47,61,62,100].

Figure 35 - (a) ORR Polarization curves for PdCu/C and Pd/C catalysts measured in 0.5 M H_2SO_4 solution saturated with O_2 (b) H_2O_2 oxidation currents at the ring. Inset: Percentage of H_2O_2 formed at disk potential of 0.6 V vs. atomic percent of Cu. Rotation rate: 2500 rpm. Sweep rate: 0.005 V s^{-1}.

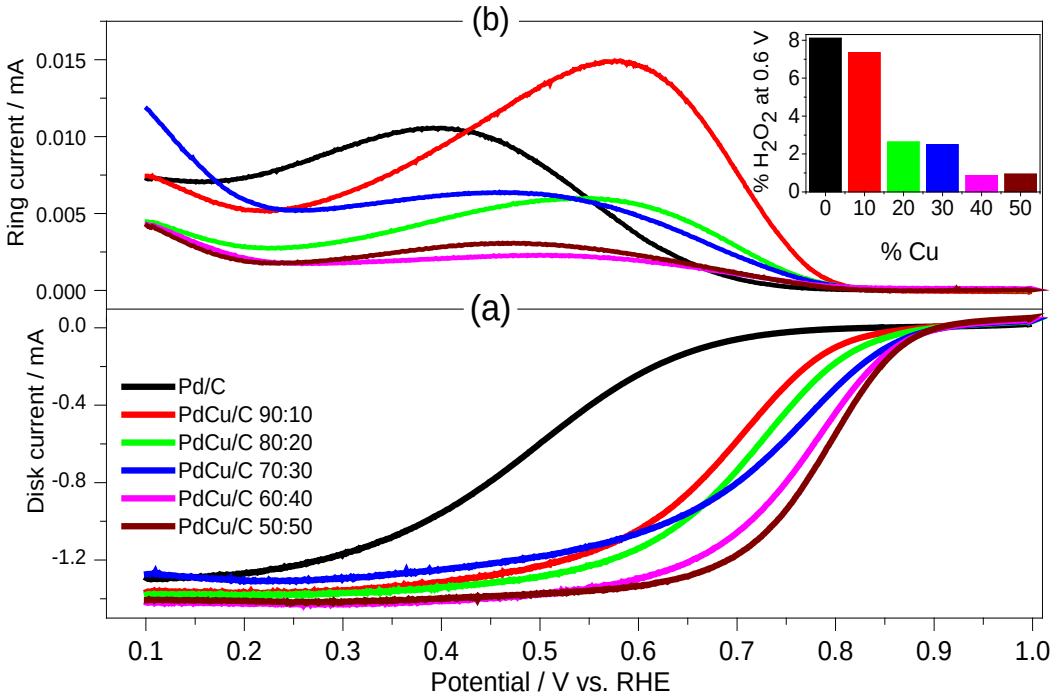

The kinetic current (ik) at 0.80 V calculated using the Koutecky- Levich equation (equation 19) was used to evaluate the mass activity (equation 20) and specific activity (equation 21) of PdCu/C catalysts, which are presented in Figure 36.

Figure 36 - Mass activity (a) and specific activity (b) at 0.8 V for ORR in 0.5 M H_2SO_4 solution against atomic percentage of Cu.

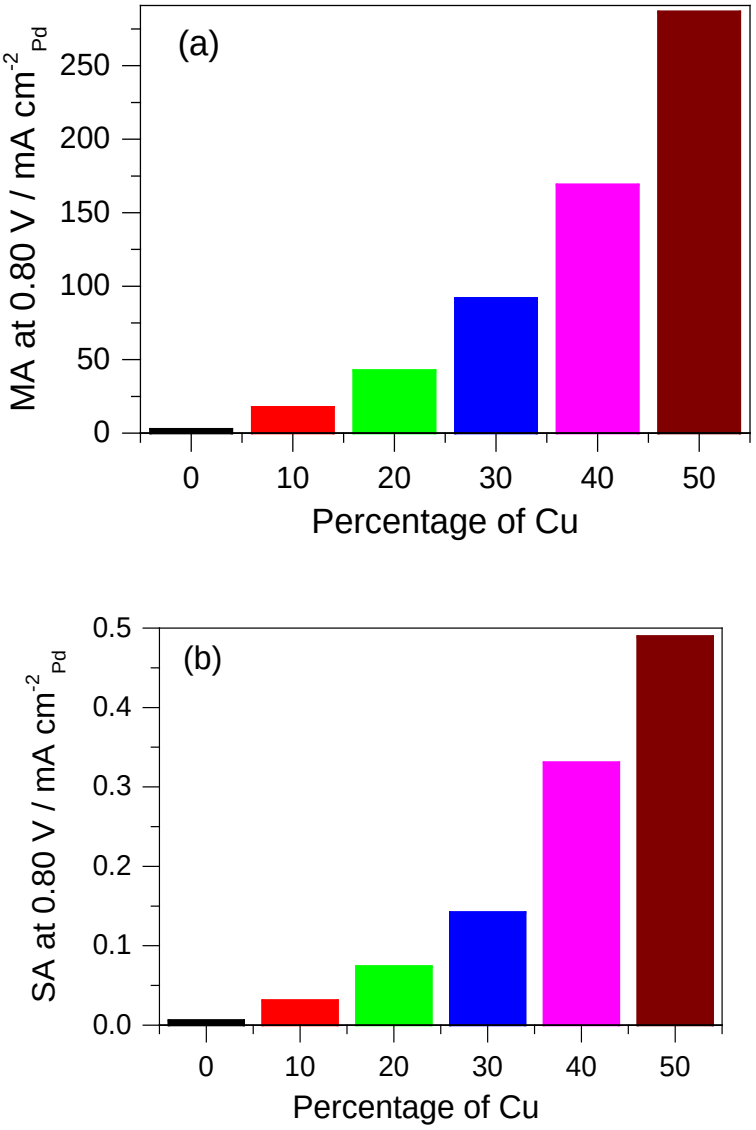

The ECSA-normalized currents are plotted against the integral value of the Lorentzian curve adjusted to XAS spectra and against the Pd-Pd distance in Figure 37.

Figure 37 - Current density for ORR at 0.80 V in 0.5 M H_2SO_4 solution of Pd/C and PdCu/C of different compositions. (a) Against the integral of Lorentzian curve adjusted to XAS spectra. (b) Against the XRD-derived Pd-Pd distance.

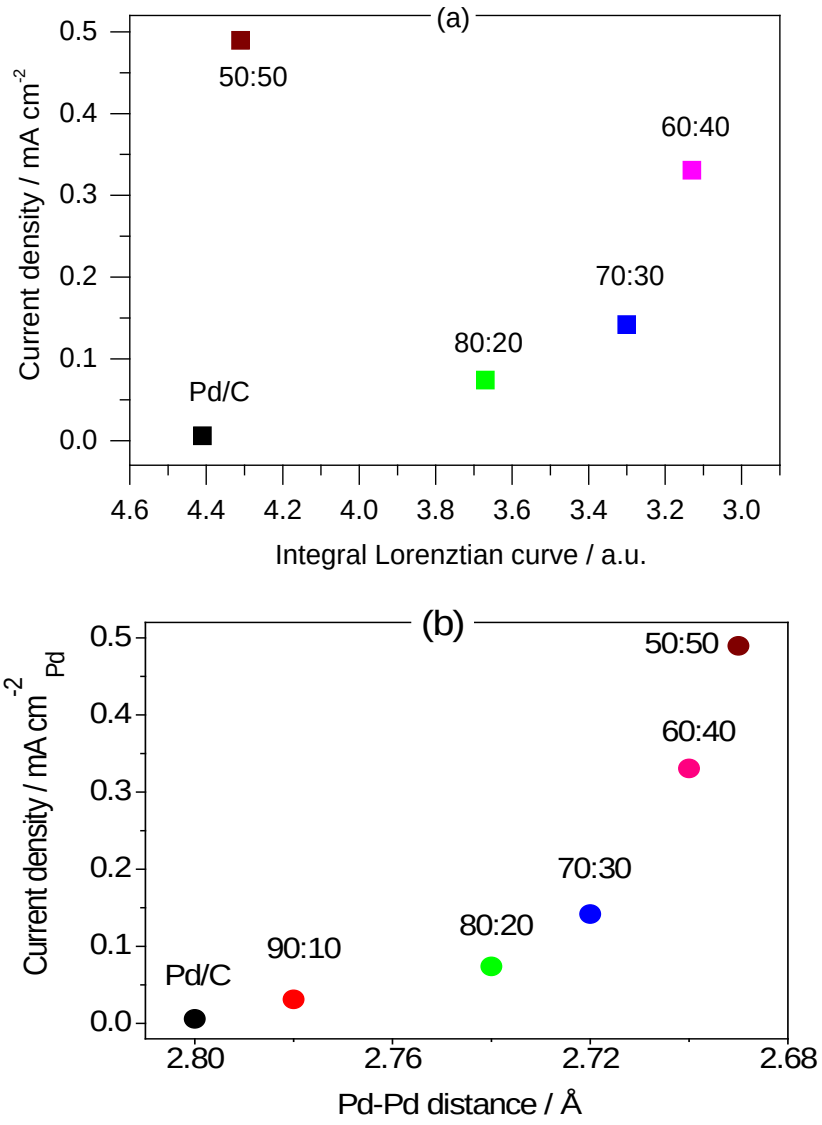

The ECSA-normalized currents of Figure 37 show that, as for PdNi/C catalysts, the current density follows the change in Pd-Pd distance. In the case of PdCu/C, a general trend with the increase of occupancy of 4d band of Pd is observed with PdCu/C 50:50 having a distinct behavior that cannot be explained at present. Generally, in acidic solution the Pd-Pd distance and the electronic properties appear to have a role in the ORR on PdCu/C.

Interestingly, our PdCu/C 50:50 shows higher activities than Pt/C and than nanoporous PdCu/C of three different compositions Pd:Cu (50:50, 70:30 and 75:25) reported in the literature [61,62].

Regarding the Tafel plots (Figure 38), the two regions of 60 and 120 mV/dec are clearly evidenced in agreement with our results for PdNi/C and with literature [23,24].

Figure 38 - Mass-transport corrected Tafel plots of ORR on PdCu/C samples. Lines with slopes of 60 mv/dec and 120 mV/dec are shown. Data for Pd/C are not shown because they appear at much lower values of log ik.

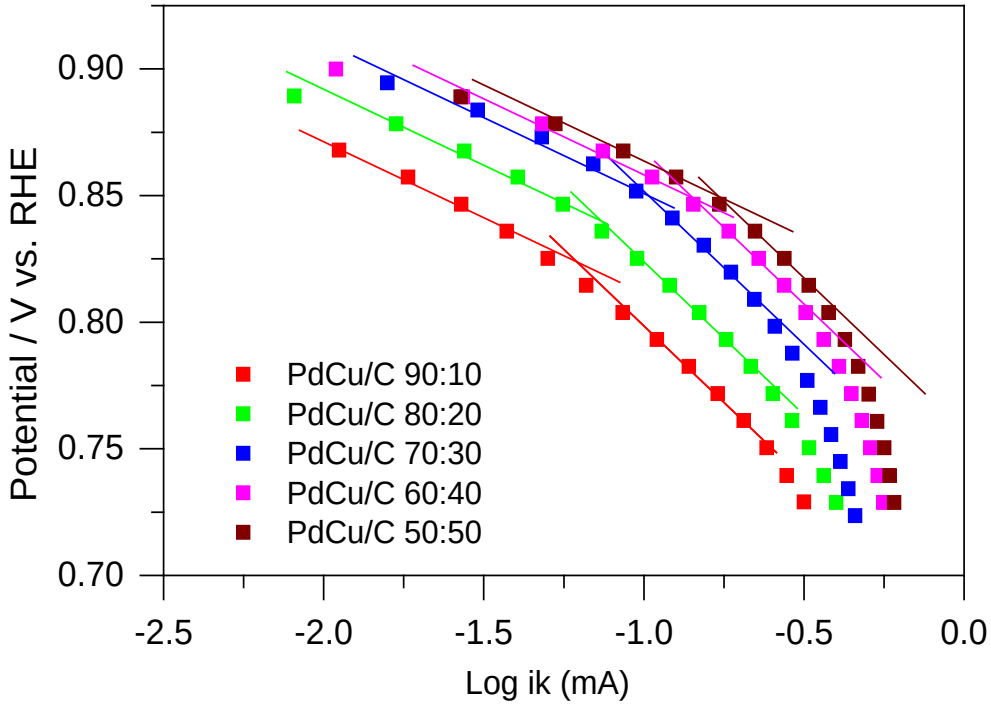

4.2.6. Stability tests in H_2SO_4 solution

The stability of the PdCu/C electrocatalysts of different compositions was examined by continuously cycling the potential, as described for PdNi/C. The sets of CV curves between 0.05 V and 1.0 V taken in 0.5 M H_2SO_4 solution are depicted in Figure 39.

Figure 39 - Cyclic voltammetry curves taken for stability tests for Pd/C and PdCu/C catalyst in 0.5 M H_2SO_4 solution from 0.050 to 1.0 V vs RHE. Sweep rate 0.050 V s^{-1}.

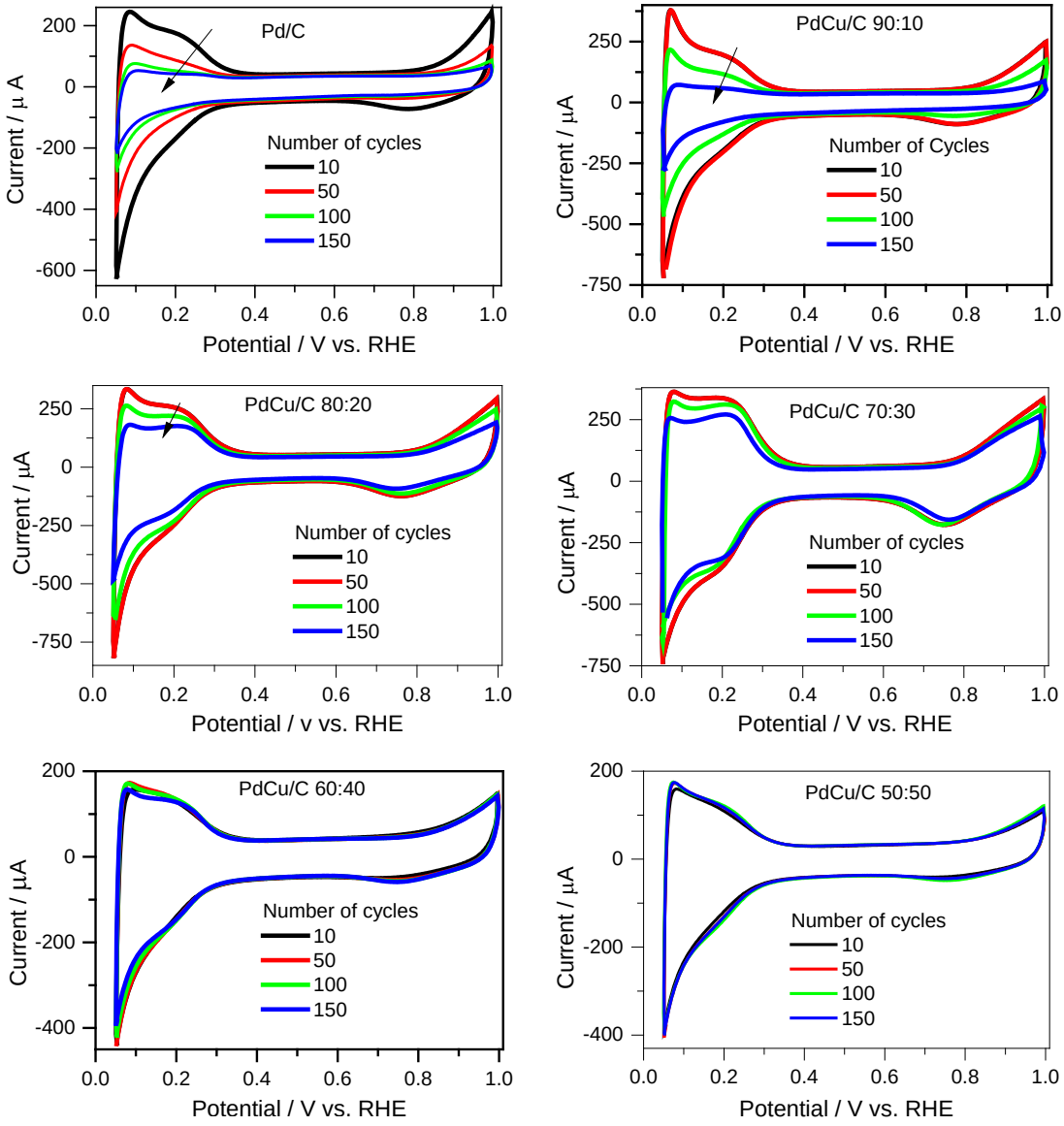

It is seen in Figure 39 that repetitions in potential cycling has a marked effect on Pd/ and on PdCu/C 90:10 which revealed a marked loss of charge. PdCu/C 80:20 and PdCu/C 70:30 follow the same trends but suffer smaller degradation changes. CV curves of stability test for PdCu/C 60:40 still show some charge variation, while for PdCu/C 50:50 they show that this samples presents high stability over potential cycling.

In general, all PdCu/C materials show better stability than the Pd/C reference sample, as evidenced by the relative variation of the total charge presented in Figure 40. Generally, the relative charge drop is less pronounced as the percentage of Cu in the catalyst increases. Pd/C and PdCu/C 90:10 lost about 80 % of the charge. Interestingly, the relative charge for PdCu/C 50:50 is almost unchanged.

Figure 40 - Relative charge variations during accelerated stability tests for Pd/C and PdCu/C in 0.5 M H_2SO_4.

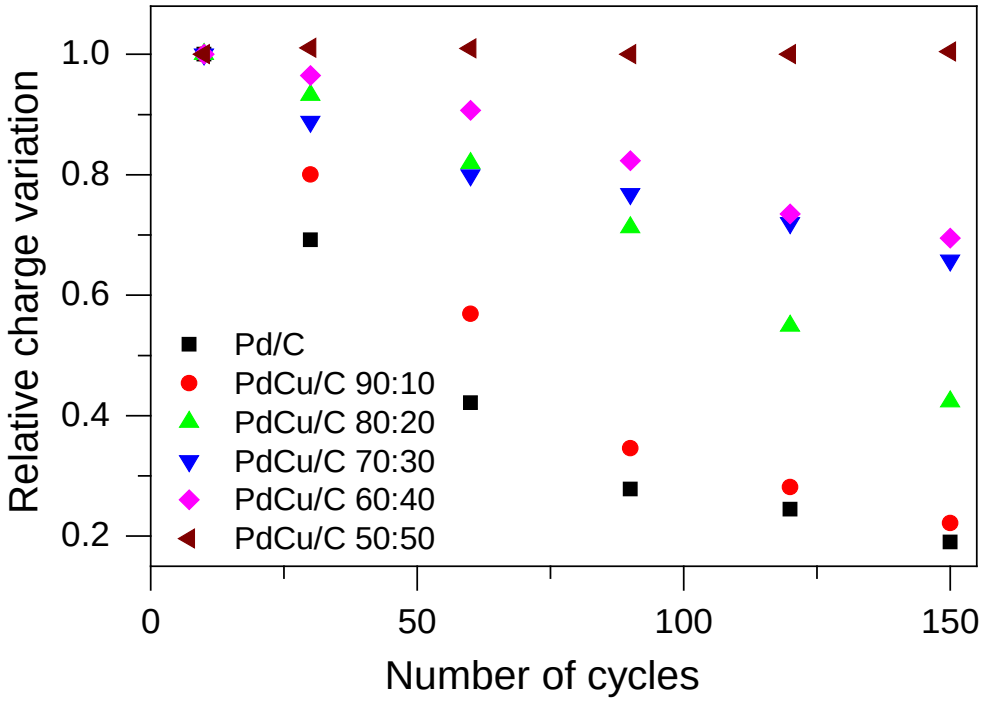

4.2.7. Cyclic voltammetry experiments in alkaline solution

The cyclic voltammograms of Pd/C and PdCu/C electrocatalysts registered in Ar-saturated 0.1 M NaOH solution are presented in Figure 41. The current-potential profiles are similar to those of PdNi/C in alkaline solution (presented in Figure 18). In detailed analysis, remarkable charge differences are seen in the region of formation and reduction of oxides that exceed the variation in the hydrogen adsorption/desorption region. The higher charges might be attributed to the overlap of Pd and Cu surface processes. In the potential range about 0.5

V to 1.0 V there is a slight shift to lower positive values of the onset potential of the oxides formation as the Cu content increases. Some differences are also seen in the region about 0.45 and 0.65 V where adsorption of OH^- partially overlaps with the hydrogen desorption peak that are likely to be due to Cu on the surface.

Figure 41 - Cyclic voltammetry curves of the Pd/C and PdCu/C catalysts in Ar-saturated 0.1 M NaOH. Sweep rate: 0.05 V s^{-1}.

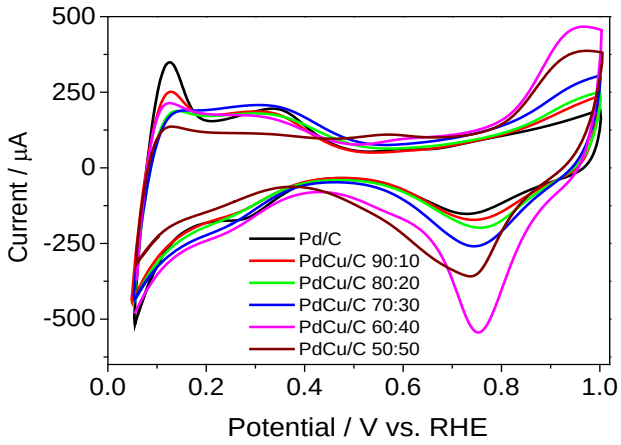

4.2.8. Performance of PdCu/C catalysts for the ORR in alkaline medium

The ORR study was performed a previously described for PdNi/C catalysts, registering ORR polarization curves at several rotation speeds and keeping a continuous flow of O_2. These ORR experiments were carried out at 0.1 M NaOH medium, on similar conditions that those set for ORR measurements in acidic medium. Polarization curves are shown in Figure 42. It is seen that the ORR curves for Pd/C and PdCu/C catalysts in alkaline medium have a limiting current region that extends over a potential range much wider than in acidic medium.

Figure 42 - ORR polarization curves at various rotation rates for Pd/C and PdCu/C catalysts in 0.1 M NaOH solution. Sweep rate: 0.005 V s^{-1}.

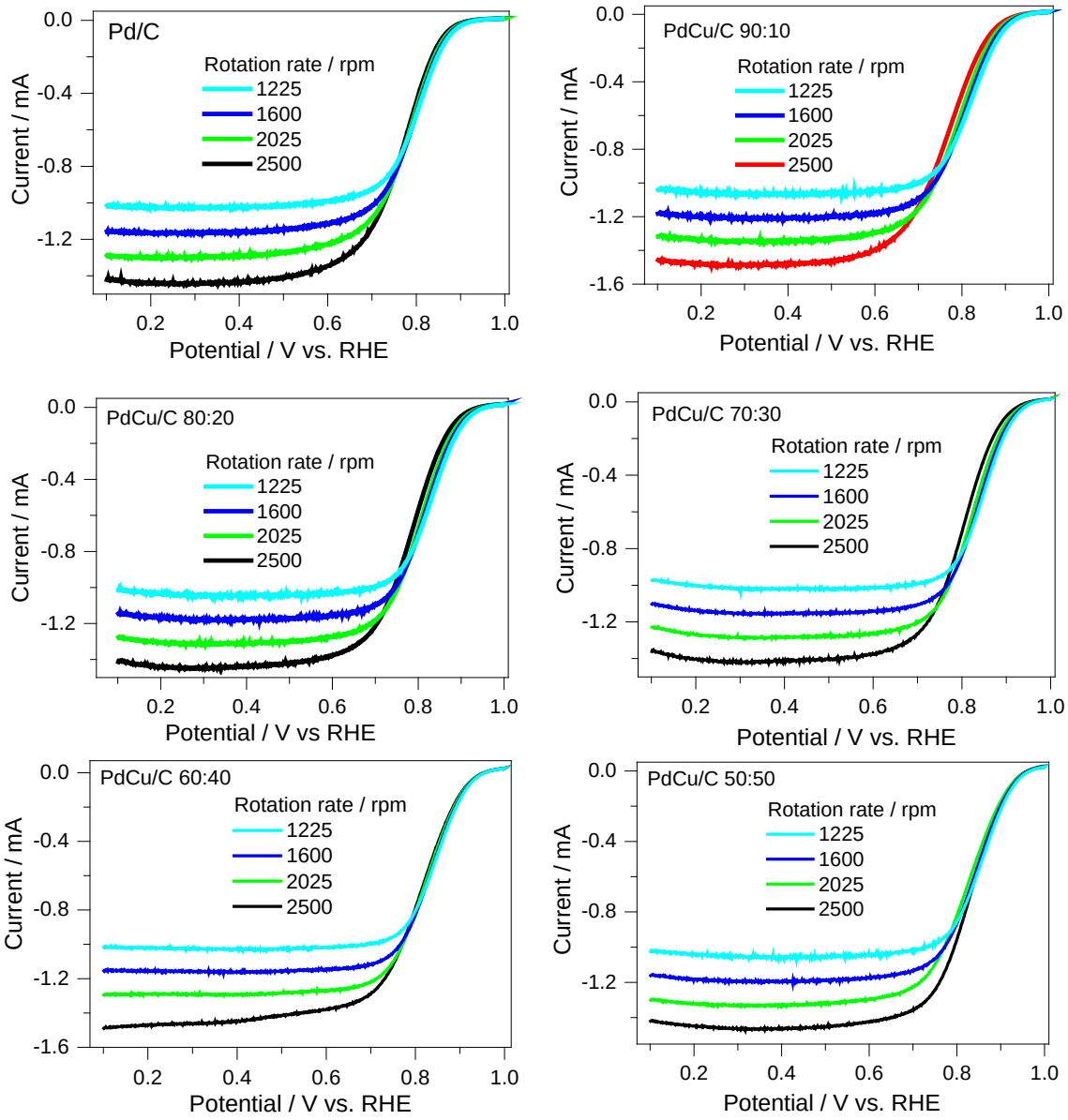

Figure 43 presents the Levich plots derived from the ORR curves for Pd/C and PdCu/C of different compositions. As expected, it is seen that they are linear with a small positive intercept due to O_2 diffusion in the catalyst layer.

Figure 43 - Levich plots for Pd/C and PdCu/C catalysts. The linear fit is shown only for PdCu/C 90:10 and 70:30, for clarity.

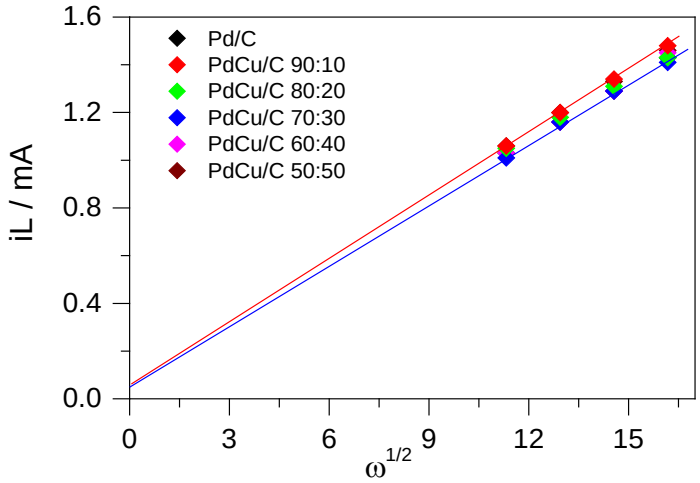

The ORR polarization curves and the hydrogen peroxide oxidation currents registered at 2500 rpm for Pd/C and PdCu/C samples are presented in Figure 44.

Figure 44 - (a) ORR Polarization curves for PdCu/C and Pd/C catalysts measured in 0.1 M NaOH solution saturated with O_2 (b) H_2O_2 oxidation currents at the ring. Inset: Percentage of H_2O_2 formed at disk potential of 0.80 V vs. atomic percent of Cu. Rotation rate: 2500 rpm. Sweep rate: 0.005 V s^{-1}.

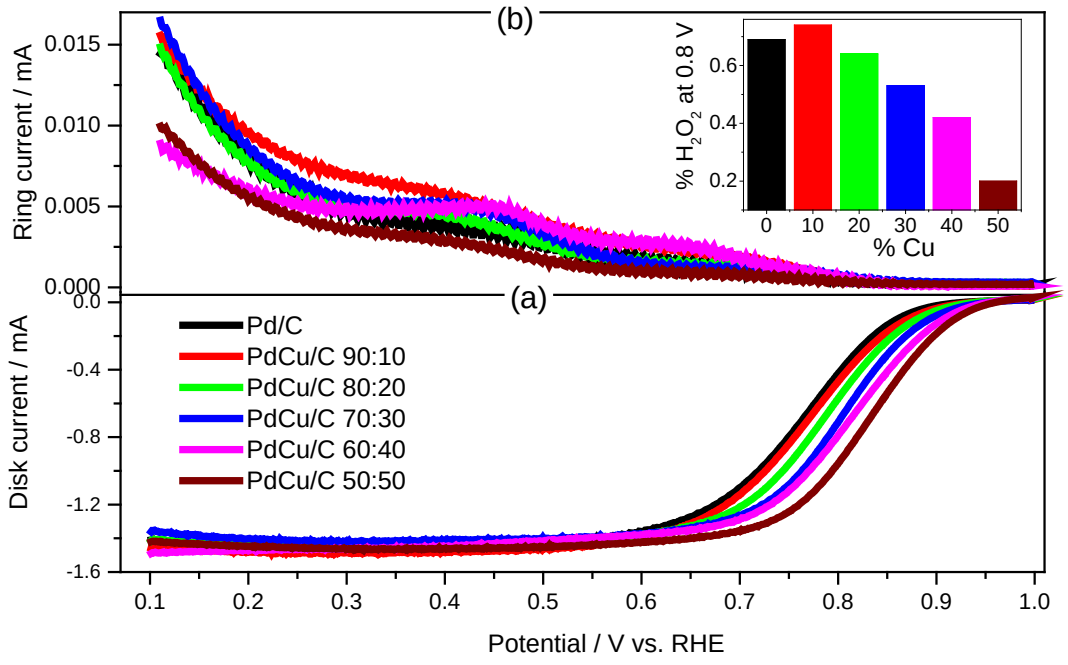

Compared to Pd/C, it is seen that the ORR polarization curves are shifted toward positive potential for PdCu/C as the percentage of Cu increases. Thus, it is clear that Cu in alkaline solution also has an enhancing effect on ORR. The small hydrogen peroxide oxidation currents show the 4-electron path is considerably favored [23].

The kinetic current (ik) at 0.80 V was calculated using the Koutecky- Levich equation (equation 19) to evaluate the mass activity (equation 20) and specific activity (equation 21) of PdCu/C catalysts, which are depicted as a function of Cu percentage in Figure 45.

Figure 45 - Mass activity (a) and specific activity (b) at 0.85 V for ORR in 0.1 M NaOH solution against atomic percentage of Cu.

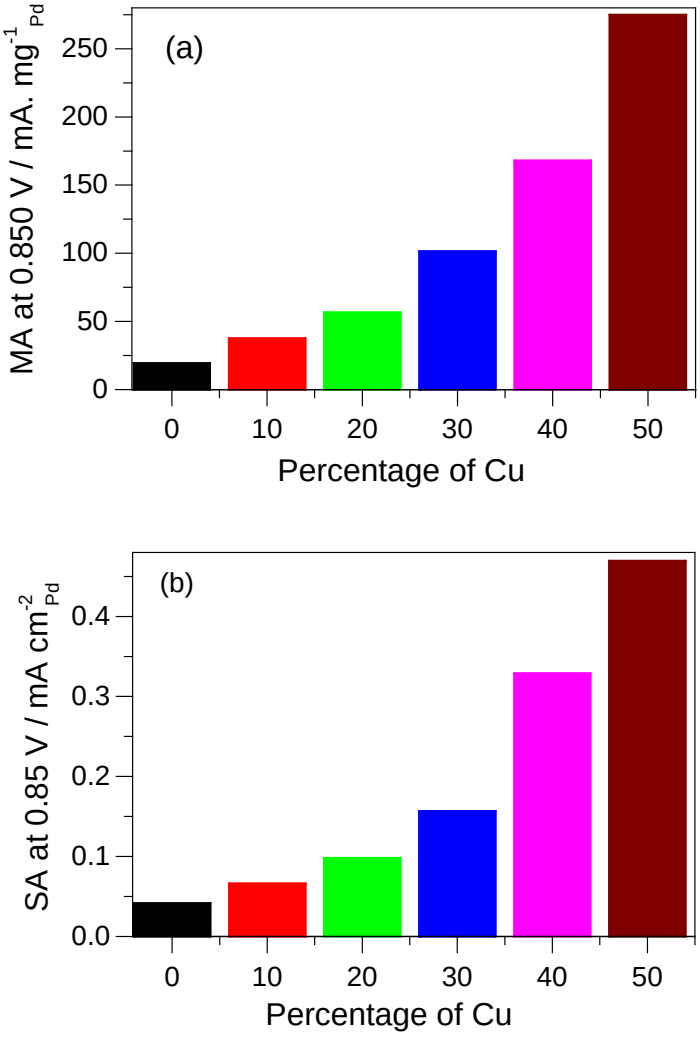

It is clearly seen that both parameters indicate that PdCu/C samples are more active for ORR than Pd/C. Similarly, the plots show that enhancement of activity increases following the Cu percentage in the material. Our data show that Cu addition to Pd lead to enhancement of ORR activity in alkaline solution, in agreement with literature reports [59,100,101].

The plots of current density at 0.850 V against the area of the Lorentzian curve and against the Pd-Pd interatomic distance, which given in Figure 46, look like those obtained for acidic medium. Again, it is not possible to say that one effect is dominant, so it is likely that both have a role in the ORR in alkaline solutions.

Figure 46 - Current density for ORR at 0.850 V in alkaline solution of Pd/C and PdCu/C of different compositions. (a) Against the integral of Lorentzian curve adjusted to XAS spectra. (b) Against the XRD-derived Pd-Pd distance.

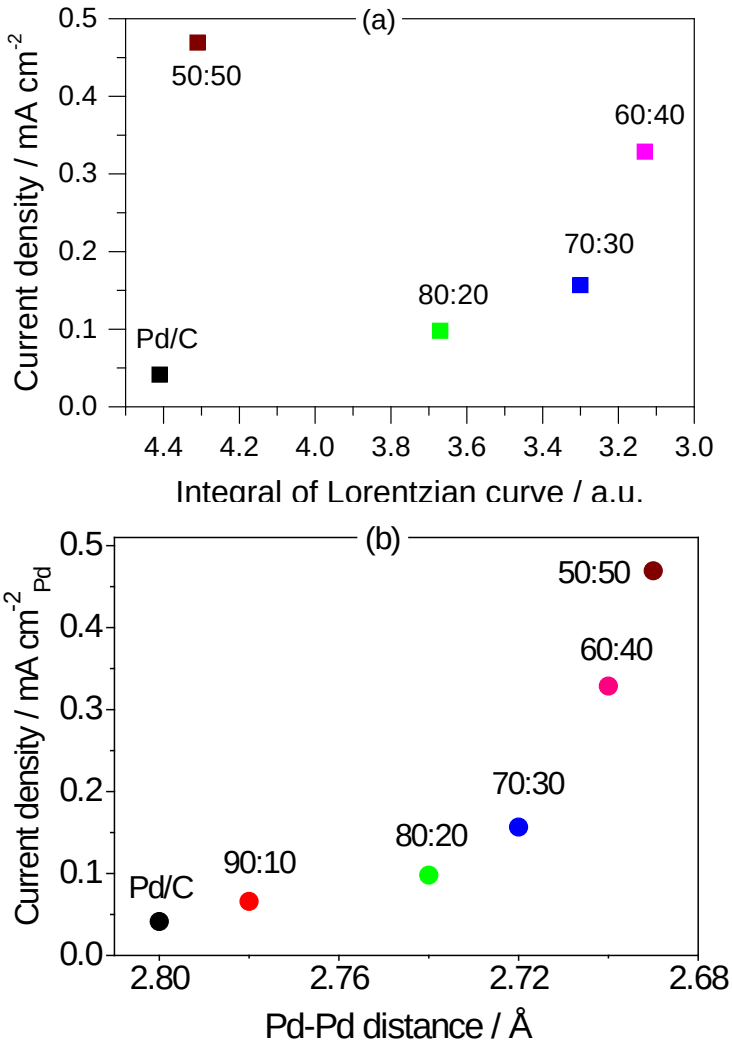

For this set of PdCu/C catalysts, the Tafel plots for alkaline medium also show two regions with different slope, as presented in Figure 47. It is interesting to notice the shift toward higher values of kinetically controlled current of data for PdCu/C 50:50.

Figure 47 - Mass-transport corrected Tafel plots of ORR on PdCu/C samples. Lines with slopes of 60 mv/dec and 120 mV/dec are shown.

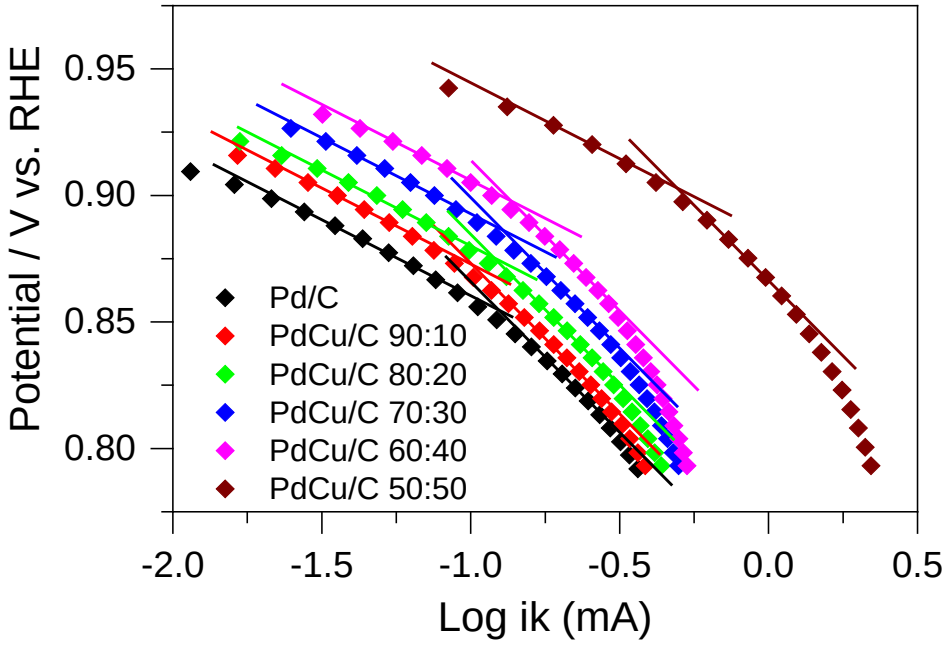

4.2.9. Accelerated stability test in 0.1 M NaOH solution

The cyclic voltammetry curves registered for evaluating stability of Pd/C and PdCu/C electrocatalysts up to 1000 potential cycles in alkaline solution are presented in Figure 48.

Figure 48 - Cyclic voltammetry curves taken for stability tests for Pd/C and PdCu/C catalyst in 0.1 M NaOH solution from 0.050 to 1.0 V vs RHE. Sweep rate 0.050 V s^{-1}.

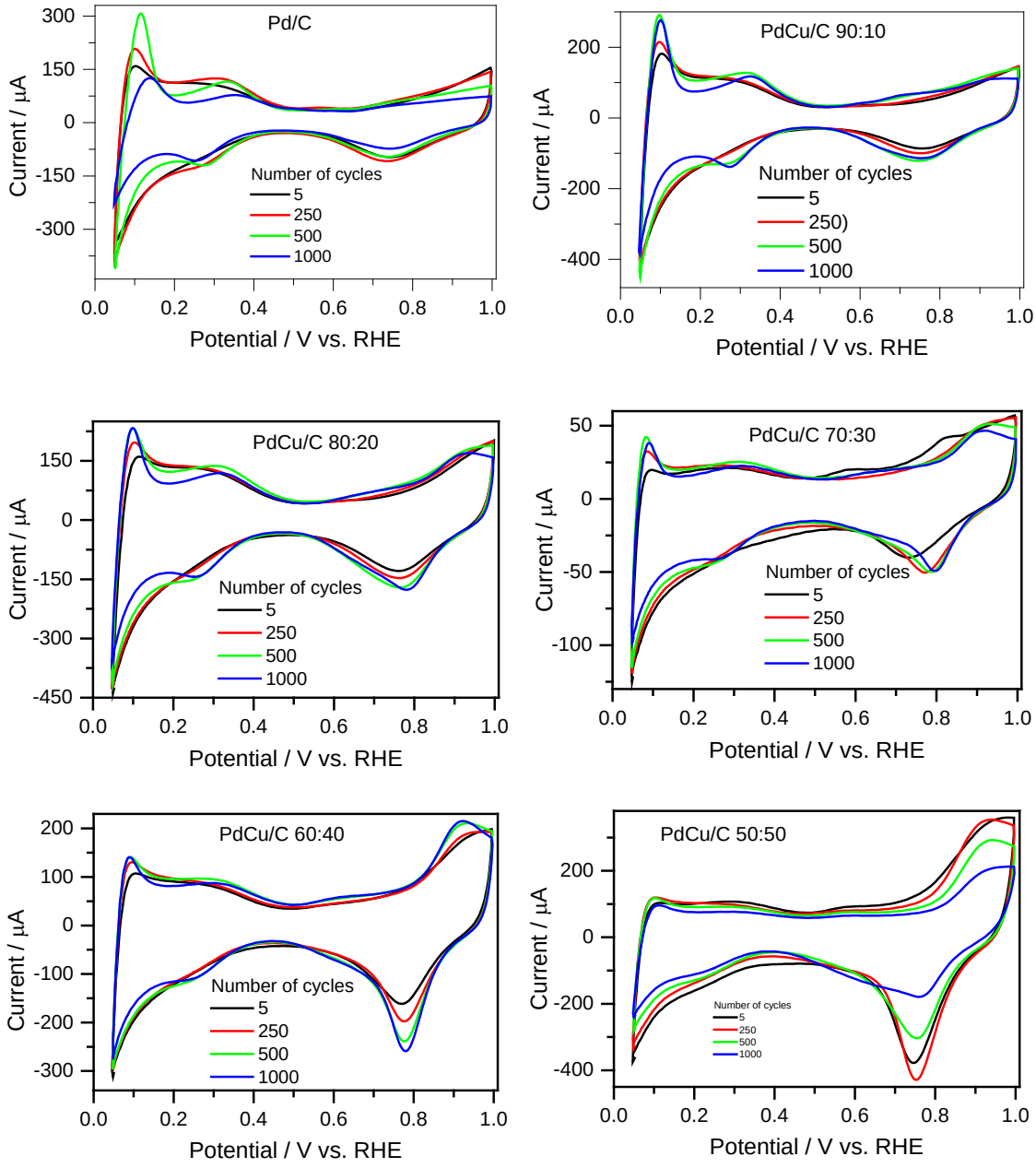

The changes in the total relative charge are presented in Figure 49. It is seen that for PdCu/C samples, the relative total charge increases and then decreases during the continuous cycling. The changes indicate lack of good stability of PdCu/C samples during continuous potential cycling in alkaline medium.

Figure 49 - Relative charge variations during accelerated stability tests for Pd/C and PdCu/C in 0.1 M NaOH.

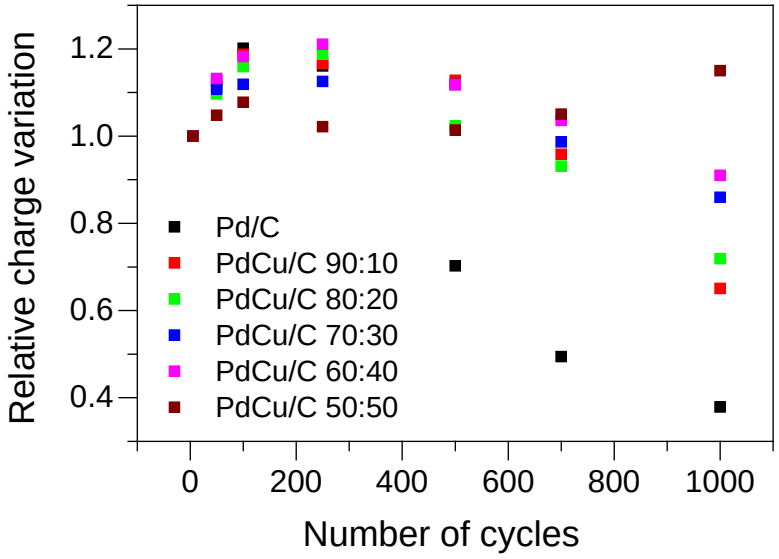

4.3. Comparison between PdNi/C and PdCu/C in acidic and alkaline media

The mass activities and specific activities for the ORR at 0.80 V in 0.5 M H_2SO_4 solution calculated for PdNi/C and PdCu/C catalysts of different compositions are compared in Table 10.

Table 10 - ORR mass activities and specific activities at 0.80 V for PdNi/C and PdCu/C electrocatalysts in 0.5 M H_2SO_4.

PdNi/C	MA (mA/mg)	SA (mA/cm^2)	PdCu/C	MA (mA/mg)	SA (mA/cm^2)
90:10	2.9	0.01	90:10	17.6	0.03
80:20	9.6	0.03	80:20	42.6	0.07
70:30	20.0	0.08	70:30	91.8	0.14
60:40	43.1	0.17	60:40	168.9	0.33
50:50	98.1	0.47	50:50	286.6	0.49

It is seen that in acidic solution mass and specific activities of PdCu/C catalysts are better than those of PdNi/C. For the most active materials of each set, the specific activity is not very different and the mass activity is much better for PdCu/C. Also, stability tests in acidic medium (Figure 17 for PdNi/C and Figure 40 for PdCu/C samples) show that PdCu/C would be also more stable. Thus, PdCu/C 50:50 would be a better cathode material than PdNi/C 50:50 in acidic medium.

The mass activities and specific activities for the ORR at 0.85 V in 0.1 M NaOH solution are compared in Table 11. It is seen that PdNi/C samples have better specific activities than PdCu/C. Mass activities are higher for PdCu/C up to 40% Cu and similar for PdNi/C 50:50 and PdCu/C 50:50. In alkaline medium, PdNi/C and PdCu/C have much better activities than Pd/C but showed degradation (extent depending on second metal percentage) during continuous potential cycling.

Table 11 - ORR mass activities and specific activities at 0.85 V for PdNi/C and PdCu/C electrocatalysts in 0.1 M NaOH.

PdNi/C	MA (mA/mg)	SA (mA/cm^2)	PdCu/C	MA (mA/mg)	SA (mA/cm^2)
90:10	32.0	0.08	90:10	37.5	0.07
80:20	44.7	0.15	80:20	56.5	0.10
70:30	92.9	0.39	70:30	101.4	0.16
60:40	123.8	0.49	60:40	167.9	0.33
50:50	296.1	1.42	50:50	274.8	0.47

For all studied materials, the ORR activities are higher in alkaline medium compared to acidic solutions as expected. In both environments and for all catalysts, ORR reaction proceeds in all cases mainly via 4-electron path, i.e., producing water. The amount of hydrogen peroxide produced is very small for all sample. Moreover, it seems to decrease a little in both media, acidic and alkaline, with addition of the second metal.

In both cases, the addition of the second metal (Ni or Cu) lead to increased occupation of Pd 4d band and to lower values of lattice constant and Pd-Pd distance. Overall, mass activities and specific activities correlate with the electronic properties and the Pd-Pd distance. So, it is not possible to tell that one of these properties determines the ORR catalytic activity. Most likely, the two properties might play a role.

Continuous potential cycling (up to 150 cycles) in acidic medium show that bimetallic samples are generally more stable than Pd/C, in good agreement with previous reports. Continuous potential cycling in alkaline medium (up to 1000 cycles) showed that PdNi/C and PdCu/C samples degrade less than Pd/C but stability is still low. In alkaline solution, marked degradation of most samples occurred.

In summary, PdCu/C 50:50 is the most active and stable sample in acidic medium. PdNi/C 50:50 is the most active in basic medium but is not very stable.

5. CONCLUSIONS

In the present study, carbon-supported PdNi and PdCu nanoparticles have been prepared successfully by a modified polyol method. Based on the results obtained, we can conclude that:

✓ Alloys were formed leading to decrease in lattice parameter (for both systems);

✓ The addition of second metal (Ni or Cu) lead to an increase in the occupation of the 4d band of Pd. Distinct behavior was observed for PdCu/C 50:50;

✓ Addition of Ni or Cu lead to better ORR activity for oxygen reduction in dilute H_2SO_4 and NaOH solutions, compared with Pd/C.

✓ For all bimetallic materials, ORR activity improves as the percentage of second metal (Ni or Cu) increases. Samples of 50:50 composition are the most active.

✓ Activity for ORR of all studied materials is higher in alkaline solution than in acidic solution, as expected.

✓ In acidic medium, PdCu/C catalysts are more active than PdNi/C materials of similar nominal percentage of second metal. PdCu/C 50:50 has the best performance and stability;

✓ In alkaline medium, PdNi/C catalysts have higher ORR activity than PdCu/C, but all PdNi/C and PdCu/C samples degrade (extent depending of composition),

✓ Generally, the kinetic current density increases as the 4d band of Pd is more filled and as the Pd-Pd distance decreases. So, it is likely that both properties play a role.

✓ The amount of hydrogen peroxide produced is small on the studied materials. So, in all cases the oxygen reduction reaction proceeded via 4-electrons mechanism (acidic and basic media).

6. REFERENCES

1. SRINIVASAN, S. **Fuel Cells. From Fundamentals to Applications**. Springer US, 2006. ISBN 978-0-387-25116-5.

2. BAGOTSKY, V. S. **Fuel Cells. Problems and Solutions**. Wiley, New York. 2012. ISBN 9780470232897.

3. STAMBOULI, A. B. Fuel cells: The expectations for an environmental-friendly and sustainable source of energy. **Renewable & Sustainable Energy Reviews,** v. 15, n. 9, p. 4507-4520, 2011.

4. GROVE, W. R. XXIV. On voltaic series and the combination of gases by platinum. **The London, Edinburgh, and Dublin Philosophical Magazine and Journal of Science,** v. 14, n. 86-87, p. 127-130, 1839.

5. PERRY, M. L.; FULLER, T. F. A historical perspective of fuel cell technology in the 20th century. **Journal of the Electrochemical Society,** v. 149, n. 7, p. S59-S67, 2002.

6. MAURYA, S. et al. A review on recent developments of anion exchange membranes for fuel cells and redox flow batteries. **Rsc Advances,** v. 5, n. 47, p. 37206-37230, 2015.

7. CARRETTE, L.; FRIEDRICH, K. A.; STIMMING, U. Fuel Cells - Fundamentals and Applications. **Fuel Cells,** v. 1, n. 1, p. 5-39, 2001.

8. AN, L.; ZHAO, T. S.; LI, Y. S. Carbon-neutral sustainable energy technology: Direct ethanol fuel cells. **Renewable & Sustainable Energy Reviews,** v. 50, p. 1462-1468, 2015.

9. LI, X. L.; FAGHRI, A. Review and advances of direct methanol fuel cells (DMFCs) part I: Design, fabrication, and testing with high concentration methanol solutions. **Journal of Power Sources,** v. 226, p. 223-240, 2013.

10. DEKEL, D. R. Review of cell performance in anion exchange membrane fuel cells. **Journal of Power Sources,** v. 375, p. 158-169, 2018.

11. GE, X. M. et al. Oxygen Reduction in Alkaline Media: From Mechanisms to Recent Advances of Catalysts. **Acs Catalysis,** v. 5, n. 8, p. 4643-4667, 2015.

12. ANTOLINI, E.; GONZALEZ, E. R. Alkaline direct alcohol fuel cells. **Journal of Power Sources,** v. 195, n. 11, p. 3431-3450, 2010.

13. ZHANG, H. W. et al. Anion-Exchange Membranes for Fuel Cells: Synthesis Strategies, Properties and Perspectives. **Fuel Cells,** v. 15, n. 6, p. 761-780, 2015.

14. DUBAU, L. et al. A review of PEM fuel cell durability: materials degradation, local heterogeneities of aging and possible mitigation strategies. **Wiley Interdisciplinary Reviews-Energy and Environment,** v. 3, n. 6, p. 540-560, 2014.

15. PAN, Z. F. et al. Alkaline anion exchange membrane fuel cells for cogeneration of electricity and valuable chemicals. **Journal of Power Sources,** v. 365, p. 430-445, 2017.

16. WANG, Y. et al. A review of polymer electrolyte membrane fuel cells: Technology, applications, and needs on fundamental research. **Applied Energy,** v. 88, n. 4, p. 981-1007, 2011.

17. SEN, R. K.; ZAGAL, J.; YEAGER, E. The electrocatalysis of molecular oxygen reduction. **Inorganic Chemistry,** v. 16, n. 12, p. 3379-3380, 1977.

18. YEAGER, E. Electrocatalysts for O2 reduction. **Electrochimica Acta,** v. 29, n. 11, p. 1527-1537, 1984.

19. WATANABE, M. et al. Overview of recent developments in oxygen reduction electrocatalysis. **Electrochimica Acta,** v. 84, p. 187-201, 2012.

20. SHAO, M. H. et al. Recent Advances in Electrocatalysts for Oxygen Reduction Reaction. **Chemical Reviews,** v. 116, n. 6, p. 3594-3657, 2016.

21. SONG, C.; ZHANG, J. Electrocatalytic Oxygen Reduction Reaction. In: ZHANG, J. (Ed.). **PEM Fuel Cell Electrocatalysts and Catalyst Layers: Fundamentals and Applications**. London: Springe, 2008. p.89-134. ISBN 978-1-84800-936-3.

22. YEAGER, E. DIOXYGEN ELECTROCATALYSIS - MECHANISMS IN RELATION TO CATALYST STRUCTURE. **Journal of Molecular Catalysis,** v. 38, n. 1-2, p. 5-25, 1986.

23. TARASEVICH, M. R.; SADKOWSKI, A.; YEAGER, E. Oxygen Electrochemistry. In: CONWAY, B. E.;BOCKRIS, J. O. M.*, et al.* (Ed.). **Comprehensive Treatise of Electrochemistry: Volume 7 Kinetics and**

Mechanisms of Electrode Processes. Boston, MA: Springer US, 1983. p.301-398. ISBN 978-1-4613-3584-9.

24. MALHEIRO, A. R.; PEREZ, J.; VILLULLAS, H. M. Well-Alloyed PtFe/C Nanocatalysts of Controlled Composition and Same Particle Size: Oxygen Reduction and Methanol Tolerance. **Journal of the Electrochemical Society,** v. 156, n. 1, p. B51-B58, 2009.

25. SHUKLA, A. K. et al. Carbon-supported Pt-Fe alloy as a methanol-resistant oxygen-reduction catalyst for direct methanol fuel cells. **Journal of Electroanalytical Chemistry,** v. 563, n. 2, p. 181-190, 2004.

26. LUO, Y.; ALONSO-VANTE, N. The Effect of Support on Advanced Pt-based Cathodes towards the Oxygen Reduction Reaction. State of the Art. **Electrochimica Acta,** v. 179, p. 108-118, 2015.

27. CZERWIŃSKI, A. The adsorption of carbon oxides on a palladium electrode from acidic solution. **Journal of Electroanalytical Chemistry,** v. 379, n. 1, p. 487-493, 1994.

28. MALHEIRO, A. R.; PEREZ, J.; VILLULLAS, H. M. Surface structure and electronic properties of Pt-Fe/C nanocatalysts and their relation with catalytic activity for oxygen reduction. **Journal of Power Sources,** v. 195, n. 10, p. 3111-3118, 2010.

29. MALHEIRO, A. R.; PEREZ, J.; VILLULLAS, H. M. Dependence on composition of electronic properties and stability of Pt-Fe/C catalysts for oxygen reduction. **Journal of Power Sources,** v. 195, n. 21, p. 7255-7258, 2010.

30. YANO, H. et al. Oxygen reduction activity of carbon-supported Pt-M (M = V, Ni, Cr, Co, and Fe) alloys prepared by nanocapsule method. **Langmuir,** v. 23, n. 11, p. 6438-6445, 2007.

31. SANTIAGO, E. I.; VARANDA, L. C.; VILLULLAS, H. M. Carbon-supported Pt-Co catalysts prepared by a modifled polyol process as cathodes for PEM fuel cells. **Journal of Physical Chemistry C,** v. 111, n. 7, p. 3146-3151, 2007.

32. RAND, D. A. J.; WOODS, R. Nature of adsorbed oxygen on rhodium, palladium and gold electrodes. **Journal of Electroanalytical Chemistry,** v. 31, n. 1, p. 29-38, 1971.

33. CARBONIO, E. A. et al. Pt-Cu/C and Pd Modified Pt-Cu/C Electrocatalysts for the Oxygen Reduction Reaction in Direct Methanol Fuel Cells. **Journal of the Brazilian Chemical Society,** v. 21, n. 4, p. 590-602, 2010.

34. SUI, S. et al. A comprehensive review of Pt electrocatalysts for the oxygen reduction reaction: Nanostructure, activity, mechanism and carbon support in PEM fuel cells. **Journal of Materials Chemistry A,** v. 5, n. 5, p. 1808-1825, 2017.

35. ZHANG, C. L. et al. A review of Pt-based electrocatalysts for oxygen reduction reaction. **Frontiers in Energy,** v. 11, n. 3, p. 268-285, 2017.

36. ANTOLINI, E.; LOPES, T.; GONZALEZ, E. R. An overview of platinum-based catalysts as methanol-resistant oxygen reduction materials for direct methanol fuel cells. **Journal of Alloys and Compounds,** v. 461, n. 1-2, p. 253-262, 2008.

37. HOLTON, O. T.; STEVENSON, J. W. The Role of Platinum in Proton Exchange Membrane Fuel Cells Evaluation of platinum's unique properties for use in both the anode and cathode of a proton exchange membrane fuel cell. **Platinum Metals Review,** v. 57, n. 4, p. 259-271, 2013.

38. ANTOLINI, E. Palladium in fuel cell catalysis. **Energy & Environmental Science,** v. 2, n. 9, p. 915-931, 2009.

39. SHAO, M. Palladium-based electrocatalysts for hydrogen oxidation and oxygen reduction reactions. **Journal of Power Sources,** v. 196, n. 5, p. 2433-2444, 2011.

40. LO VECCHIO, C. et al. Investigation of Supported Pd-Based Electrocatalysts for the Oxygen Reduction Reaction: Performance, Durability and Methanol Tolerance. **Materials,** v. 8, n. 12, p. 7997-8008, 2015.

41. LIU, H.; MANTHIRAM, A. Tuning the electrocatalytic activity and durability of low cost Pd70Co30 nanoalloy for oxygen reduction reaction in fuel cells. **Electrochemistry Communications,** v. 10, n. 5, p. 740-744, 2008.

42. GIACOMINI, M. T. et al. Characterization of the activity of palladium-modified polythiophene electrodes for the hydrogen oxidation and oxygen reduction reactions. **Journal of the Electrochemical Society,** v. 150, n. 5, p. A588-A593, 2003.

43. RAND, D. A. J.; WOODS, R. Study of dissolution of platinum, palladium, rhodium and gold electrodes in 1 M sulfuric-acid by cyclic voltammetry. **Journal of Electroanalytical Chemistry,** v. 35, n. NMAR, p. 209-&, 1972.

44. PIRES, F. I.; VILLULLAS, H. M. Pd-based catalysts: Influence of the second metal on their stability and oxygen reduction activity. **International Journal of Hydrogen Energy,** v. 37, n. 22, p. 17052-17059, 2012.

45. JUODKAZIS, K. et al. Anodic dissolution of palladium in sulfuric acid: An electrochemical quartz crystal microbalance study. **Russian Journal of Electrochemistry,** v. 39, n. 9, p. 954-959, 2003.

46. RAMOS-SANCHEZ, G.; YEE-MADEIRA, H.; SOLORZA-FERIA, O. PdNi electrocatalyst for oxygen reduction in acid media. **International Journal of Hydrogen Energy,** v. 33, n. 13, p. 3596-3600, 2008.

47. BAMPOS, G. et al. Comparison of the Activity of Pd-M (M: Ag, Co, Cu, Fe, Ni, Zn) Bimetallic Electrocatalysts for Oxygen Reduction Reaction. **Topics in Catalysis,** v. 60, n. 15-16, p. 1260-1273, 2017.

48. SAVADOGO, O. et al. Investigation of some new palladium alloys catalysts for the oxygen reduction reaction in an acid medium. **Journal of New Materials for Electrochemical Systems,** v. 7, n. 2, p. 77-83, 2004.

49. FOUDA-ONANA, F.; BAH, S.; SAVADOGO, O. Palladium-copper alloys as catalysts for the oxygen reduction reaction in an acidic media I: Correlation between the ORR kinetic parameters and intrinsic physical properties of the alloys. **Journal of Electroanalytical Chemistry,** v. 636, n. 1-2, p. 1-9, 2009.

50. HSUEH, K. L.; GONZALEZ, E. R.; SRINIVASAN, S. Electrolyte effects on oxygen reduction kinetics at platinum - a rotating-ring disk electrode analysis **Electrochimica Acta,** v. 28, n. 5, p. 691-697, 1983.

51. ZHAO, J.; SARKAR, A.; MANTHIRAM, A. Synthesis and characterization of Pd-Ni nanoalloy electrocatalysts for oxygen reduction reaction in fuel cells. **Electrochimica Acta,** v. 55, n. 5, p. 1756-1765, 2010.

52. JIANG, L. et al. Oxygen Reduction Reaction on Carbon Supported Pt and Pd in Alkaline Solutions. **Journal of the Electrochemical Society,** v. 156, n. 3, p. B370-B376, 2009.

53. ERIKSON, H. et al. Electrochemical reduction of oxygen on palladium nanocubes in acid and alkaline solutions. **Electrochimica Acta,** v. 59, p. 329-335, 2012.

54. ERIKSON, H. et al. Recent progress in oxygen reduction electrocatalysis on Pd-based catalysts. **Journal of Electroanalytical Chemistry,** v. 780, p. 327-336, 2016.

55. WANG, M. et al. PdNi Hollow Nanoparticles for Improved Electrocatalytic Oxygen Reduction in Alkaline Environments. **Acs Applied Materials & Interfaces,** v. 5, n. 23, p. 12708-12715, 2013.

56. SANIJ, F. D.; GHARIBI, H. Preparation of bimetallic alloyed palladium-nickel electro-catalysts supported on carbon with superior catalytic performance towards oxygen reduction reaction. **Colloids and Surfaces a-Physicochemical and Engineering Aspects,** v. 538, p. 429-442, 2018.

57. PENG, X. et al. Highly active and durable Pd-Cu catalysts for oxygen reduction in alkaline exchange membrane fuel cells. **Frontiers in Energy,** v. 11, n. 3, p. 299-309, 2017.

58. SHA, Y. et al. DFT Prediction of Oxygen Reduction Reaction on Palladium-Copper Alloy Surfaces. **Acs Catalysis,** v. 4, n. 4, p. 1189-1197, 2014.

59. AN, L. J. et al. Hollow palladium-copper bimetallic nanospheres with high oxygen reduction activity. **Electrochimica Acta,** v. 176, p. 222-229, 2015.

60. WU, J. F. et al. PdCu Nanoalloy Electrocatalysts in Oxygen Reduction Reaction: Role of Composition and Phase State in Catalytic Synergy. **Acs Applied Materials & Interfaces,** v. 7, n. 46, p. 25906-25913, 2015.

61. ZHANG, H. et al. Nanoporous PdCu alloys as highly active and methanol-tolerant oxygen reduction, electrocatalysts. **International Journal of Hydrogen Energy,** v. 38, n. 24, p. 10029-10038, 2013.

62. KARIUKI, N. N. et al. Colloidal Synthesis and Characterization of Carbon-Supported Pd-Cu Nanoparticle Oxygen Reduction Electrocatalysts. **Chemistry of Materials,** v. 22, n. 14, p. 4144-4152, 2010.

63. MARTINEZ-CASILLAS, D. C.; VAZQUEZ-HUERTA, G.; SOLORZA-FERIA, O. Electrocatalytic Properties of PdCu Oxygen Reduction for PEM Fuel Cell. In: DUDNEY, N. (Ed.). **Batteries and Energy Technology**, v.28, 2010. p.141-147. (ECS Transactions). ISBN 1938-5862 978-1-56677-856-5.

64. XU, C. X. et al. Nanotubular Mesoporous PdCu Bimetallic Electrocatalysts toward Oxygen Reduction Reaction. **Chemistry of Materials,** v. 21, n. 14, p. 3110-3116, 2009.

65. SUN, M.; LI, J. H. Recent Progress on Palladium-Based Oxygen Reduction Reaction Electrodes for Water Treatment. **Acta Physico-Chimica Sinica,** v. 33, n. 1, p. 198-210, 2017.

66. LUO, Y. et al. An easy and cheap chemical route using a MOF precursor to prepare Pd-Cu electrocatalyst for efficient energy conversion cathodes. **Journal of Catalysis,** v. 338, p. 135-142, 2016.

67. WANG, X. P. et al. Bimetallic Pd-Cu oxygen reduction electrocatalysts. **Journal of the Electrochemical Society,** v. 155, n. 6, p. B602-B609, 2008.

68. CHEN, L. Y. et al. Nanoporous PdNi Bimetallic Catalyst with Enhanced Electrocatalytic Performances for Electro-oxidation and Oxygen Reduction Reactions. **Advanced Functional Materials,** v. 21, n. 22, p. 4364-4370, 2011.

69. XU, C. X. et al. Nanoporous PdNi alloys as highly active and methanol-tolerant electrocatalysts towards oxygen reduction reaction. **Journal of Materials Chemistry A,** v. 1, n. 43, p. 13542-13548, 2013.

70. WU, J. F. et al. A review of PEM fuel cell durability: Degradation mechanisms and mitigation strategies. **Journal of Power Sources,** v. 184, n. 1, p. 104-119, 2008.

71. SCHMITTINGER, W.; VAHIDI, A. A review of the main parameters influencing long-term performance and durability of PEM fuel cells. **Journal of Power Sources,** v. 180, n. 1, p. 1-14, 2008.

72. YU, K. et al. Degradation Mechanisms of Platinum Nanoparticle Catalysts in Proton Exchange Membrane Fuel Cells: The Role of Particle Size. **Chemistry of Materials,** v. 26, n. 19, p. 5540-5548, 2014.

73. BORUP, R. L. et al. PEM fuel cell electrocatalyst durability measurements. **Journal of Power Sources,** v. 163, n. 1, p. 76-81, 2006.

74. KNIGHTS, S. D. et al. Aging mechanisms and lifetime of PEFC and DMFC. **Journal of Power Sources,** v. 127, n. 1-2, p. 127-134, 2004.

75. YOUSFI-STEINER, N. et al. A review on polymer electrolyte membrane fuel cell catalyst degradation and starvation issues: Causes, consequences and diagnostic for mitigation. **Journal of Power Sources,** v. 194, n. 1, p. 130-145, 2009.

76. ZHANG, S. S. et al. A review of platinum-based catalyst layer degradation in proton exchange membrane fuel cells. **Journal of Power Sources,** v. 194, n. 2, p. 588-600, 2009.

77. SEVJIDSUREN, G. et al. Effect of Different Support Morphologies and Pt Particle Sizes in Electrocatalysts for Fuel Cell Applications. **Journal of Nanomaterials**, 2010.

78. ANTOLINI, E. Carbon supports for low-temperature fuel cell catalysts. **Applied Catalysis B-Environmental,** v. 88, n. 1-2, p. 1-24, 2009.

79. MENG, H.; ZENG, D. R.; XIE, F. Y. Recent Development of Pd-Based Electrocatalysts for Proton Exchange Membrane Fuel Cells. **Catalysts,** v. 5, n. 3, p. 1221-1274, 2015.

80. HIGGINS, D. et al. The application of graphene and its composites in oxygen reduction electrocatalysis: a perspective and review of recent progress. **Energy & Environmental Science,** v. 9, n. 2, p. 357-390, 2016.

81. CUI, C. H.; LI, H. H.; YU, S. H. Large scale restructuring of porous Pt-Ni nanoparticle tubes for methanol oxidation: A highly reactive, stable, and restorable fuel cell catalyst. **Chemical Science,** v. 2, n. 8, p. 1611-1614, 2011.

82. CAMACHO, B. R. et al. Enhancing oxygen reduction reaction activity and stability of platinum via oxide-carbon composites. **Catalysis Today,** v. 202, p. 36-43, 2013.

83. STACY, J. et al. The recent progress and future of oxygen reduction reaction catalysis: A review. **Renewable & Sustainable Energy Reviews,** v. 69, p. 401-414, 2017.

84. HE, Q. G.; CAIRNS, E. J. Review-Recent Progress in Electrocatalysts for Oxygen Reduction Suitable for Alkaline Anion Exchange Membrane Fuel Cells. **Journal of the Electrochemical Society,** v. 162, n. 14, p. F1504-F1539, 2015.

85. SUN, S. H. et al. Monodisperse FePt nanoparticles and ferromagnetic FePt nanocrystal superlattices. **Science,** v. 287, n. 5460, p. 1989-1992, 2000.

86. FIEVET, F.; LAGIER, J. P.; FIGLARZ, M. Preparing monodisperse metal powders in micrometer and submicrometer sizes by the polyol process. **Materials Research Society Bulletin,** v. 14, p. 29-40, 1989.

87. MALHEIRO, A. R. et al. The Extent on the Nanoscale of Pt-Skin Effects on Oxygen Reduction and Its Influence on Fuel Cell Power. **Journal of Physical Chemistry C,** v. 114, n. 47, p. 20267-20271, 2010.

88. GENTIL, R.; VILLULLAS, H. M. Oxygen reduction activity and methanol tolerance of carbon-supported PtV nanoparticles and the effects of heat treatment at low temperatures. **Journal of Solid State Electrochemistry,** v. 20, n. 4, p. 1119-1129, 2016.

89. NEWVILLE, M. Fundamentals of XAFS. In: HENDERSON, G. S.;NEUVILLE, D. R.*, et al.* (Ed.). **Spectroscopic Methods in Mineralology and Materials Sciences**, v.78, 2014. p.33-74. (Reviews in Mineralogy & Geochemistry). ISBN 978-0-939950-93-5.

90. SCHMIDT, T. J. et al. Characterization of high-surface area electrocatalysts using a rotating disk electrode configuration. **Journal of the Electrochemical Society,** v. 145, n. 7, p. 2354-2358, 1998.

91. CULLITY, B. C. **Elements of X-ray Diffraction**. Second.Addison-Wesley Publishing Company, Inc., London. 1978.

92. BIDWELL, L. R.; SPEISER, R. Unit-cell dimensions of Ni-Pd alloys at 25 and 900 degrees C. **Acta Crystallographica,** v. 17, n. 11, p. 1473-&, 1964.

93. RAVEL, B.; NEWVILLE, M. ATHENA, ARTEMIS, HEPHAESTUS: data analysis for X-ray absorption spectroscopy using IFEFFIT. **Journal of Synchrotron Radiation,** v. 12, p. 537-541, 2005.

94. FANG, L. L. et al. Determination of the Real Surface Area of Palladium Electrode. **Chinese Journal of Chemical Physics,** v. 23, n. 5, p. 543-548, 2010.

95. BARD, A. J.; FAULKNER, L. R. **Electrochemical Methods: Fundamentals and Applications**. Second.Wiley, NY. 2000. ISBN 978-0-471-04372-0.

96. ERIKSON, H. et al. Oxygen reduction on electrodeposited Pd coatings on glassy carbon. **Electrochimica Acta,** v. 88, p. 513-518, 2013.

97. BIN, D. et al. Facile synthesis of PdNi nanowire networks supported on reduced graphene oxide with enhanced catalytic performance for formic acid oxidation. **Journal of Materials Chemistry A,** v. 3, n. 26, p. 14001-14006, 2015.

98. ARENZ, M. et al. The oxygen reduction reaction on thin palladium films supported on a Pt(111) electrode. **Journal of Physical Chemistry B,** v. 107, n. 36, p. 9813-9819, 2003.

99. SUBRAMANIAN, P. R.; LAUGHLIN, D. E. Cu-Pd (Copper-Palladium). **Journal of Phase Equilibria,** v. 12, n. 2, p. 231-243, 1991.

100. WU, W. P. et al. Palladium copper nanosponges for electrocatalytic reduction of oxygen and glucose detection. **Journal of Materials Chemistry A,** v. 3, n. 18, p. 9675-9681, 2015.

101. GUO, Z. F. et al. Carbon Supported Oxide-Rich Pd-Cu Bimetallic Electrocatalysts for Ethanol Electrooxidation in Alkaline Media Enhanced by Cu/CuOx. **Catalysts,** v. 6, n. 5, 2016.